Methylmercury production and export across the terrestrial-aquatic continuum in permafrost peatland catchments

by

Lauren Thompson

A thesis submitted in partial fulfillment of the requirements for the degree of

Doctor of Philosophy

in

Water and Land Resources

Department of Renewable Resources

University of Alberta

Abstract

Ongoing permafrost thaw in northern peatland catchments may increase the production and downstream delivery of neurotoxic methylmercury (MeHg) across the terrestrial-aquatic continuum. Peatlands in boreal-Arctic regions have large stocks of mercury (Hg) in frozen soils, accumulated through atmospheric deposition of natural and human-emitted Hg over thousands of years. Permafrost thaw in peatlands often leads to land surface collapse (thermokarst), which may shift environmental conditions to facilitate microbial production of MeHg (methylation). However, the degree to which Hg is methylated post-thaw and exported downstream remains uncertain in northwestern Canada and poses a potential hazard for uptake by aquatic food webs.

I initiated three field studies examining MeHg cycling throughout the peatland-rich Interior Plains of boreal western Canada – 1) examining how peatland and permafrost extent influenced MeHg concentrations through a synoptic sampling of lakes and streams, 2) determining how discharge and land cover controlled the export and concentrations of MeHg in two stream catchments with differing peatland extent, and 3) exploring the microbial production of MeHg in thermokarst wetlands compared to intact permafrost peatlands.

By sampling total Hg (THg) and MeHg concentrations from 25 lakes and 47 streams spanning 1700 km across the Interior Plains (Chapter 2), I found that peatlands were primary sources of MeHg to surface waters regardless of permafrost extent, as MeHg concentrations increased with indicators of peatland-derived water chemistry. Lakes were potential MeHg sinks, likely through solar MeHg degradation (photodemethylation), while resident microbial communities in lake sediments were most capable of gaseous Hg emission to the atmosphere rather than methylation.

To consider seasonal variation in MeHg concentrations and export, I initiated a study involving higher-frequency sampling of streams in the discontinuous permafrost region.

Alongside Dehcho-Aboriginal Aquatic Resources and Ocean Management, I monitored one peatland-dominated catchment and one mixed catchment of mountains, forests, and peatlands over three years (Chapter 3). Compared to the mixed catchment, the peatland catchment had higher MeHg and lower THg concentrations and greater inter-annual variability in solute yields driven by storage thresholds in peatlands that control runoff generation. Transport limitation primarily controlled solute concentrations in the mixed catchment, with terrestrial flushing during high flows and lower inter-annual variability of solute yields due to consistent streamflow from groundwater sources and runoff generation from steeper slopes. I then studied biogeochemical controls on Hg methylation in peatlands due to their significance as downstream MeHg sources (Chapters 2, 3).

From methylation assays and peat and porewater chemistry of twelve peatland sites in the Interior Plains (Chapter 4), I found thermokarst wetlands to have greater methylation potential than intact permafrost peatlands. The highest MeHg concentrations and potential methylation rates were observed in fens and associated with a higher water table, labile organic matter, pH, and concentrations of sulfur and iron. The continued thawing of permafrost peatlands and expansion of thermokarst wetlands will likely result in favorable conditions for MeHg production.

My findings suggest that permafrost thaw in northern peatlands will enhance Hg methylation across the landscape, although wetland trophic status and groundwater connectivity will control MeHg production, and catchment hydrological functioning will determine downstream export. This knowledge is important for public health planning and land use intervention in the face of climate change, given the high risks of MeHg in aquatic ecosystems to northern communities.

Preface

Contributions of authors

All co-authored work presented in this dissertation follows the author order convention where the first author is the lead author, followed by authors in order of contribution, with the last author as the principal investigator. Each chapter in this thesis represents a collaborative scientific effort resulting in manuscript publication or preparation for submission to peer-reviewed journals, as detailed below. For all chapters, L.M.T. and D.O. designed the study with input from co-authors; L.M.T. led fieldwork, data analysis, and manuscript writing. Laboratory analysis was primarily led by L.M.T. with analytical support from R.S., J.C.W., K.H.K., L.P.P.B., R.H.S.H., and V.M. Prior to publication, all co-authors contributed or will contribute to writing.

Chapter 2: L.M. Thompson, M.A. Kuhn, J.C. Winder, L.P.P. Braga, R.H.S. Hutchins, A.J. Tanentzap, V.L. St. Louis, and D. Olefeldt. Controls on methylmercury concentrations in lakes and streams of peatland-rich catchments along a 1700 km permafrost gradient. Limnology & Oceanography, 68: 583–597. https://doi.org/10.1002/lno.12296

> ***Dataset:*** *University of Alberta, 2022. CIMP 199: Water quality of peatland ponds and streams on a latitudinal transect (dataset). 4.0.0. DataStream. https://doi.org/10.25976/rzkg-7n02.*
>
> ***Supplemental information:*** *University of Alberta Education & Research Archive. https://doi.org/10.7939/r3-z2w3-p617*

Chapter 3: L.M. Thompson, M. Low, R. Shewan, C. Schulze, M. Simba, O. Sonnentag, S. Tank, and D. Olefeldt. Landscape drives variability in concentrations and yields of mercury, methylmercury, and dissolved organic carbon in boreal catchments. Submitted to Water Resources Research.

> ***Dataset:*** *University of Alberta and Dehcho-AAROM. 2022. Seasonal Monitoring of Smith Creek and Scotty Creek, 2019-2021 (dataset). 1.0.0. DataStream. https://doi.org/10.25976/y9yi-no57.*

Chapter 4: L.M. Thompson, R. Shewan, V. Mangal, L.I. Harris, C.H. Cheng, L.P.P. Braga, O. Kolmakova, A.J. Tanentzap, K.H. Knorr, M.A. Kuhn, C. Haugk, A. Azaroff, S. Jonsson, V.L. St. Louis, I. Lehnherr, W.L. Quinton, O. Sonnentag, and D. Olefeldt. Enhanced methylmercury formation in thawing permafrost peatlands of northwestern Canada. Manuscript in preparation.

> ***Dataset:*** *L.M. Thompson, D. Olefeldt, V. Mangal, and K.H. Knorr. 2022. Soil and porewater chemistry from peatlands of the Interior Plains, northwestern Canada (dataset). University of Alberta Education & Research Archive. https://doi.org/10.7939/r3-vp5e-aj53*

To make a precise scientific description of reality out of words is like trying to build a rigid structure out of pure quicksilver.

"Unpopular Opinions," Dorothy L. Sayers

Acknowledgements

Thank you to funders that made this work possible, including support from the Natural Sciences and Engineering Research Council of Canada (NSERC) Discovery Grant and Northern Supplement, the Campus Alberta Innovates Program, the NWT Cumulative Impact Monitoring Program, the Northern Scientific Training Program, and UAlberta North. Personal funding was provided through NSERC CGS-M, PGS-D, Weston Family Foundation, and University of Alberta.

Research for my thesis was undertaken on the lands and territories of Treaty 11, 8, and 6 of contemporary Canada. Thank you to the generous knowledge holders in the North who deepened my understanding of the muskeg and doing science in a good way. I immensely appreciate the contributions and guidance from the Dehcho-AAROM Guardians, with particular thanks to Mike Low. Additionally, thanks to Matt Munson, Trish Fontaine, and Maggie Glasgow for fostering an internship with Dene Tha` First Nation that taught me so much.

Many thanks to my supervisor, Dr. David Olefeldt, for supporting me throughout my Ph.D. David's trust in my abilities, in addition to his keen understanding of Interior Plains hydro-bio-geo-chemistry and craft for writing, has been foundational to my development. I would also like to thank Dr. Tim Moore at McGill University, who taught me so much during my formative time at Mer Bleue and whose support inspired my pursuit of graduate studies.

Thank you to my supervisory committee for your time and guidance: Drs. Suzanne Tank, Oliver Sonnentag, and Vincent St. Louis. Additional thanks go to collaborators I have been fortunate to work with and learn from, including Drs. Andrew Tanentzap, Lucas Braga, Vaughn Mangal, Klaus-Holger Knorr, and Lorna Harris. Thank you, Dr. Sofi Jonsson, for the excellent experience at Stockholm University and the opportunity to visit some beautiful Fennoscandian peatlands.

I'm grateful for the support of Catchment and Wetland Science labmates throughout my grad school journey and beyond. Thank you to Drs. Liam Heffernan, McKenzie Kuhn, Emily Pugh, Carolyn Gibson, as well as Christopher Schulze, Julia Orlova, Rebecca Frei, Renae Shewan, and Jessica Lagroix. Fieldwork takes a village; my labmates and the many brilliant undergraduates who worked with CAWS made fieldwork into dream work, including Johanna Winder, Maya Frederickson, Theresa Wilkes, Erik Umbach, and Kate Marouelli. I am thankful for the many times

you all answered the call to be a second pair of hands for sampling and generous lab support in Edmonton whenever I was away.

I can't thank my friends and family – the Thompsons and Rezansoffs – enough for their unwavering encouragement and support. I'm incredibly grateful to my parents, Donna and Gord, and siblings, Duncan and Erin, for cheering me on, no matter what. Finally, to Evan. You kept me together with your patience and care during this adventure that took me away for countless days, kept Wrigley fed and walked when I was in the depths of thesis writing, and never hesitated to help me rewire my scientific instruments or troubleshoot truck issues over the phone – I love and appreciate you to the moon and back. This thesis would not have been possible without you.

Table of Contents

List of Tables

List of Figures

List of Abbreviations and Symbology

%MeHg	Percent methylmercury; the ratio of methylmercury to total mercury
$\delta^{13}C$	Ratio of ^{13}C and ^{12}C
$\delta^{15}N$	Ratio of ^{15}N and ^{14}N
β	Log-log slope between discharge and solute
A_{254}	Absorbance at 254 nm
ACW	Anticlockwise
AIC	Akaike Information Criterion
AMLE	Adjusted Maximum Likelihood Estimator
BIX	Biological index
C	Carbon
C1	PARAFAC Component 1
C2	PARAFAC Component 2
C3	PARAFAC Component 3
C4	PARAFAC Component 4
C5	PARAFAC Component 5
Ca	Calcium
CDEM	Canadian Digital Elevation Model
Cl	Chloride
Cu	Copper
CV	Coefficient of variation
CV_C/CV_Q	Coefficients of variation of solute concentration over discharge
CW	Clockwise
DOC	Dissolved organic carbon
DOM	Dissolved organic matter
EC	Electrical conductivity
EEM	Emission-excitation matrix
Fe	Iron
FI	Fluorescence index
Fmax	Maximum fluorescence of excitation and emission in Raman units
FTICR	Fourier-transform ion cyclotron resonance
FTIR	Fourier-transform infrared
H	Hydrogen
Hg	Mercury
Hg^0	Elemental mercury
Hg^{II}	Divalent inorganic mercury
hgcAB	Hg^{II} methylating gene
HIX	Humification index
ICP-MS	Inductively coupled plasma-mass spectrometer
ICP-OES	Inductively coupled plasma optical emission spectroscopy

K	Potassium
k_m	Potential methylation rate
MAAT	Mean annual air temperature
MeHg	Methylmercury
merA	Hg^{II} reducing gene
merB	MeHg demethylating gene
Mg	Magnesium
Mn	Manganese
Na	Sodium
NH	No hysteresis
NH_4-N	Ammonium-as-nitrogen
NO_2-N	Nitrite-as-nitrogen
NO_3-N	Nitrate-as-nitrogen
NOSC	Nominal oxygen state of carbon
O	Oxygen
P	Phosphorus
PARAFAC	Parallel factor analysis
PCA	Principle component analysis
PD	Photodemethylation
perANOVA	Permutational analysis of variance
perMANOVA	Permutational multivariate analysis of variance
PFD	Photon flux density
PO_4-P	Orthophosphate-as-phosphorus
Q	Discharge
QA/QC	Quality assurance/quality control
RDA	Redundancy analysis
S	Sulfur
SD	Standard deviation
SE	Standard error
SO_4^{-2}-S	Sulfate-as-sulfur
SSPs	Shared Socio-economic Pathways
$SUVA_{254}$	Specific ultraviolet absorbance at 254 mn
TDN	Total dissolved nitrogen
TEA	Terminal electron acceptor
THg	Total mercury
UV	Ultraviolet
UV-A	Ultraviolet A
UV-B	Ultraviolet B
Zn	Zinc

1. Introduction

1.1 Mercury accumulation in northern peatlands

Mercury (Hg) is a neurotoxic contaminant of global concern due to the tendency of its organic form, methylmercury (MeHg), to biomagnify as it travels up trophic levels and bioaccumulate in fatty tissues over the lifetime of aquatic biota (Mergler et al., 2007). The biogeochemical transformation of main Hg species (elemental Hg – Hg^0, divalent inorganic Hg – Hg^{II}, MeHg) mediates the cycling of Hg through the soil, air, and water. Peatland ecosystems have accumulated Hg stores over millennia from atmospheric deposition of Hg binding to plants and soil organic matter (Grigal, 2003), where abundant thiol or sulfhydryl groups in organic matter have a high capacity for Hg complexation (Skyllberg, 2008). Long-distance atmospheric transport drives Hg pollution to Arctic and sub-Arctic ecosystems (Ariya et al., 2015). Rock weathering, volcanoes, and geothermal sources naturally emit Hg, while anthropogenic sources arise from industrial processes or intentional use as an amalgam in dentistry and gold mining (Pacyna et al., 2016). Hg^0 is the primary Hg species in the atmosphere, driving vegetation and soil uptake of Hg in tundra and peatlands (Jiskra et al., 2015, 2018). Atmospheric Hg^{II} deposition may occur near its source through dry or wet deposition or form through oxidation of Hg^0 (Amos et al., 2012).

Long-term increasing Hg concentration trends within fish in the peatland-rich Interior Plains of western Canada have led to fish consumption advisories, with Hg release from thawing permafrost peatlands identified as a possible driver (Laird et al., 2018; Moslemi-Aqdam et al., 2023). Schuster et al. (2018) have estimated the top three meters of permafrost soils to contain ~1600 Gg Hg, twice as much Hg as all other soils, the ocean, and the atmosphere combined, based on soil samples from Alaska. By contrast, Lim et al. (2020) presented a significantly lower estimate of ~600 Gg Hg based on peatland samples from the Western Siberian Lowlands. Despite uncertainty in quantifying the permafrost Hg stock, its vulnerability due to permafrost thaw and the potential for microbial production of neurotoxic MeHg after thaw is a global concern (AMAP, 2021; Jonsson et al., 2022). Understanding the cycling and bioavailability of Hg post-thaw is particularly important for northern Indigenous communities who rely on higher trophic level animals such as fish as a nutritionally and culturally important country food (Basu et al., 2022; Houde et al., 2022).

1.2 The rapidly changing Interior Plains of northwestern Canada

The Interior Plains of northwestern Canada, spanning the Taiga Plains and Boreal Plains ecozones, are characterized by widespread peatlands that began developing after the last glacial maximum (Ecosystem Classification Group, 2009). Permafrost aggraded in the region 1200–4500 years ago (Heffernan et al., 2020; Pelletier et al., 2017) and is relatively thin and warm and thus susceptible to thaw (Holloway & Lewkowicz, 2020; Spence et al., 2020). Peatlands protect the southern fringes of permafrost due to the insulating properties of peat; relatively dry, treed peat plateaus are the predominant permafrost landform (Wright et al., 2022). The climate of the Interior Plains is cool and dry, with highly variable catchment runoff regimes that are sensitive to the balance of precipitation and evapotranspiration (Burd et al., 2018; Mack et al., 2021).

Rapid warming (Vincent et al., 2015) and increasing wildfire regimes (Gibson et al., 2018) are driving extensive permafrost thaw in the Interior Plains. Thawing of ice-rich permafrost leads to land surface collapse (thermokarst) and drastically alters environmental conditions (Quinton et al., 2011) with implications for the production of MeHg (Tarbier et al., 2021). Throughout the Holocene, cycles of permafrost aggradation and degradation have occurred in the region's peatlands (Zoltai, 1993). However, thermokarst wetlands may now be considered irreversibly thawed since far greater permafrost degradation than aggradation is occurring (Gibson et al., 2018, 2021; Quinton et al., 2011).

Plateau-wetland complexes (Figure 1.1) are ubiquitous across the Interior Plains, in which intact permafrost peatlands are surrounded by permafrost-free thermokarst wetlands (i.e., bogs and fens). Hydrological implications of thaw are complex and can lead to enhanced surface and subsurface connectivity (Connon et al., 2014) alongside temporary increases in groundwater storage within thermokarst bogs that may subsequently drain (Carpino et al., 2021; Connon et al., 2014) and result in a decline of basin storage (Haynes et al., 2018). These land cover changes, alongside potential activation of groundwater flow paths, may explain observations of increased streamflow in the Interior Plains despite non-significant precipitation changes (Mack et al., 2021; Wright et al., 2022).

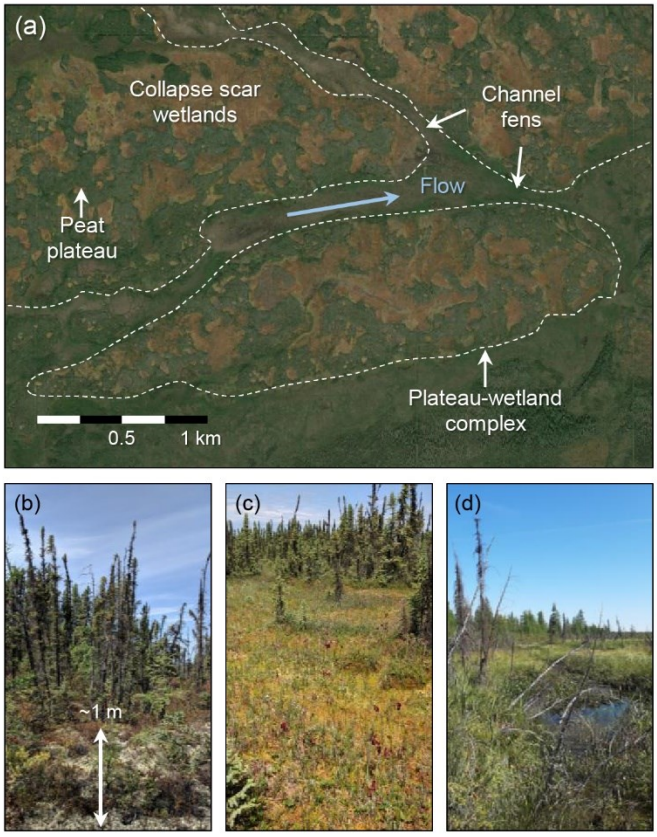

Figure 1.1. Plateau-wetland complexes in the Interior Plains. A) Green areas are intact permafrost-underlain peat plateaus, dark grey areas are permafrost-free runoff conveying channel fens, and orange/brown areas are permafrost-free collapse scar (thermokarst) bogs and poor fens. B) A treed peat plateau, C) thermokarst bog, and D) channel fen. Satellite imagery from Esri Canada and photos by L. M. Thompson and S. N. Wright. Adapted from Wright et al. (2022).

1.3 Microbial methylmercury production in peatlands

Peatlands have long been recognized as sites of MeHg production and export (St. Louis et al., 1994). The environmental conditions of waterlogged thermokarst wetlands can promote high Hg^{II} methylation efficiency (Fahnestock et al., 2019; Roth et al., 2021), dependent on the balance of microbial community, dissolved organic matter (DOM) quantity and composition, Hg bioavailability, and the abundance of terminal electron acceptors (Bravo & Cosio, 2020). Dissolved organic matter (DOM) may promote microbial activity and methylation (Hall et al., 2004). Hg^{II}-DOM complexation can facilitate bacterial uptake and increase Hg^{II} bioavailability (Chiasson-Gould et al., 2014). However, bioavailability becomes limited at high DOM concentrations (Chiasson-Gould et al., 2014), which is common in peatlands. The low pH conditions in wetlands can increase microbial Hg^{II} uptake (Kelly et al., 2003) and trigger the

displacement of Hg^{II} from particles and DOM (Ullrich et al., 2001). Sulfide-Hg^{II} complexes can likewise enhance methylation (Graham et al., 2012) but reach a threshold where bioavailability is inhibited at high concentrations (Hsu-Kim et al., 2013). Reduced iron forms can scavenge sulfide or complex sulfur, which may free up Hg for methylation (Bravo et al., 2015).

Microbes play a vital role in the production of MeHg. Bacteria were identified as likely producers of MeHg in the late 1960s (Jensen & Jernelöv, 1969). Sulfate-reducing bacteria, iron-reducing bacteria, and methanogens are considered the primary Hg^{II} methylators in wetlands (Bravo & Cosio, 2020). The linkage of *hgcAB* genes with Hg^{II} methylation has led to advancement in distinguishing potential methylators (Parks et al., 2013). An *hgcA*-encoded protein initiates the transfer of a negatively charged methyl carbanion to a Hg^{II} substrate, and *hgcB* encodes a ferredoxin-like protein to provide an electron donor for *hgcA* (Zhou et al., 2014). Recent work has recorded abundant *hgcA* genes and putative methylators in thermokarst wetlands (Fahnestock et al., 2019; McDaniel et al., 2020; Roth et al., 2021). Fens with intermediately-rich conditions are highly suited for methylation (Fahnestock et al., 2019; Gordon et al., 2016; Poulin et al., 2019; Tjerngren et al., 2012), a factor likely tied to the inputs of terminal electron acceptors such as sulfate and iron delivered from groundwater. Expansion of fens across the Interior Plains and activation of groundwater flow paths may result in the more efficient delivery of terminal electron acceptors that enhance Hg^{II} methylation.

1.4 Methylmercury production and degradation in lakes

Thermokarst peatland lakes release Hg and carbon (Klaminder et al., 2008; Rydberg et al., 2010), and organic-rich thaw ponds in the High Arctic can be sites with high sediment Hg^{II} methylation and high %MeHg (MeHg:Hg) (Lehnherr, St. Louis, & Kirk, 2012; MacMillan et al., 2015; St. Louis et al., 2005). Small peatland lakes in the Northwest Territories had high DOM concentrations and %MeHg (Evans et al., 2005), suggesting high Hg^{II} production within the lake sediments. However, the predominant Hg cycling model of lake sediments as the primary site for MeHg production within a catchment may not hold for wetland-influenced lakes. DOM can be a primary vector of MeHg from external sources such as wetlands to lakes dominated by allochthonous DOM (Branfireun et al., 2020; Bravo et al., 2017), such as those in the Interior Plains (Pugh et al., 2021). Lower Hg^{II} methylation rates in lakes have been associated with allochthonous, aromatic DOM

relative to labile, autochthonous DOM (Branfireun et al., 2020; Bravo et al., 2017). The Hg^{II} methylation capacity of peatland lake sediments in permafrost regions has not been investigated to date, and a knowledge gap remains for the methylating capability of sediment microbial communities.

Understudied relative to methylation, MeHg demethylation can be biotic or abiotic. Solar degradation (photodemethylation) is the dominant MeHg sink in freshwater systems, and its effectiveness decreases with depth (Lehnherr & St. Louis, 2009). In particular, aromatic DOM inhibits photodemethylation by attenuating radiation (Klapstein et al., 2018; Zhang et al., 2017). As increased DOM concentrations are expected with the expansion of thermokarst wetlands (Frey & Smith, 2005; Olefeldt et al., 2014), reduced capacity for photodemethylation is a potential cascading consequence of thaw (Chételat et al., 2022).

1.5 Mercury and methylmercury export in riverine environments

Streams and rivers are important pathways for Hg transportation that integrate contributions within their catchment. Hg export in Arctic rivers is closely tied to water discharge and suspended sediment load (Åkerblom et al., 2022; Emmerton et al., 2013; Zolkos et al., 2020); high loadings of sediment-bound Hg have been observed downstream of glaciers and retrogressive thaw slumps (St. Pierre et al., 2018; Vermilyea et al., 2017). Relatively higher MeHg concentrations have been observed downstream of wetland environments, where Hg species tend to be in the dissolved phase and coupled with DOM (Nagorski et al., 2014; Vermilyea et al., 2017). Spring freshet is a crucial period for Hg and MeHg export in major Arctic Rivers, comprising 50-65% of annual export, where frozen ground conditions ensure a flush of solutes from surficial soils alongside the delivery of Hg deposited in the snow (Dastoor et al., 2022; Emmerton et al., 2013; Zolkos et al., 2020). While the export of Hg from major Arctic rivers to the ocean has been relatively well constrained (AMAP, 2021), there is a distinct lack of studies focusing on MeHg export in northern regions, particularly in small catchments (Jonsson et al., 2022). Considering rapid permafrost thaw in the Interior Plains and observed increases in streamflow (Connon et al., 2014; Mack et al., 2021; Wright et al., 2022), changes to downstream Hg and MeHg export to the Mackenzie River, and eventually, the Arctic Ocean can be expected in the short- and long-term (Dastoor et al., 2022).

1.6 Connecting mercury cycling and permafrost thaw to capitalism and colonialism

Although this thesis focuses on Hg biogeochemistry, the systems that drive geoscientific research have deep and inextricable links to colonialism and extractive capitalism (Yusoff, 2018), as do the forces that shape anthropogenic Hg pollution. Beginning in the sixteenth century, the Spanish colonial government in the Americas used the forced labor of Indigenous peoples for Hg and silver mining economies; locally mined Hg was used to refine silver deposits which destabilized Andean communities through devastating health impacts on the laborers and still-lingering ecological consequences (Robins, 2011). The use of Hg as an amalgam (and its ecological consequences) continues today in artisanal and small-scale gold mining, a practice primarily undertaken by those facing poverty (Esdaile & Chalker, 2018; Mawowa, 2013). Canada's worst environmental disaster stems from industrial Hg pollution – Asubpeeschoseewagong First Nation (Grassy Narrows) has faced the erosion of land-based traditions and ongoing health impacts from Hg poisoning. Large quantities of Hg remain in the catchment to this day from the discharge of 10,000 kg of Hg from a chlor-alkali plant into the Wabigoon River in the 1960s by the Dryden Chemical Company (Armstrong & Hamilton, 1973; Ilyniak, 2014; Rudd et al., 2021). Members of Grassy Narrows continue to advocate for environmental and health justice in the struggle against colonial control of lands and resources that led to Hg poisoning in 90% of their community (Ilyniak, 2014; Porter, 2017).

Fossil fuels emitted from polluting industries continue to perturb the cycling of Hg and shape climate change across the globe. Coal is the greatest contributor to Hg pollution among fossil fuels, predominantly through coal combustion and secondarily during a preparatory coal washing phase (AMAP, 2019). Despite a temporary COVID-19-related decrease in global fossil carbon dioxide emissions, the anthropogenic release of climate-forcing gases is rebounding and is expected to continue accelerating (Friedlingstein et al., 2022). Indigenous communities in northern Canada have been disproportionately impacted by rapidly increasing air temperature and long-range Hg emissions due to economic decisions in highly polluting, distant regions. Changes to the muskeg (peatlands) due to permafrost thaw have important implications on cultural practices. As Dene Tha' Elder, Roy Salopree, stated about the culturally and muskeg-rich M'behcho (Bistcho Lake; R. Salopree, personal communication, September 17, 2022), "Muskeg is one of the important things in our culture, in our life. We use the spruce for medicine, to heal ourselves. We have to

live with [the muskeg] and take care of it, and do as much as we can to save it." In addition, Arctic communities have some of the highest Hg exposure globally due to foodborne intake, which requires careful risk assessment as the nutritional and cultural impacts of country foods are immense (Basu et al., 2022). In response, northern Indigenous communities are utilizing traditional knowledges to monitor Hg in their lands and waters (Houde et al., 2022). While interventions to reduce Hg pollution have been effective in decreasing atmospheric emissions, the release of legacy Hg emissions through climate-mediated changes (i.e., permafrost thaw, glacier melt, and coastal erosion) remains a concern (AMAP, 2021).

1.7 Objectives

My research focuses on the impacts of permafrost thaw on MeHg cycling in the Interior Plains. This thesis will investigate mechanisms that control the transformation of MeHg and its downstream delivery in permafrost peatland catchments. Chapter 2 evaluated variation in MeHg and Hg concentrations on a 1700 km permafrost gradient in western Canada. Chapter 3 monitored stream catchments for seasonal concentrations and export of Hg, MeHg, and DOC that flow from thawing permafrost peatlands. Finally, Chapter 4 investigated methylation potential in thermokarst wetlands compared to intact permafrost peatlands. My specific objectives are:

O1: Characterize patterns of MeHg and Hg concentrations from streams and lakes on a permafrost gradient in western Canada to assess the role of peatland cover and whether elevated concentrations are found in regions of rapid permafrost thaw.

O2: Assess temporal concentration and export trends for MeHg, Hg, and DOC from two contrasting boreal catchments to determine the role of the landscape in driving solute export.

O3: Determine methylation potential and controls on MeHg concentrations in thermokarst wetlands and intact peat plateaus in the sporadic and discontinuous permafrost region to assess how biogeochemical conditions influence potential MeHg production.

2. Controls on methylmercury concentrations in lakes and streams of peatland-rich catchments along a 1700 km permafrost gradient

Abstract

Permafrost thaw may increase the production of neurotoxic methylmercury (MeHg) in northern peatlands, but the downstream delivery of MeHg is uncertain. We quantified total mercury (THg) and MeHg concentrations in lakes and streams along a 1700 km permafrost transect in boreal western Canada to determine the influence of regional permafrost extent compared to local lake and catchment characteristics. In lakes, we assessed sediment microbial communities and modeled potential rates of water column photodemethylation. Regardless of permafrost conditions, peatlands were the primary sources of MeHg across the transect as MeHg concentrations in streams increased with aromatic dissolved organic carbon (DOC), iron, and lower pH. Higher DOC and greater catchment peatland extent were further associated with higher stream %MeHg (MeHg/THg). Peatland lakes were potential MeHg sinks, with lower MeHg concentrations than streams (mean±1SD: 0.19±0.23 and 0.47±0.77 ng MeHg L^{-1}, respectively), and larger stream catchments had lower %MeHg where photodemethylation may occur in abundant small lakes. Microbial communities in lake sediments showed that the abundance of Hg-reducing genes (*merA*) predominated over Hg methylating (*hgcA*) and MeHg demethylating (*merB*) genes. The effects of permafrost extent on MeHg processes in lakes were secondary to the influence of local catchment characteristics, but lakes in regions with less permafrost had higher DOC concentrations, higher %MeHg, and lower potential rates of photodemethylation. Our study highlights a need to understand the impacts of climate change on MeHg source and sink processes, particularly as mediated through changes to peatland DOC, to improve projections of future MeHg concentrations in northern catchments.

2.1 Introduction

Climate warming and permafrost thaw (Gibson et al., 2021) will likely affect concentrations of neurotoxic methylmercury (MeHg) in northern peatland-rich catchments (Gordon et al., 2016; Tarbier et al., 2021). Many northern boreal catchments have widespread peatlands with large stocks of atmospherically deposited mercury (Hg) bound to soil organic matter (Schuster et al., 2018). Favorable environmental conditions for MeHg production render peatlands as important sources of MeHg in boreal catchments (St. Louis et al., 1994), but the presence of permafrost in peatlands may influence MeHg production, degradation, and transport through its influence on groundwater connectivity and soil environmental conditions (Gordon et al., 2016; Poulin et al., 2019; Tarbier et al., 2021). Still, linkages between permafrost conditions and downstream MeHg delivery in northern catchments are poorly understood (Zolkos et al., 2020). Peatlands and peatland-rich catchments contain abundant shallow lakes connected to the stream network (Olefeldt et al., 2021), yet in these lakes, the balance between MeHg production and degradation through microbial and photochemical processes is unknown. Understanding spatial trends of MeHg concentrations in northern catchments can inform our ability to project future changes to MeHg cycling and how these changes may impact Indigenous peoples' cultural and physical well-being who rely on fish as healthy traditional food (Wheatley & Wheatley, 2000).

Microbes with the *hgcAB* gene cluster methylate inorganic divalent Hg^{II} into MeHg, but methylation additionally depends on environmental conditions and Hg^{II} bioavailability (Bravo & Cosio, 2020; Parks et al., 2013). High Hg^{II} methylation efficiency is often associated with anoxic conditions rich with alternative terminal electron acceptors (e.g., sulfate [SO_4^{-2}] or ferric iron; Bravo & Cosio, 2020), although elevated SO_4^{-2} concentrations may limit methylation in lakes (Gilmour et al., 1992; Shao et al., 2012). Labile dissolved organic matter (DOM) can further stimulate microbial activity and Hg bioavailability (Chiasson-Gould et al., 2014; Klapstein & O'Driscoll, 2018). Thus, certain regions in wetlands and lakes are often favorable locations for methylation (Branfireun et al., 2020; Mitchell et al., 2008b). In addition, permafrost thaw in peatlands often leads to land surface collapse, inundation, and increased groundwater interactions, creating Hg^{II} methylation hotspots (Fahnestock et al., 2019; Gordon et al., 2016; Poulin et al., 2019; Tarbier et al., 2021).

Degradation of MeHg through microbial and photochemical processes can influence MeHg concentration in freshwaters following its production. The microbial pathways of Hg^{II} reduction and reductive demethylation are associated with the detoxifying *mer* operon, where *merB* cleaves MeHg into Hg^{II} and methane, and *merA* reduces Hg^{II} into volatile gaseous Hg^0 that can be emitted to the atmosphere (Boyd & Barkay, 2012). Whereas microbial MeHg production occurs primarily in anoxic environments, the *mer* operon occurs in both aerobic and anaerobic microbes (Christakis et al., 2021). Solar breakdown (photodemethylation) of MeHg is considered the primary MeHg sink in northern lakes (Lehnherr & St. Louis, 2009). A key control on photodemethylation is water column ultraviolet (UV) radiation intensity. High DOM concentrations in small peatland lakes can rapidly attenuate UV radiation through the water column, inhibiting demethylation (Klapstein et al., 2018). The balance between Hg^{II} methylation and MeHg demethylation can vary among lakes, affecting lake MeHg concentrations and downstream transport (Branfireun et al., 2020; Girard et al., 2016; Hammerschmidt et al., 2006; Lehnherr, St. Louis, Emmerton, et al., 2012).

Here, we assessed concentrations of Hg and MeHg within lakes and streams within peatland-rich catchments on a 1700 km latitudinal and permafrost transect in the Interior Plains region of northwestern Canada (Figure 2.1). Some of the most rapid warming on Earth has occurred in this region, leading to extensive permafrost thaw in peatlands (Gibson et al., 2021). The transect provides a space-for-time substitution for projecting climate change; southern sites can be considered an analog for future conditions in northern sites where climate and permafrost conditions vary along otherwise similar physiography and land cover (Kuhn, Thompson, et al., 2021). Our focal research aims were: i) Determining how permafrost conditions and peatland extent interact in determining MeHg concentrations in lakes and streams and ii) Examining how microbial and photochemical processes may influence MeHg concentrations in small, organic-rich lakes. We anticipated that higher MeHg concentrations would covary with a greater extent of peatlands and occur within the rapidly thawing discontinuous permafrost regions. In northern freshwaters, reduced photodemethylation is predicted to occur with permafrost thaw and the associated release of DOM (Chételat et al., 2022). Our investigation of microbial driven methylation was exploratory since connections between *hgcA* gene abundance and MeHg concentrations remain unclear (Christensen et al., 2019). Our study will thus provide knowledge to help us understand future MeHg concentrations and export from northern peatland-rich catchments.

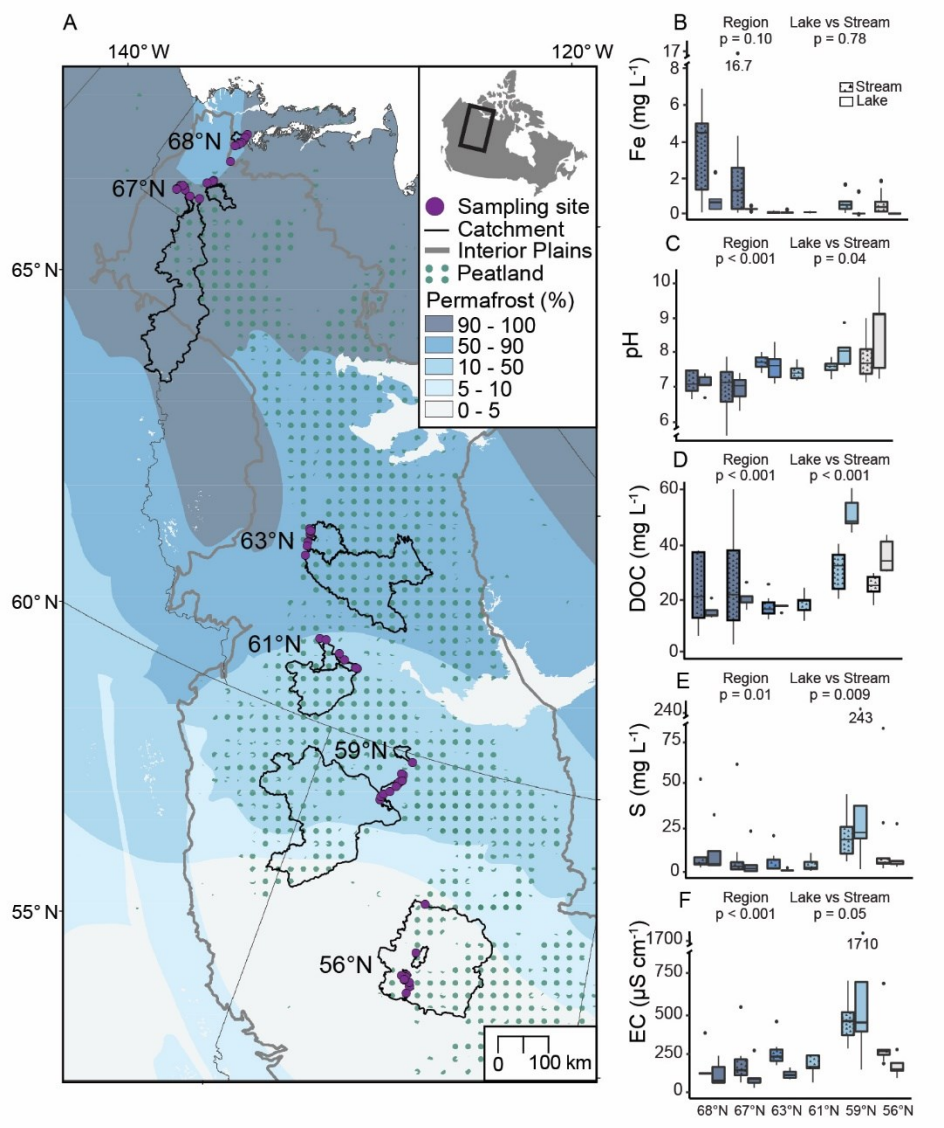

Figure 2.1. Study region and water chemistry characteristics. A) Interior Plains of western Canada with the sampled lakes and streams locations within six regions along the transect, permafrost extent (Brown, Ferrians, Melnikov, et al., 2002), peatland cover >20% (Hugelius et al., 2020), and the outlines of the sampled catchments. The supplemental document contains satellite imagery, hydrographs of major rivers, and catchment flow paths of the study regions (Figure A.2.1). B)–F) Box plots of the median, first, and third quartiles, whiskers of 1.5 times the interquartile range, and outliers of B) iron (Fe), C) pH, D) dissolved organic carbon (DOC), E) sulfur (S) concentrations, and F) electrical conductivity (EC); box plots are separated into lake and stream, and lakes were not sampled at 61°N. The *p*-values from testing the variability of waterbody type and region with permutational analysis of variance (perANOVA) are displayed (Table A.2.1).

2.2 Materials and methods

2.2.1 Study area

We sampled 25 lakes and 47 streams within the Interior Plains of northwestern Canada, spanning a 1700 km latitudinal gradient from 55.8°N to 68.9°N (Figure 2.1, Figure A.2.1). The streams ranged in size from headwaters to major rivers (Table 2.1), and the small lakes and streams were nested within larger catchments at several sites (see Figure A.2.1). The study encompassed lands of the Dehcho Dene, Gwich'in, Inuvialuit, Dene Tha', Woodland Cree, Big Stone Cree, and Métis people. The surficial geology is predominantly glacial, and glaciolacustrine sediments (Fulton, 1995), and the catchments contain widespread peatlands (Hugelius et al., 2020; Figure 2.1). The sampling locations were clustered in six regions (Table 2.1) where within each region, all sampling sites were <200 km apart (Figure A.2.1). White spruce (*Picea glauca*), balsam poplar (*Populus balsamifera*), balsam fir (*Abies balsamea*), and trembling aspen (*Populus tremuloides*) were the main tree species in upland forests, with deciduous species decreasing with latitude. Peatlands in the study area from 59°N and northward were complexes of permafrost peat plateaus and permafrost-free bogs and fens (Ecosystem Classification Group, 2009; Olefeldt et al., 2021), and at 56°N complexes of permafrost-free bogs and fens, either non-treed or containing sparse canopies of black spruce (*Picea mariana*), and tamarack (*Larix laricina*) (Olefeldt et al., 2014). Small (area < 0.1 km^2) to midsize (<10 km^2) organic-rich lakes are a common landscape feature of the catchments (Olefeldt et al., 2021). The regional climate is cool and sub-humid, with mean annual air temperature (MAAT) ranging from 1.4°C in the southernmost sites to -9.1°C in the northernmost sites (Table 2.1; Fick & Hijmans, 2017).

Table 2.1. Characteristics of the stream and lake catchments. Mean average annual air temperature (MAAT) (Fick & Hijmans, 2017), lake and catchment areas, and peatland extent within each catchment. Peatland extent was approximated (Olefeldt et al., 2014) by the proportion of the catchment with slope (Natural Resources Canada, 2013) less than 1° with waterbodies (Natural Resources Canada, 2022) masked.

Region	Permafrost Extent	MAAT (°C)	Type	*n*	Lake Area (km^2)		Catchment Area (km^2)		Peatland (%)	
					Range	Median	Range	Median	Range	Median
68°N	Continuous	-9.1	Lake	5	0.007–0.74	0.06	0.25–13	3.5	5.9–44	17
			Stream	5	-	-	7.2–320	28	5.2–34	16
67°N	Continuous	-7.2	Lake	5	0.008–0.07	0.02	0.12–0.15	0.34	46–77	51
			Stream	10	-	-	3.0–22,000	52	22–78	49
63°N	Discontinuous	-5	Lake	5	0.006–0.13	0.04	0.09–0.42	0.34	43–70	52
			Stream	8	-	-	0.14–21,000	41	11–81	42
61°N	Sporadic	-2.2	Stream	7	-	-	1.0–9,000	113	51–83	70
59°N	Sporadic	-1.1	Lake	5	0.001–0.09	0.02	0.20–4.0	0.54	42–77	65
			Stream	8	-	-	8.9–37,000	105	34–86	81
56°N	Absent	1.4	Lake	5	0.003–0.11	0.03	0.05–1.7	0.19	31–95	77
			Stream	9	-	-	16–31,000	42	46–84	70

Catchment boundaries and area (Table 2.1) were determined with the hydrology toolset on ArcGIS 10.3 using the Canadian Digital Elevation Model (CDEM; Natural Resources Canada, 2013), with manual adjustments required in some regions of low relief using the National Hydro Network (Natural Resources Canada, 2022) as reference. The proportion of lowland in each catchment (Table 2.1) was determined using the slope tool on ArcGIS 10.3. After masking waterbodies from the National Hydro Network (Natural Resources Canada, 2022), areas with slopes <1° were classified as lowland and presumed proportional to peatland cover (Olefeldt et al., 2014). Although lowlands are dominated by organic peatland soils in the region (Ecosystem Classification Group, 2009), some small, disconnected peatlands or uplands may have been misclassified due to the 30×30 m resolution of the CDEM.

2.2.2 Water sampling and analysis

Sampling was conducted in July 2019 to capture representative mid-summer conditions, avoiding the peak and low flows (Figure A.2.1). We collected unfiltered and filtered water samples from

the edges of lakes and streams for total Hg (THg) (2×125 mL) and MeHg (2×250 mL) analysis following clean hands-dirty hands protocol (St. Louis et al., 1994). All samples were collected in certified pre-cleaned glass amber bottles (Environmental Supply Company, Inc., US). Filtered THg and MeHg samples were obtained by filtering one of the two samples through pre-cleaned Nalgene 0.45 µm cellulose nitrate filter towers within 24 hours. The filtrate was then transferred to a new bottle. All THg and MeHg samples were preserved with 0.2% and 0.4% trace-metal grade HCl, respectively.

Hg samples were analyzed in the Canadian Association for Laboratory Accreditation-certified Biogeochemical Analytical Service Laboratory (University of Alberta). Water samples were analyzed for THg concentrations on a Tekran 2600 Mercury Analyzer. Water samples were analyzed for MeHg using isotope dilution, distillation, and analyses on a Tekran 2700 Methylmercury Analyzer coupled to an Agilent 7900 inductively coupled plasma-mass spectrometer (ICP-MS).

We measured the physical parameters, nutrients, major ions, and DOM characteristics of each site. Electrical conductivity (EC), pH, and water temperature were measured on-site with calibrated PT1 and PT2 Ultrapens (Myron L Company, US). We collected two additional filtered (0.7 µm Grade GF/F, Whatman) 60 mL water samples in acid-washed amber glass bottles, one of which was preserved with 0.6 mL of 2M HCl for dissolved organic carbon (DOC) and metal analysis while the other sample remained non-acidified for nutrient analysis, DOM absorbance, and fluorescence spectroscopy. All water samples were kept cool in transit to the laboratory and remained refrigerated until analysis.

The Natural Resources Analytical Laboratory (University of Alberta) analyzed samples for DOC, metals, and nutrients. A TOC-L combustion analyzer with a TNM-L module (Shimadzu, Japan) measured DOC and total dissolved nitrogen (TDN) concentrations. Colorimetry (Thermo Gallery Plus Beermaster Autoanalyzer, Thermo Fisher Scientific, US) determined concentrations of chloride (Cl), nitrate (NO_3-N), nitrite (NO_2-N), ammonium (NH_4-N), phosphate (PO_4-P), and sulfate (SO_4^{-2}-S). Concentrations of sodium (Na), potassium (K), calcium (Ca), manganese (Mn), iron (Fe), copper (Cu), zinc (Zn), magnesium (Mg), phosphorus (P), and sulfur (S) were measured

by inductively coupled plasma optical emission spectroscopy (ICP-OES, iCAP6300 Duo, Thermo Fisher Scientific, US).

We assessed the aromaticity of the DOM using the specific ultraviolet absorbance ($SUVA_{254}$) at 254 nm, where $SUVA_{254}$ values increase with DOM aromaticity (Weishaar et al., 2003). The absorbance of DOM was measured from 200 to 700 nm (UV-1280, UV-VIS Spectrophotometer, Shimadzu Corporation, Japan) and corrected with Milli-Q water blanks. We calculated $SUVA_{254}$ after correcting decadal absorbance at 254 nm (A_{254}, cm^{-1}) for interference by Fe (Weishaar et al., 2003). We used an Aqualog fluorometer (Horiba Scientific, US) to measure DOM fluorescence emission-excitation matrix spectra (EEMs). Detailed methods of DOM analysis, including parallel factor analysis (PARAFAC), quality control, and quality assurance (QA/QC), are in Appendix A.2. All data are available online in the open data platform Mackenzie DataStream (University of Alberta, 2022).

2.2.3 Photodemethylation model

We modeled specific UV photodemethylation rates (UV PD, ng L^{-1} d^{-1}) in the study lakes using an experimentally derived first-rate constant of MeHg photodemethylation (k_{pd}, m^2 E^{-1}), a universal constant even though MeHg concentration and light intensity varied among sites (Lehnherr & St. Louis, 2009). We used Equation 1 to calculate the UV-A and UV-B MeHg photodemethylation rates individually, then summed the values to calculate an overall UV photodemethylation rate. The photon flux density (PFD, mol γ m^2 d^{-1}; mol photon (γ) equivalent to E) per 5 cm interval depths (z) was calculated from Equation 2. The UV-A and UV-B light attenuation coefficients (k) were derived from measured DOC concentrations (Donahue et al., 2003; Scully & Lean, 1994). The surface PFD (PFD_0) values used were representative of the latitude and time of year. PFD_0 values from 56°N region were from FluxNet Canada (FLUXNET Canada, 2016); values from 59°N are our unpublished data; values from 61°N and 68°N are unpublished data from G. Gosselin and O. Sonnentag; data from 67°N are from ERA5 (Copernicus Climate Change Service, 2019) where we converted downward solar radiation to PFD based on observational relationships provided by G. Gosselin and O. Sonnentag.

$$\text{UV PD rate} = k_{pd} \times \text{MeHg} \times \text{PFD}. \quad (1)$$

$$PFD_z = PFD_0 \times e^{-kz}. \quad (2)$$

Depth-integrated rates were calculated as Σ UV PD rates over the specified water column depth. As an exercise to estimate the areal flux of UV photodemethylation (ng m^{-2} d^{-1}) (Lehnherr & St. Louis, 2009), we calculated the depth-specific UV PD rates × the volume of water per *z*; these values were summed from the surface to the depth equivalent to 1% of the surface rate to prevent inflation from deep and/or colored lakes and normalized by the lake area.

2.2.4 Gene abundance and diversity of *hgcA* and *merAB* in lake sediments

Near the edge of 20 lakes (excluding 68°N sites), we collected the top 10 cm of sediment using a sterile trowel and sterile gloved hands for microbial analyses at three locations. Samples from the three locations per lake were combined, then mixed and stored in sterile Whirl-Paks (Nasco, US) with the air pressed out to minimize oxygen exposure at 2–8°C until transferred to a -20°C freezer within 5 d and subsequently to a -80°C freezer within 14 d.

DNA was extracted in duplicate from 0.65 g of homogenized wet sediments using the DNeasy PowerSoil kit (QIAGEN N.V., Germany). Duplicates were pooled and concentrated by ethanol precipitation (3× volume) with sodium acetate (1/10 volume) and resuspended in Tris-Cl (10 mM, pH 8.5). A nuclease-free water-only negative control and a positive control consisting of a ZymoBIOMICS Microbial Community Standard (Zymo Research Corporation, US) were also extracted in duplicate and pooled.

We prepared sequencing libraries from 250 ng DNA per sample. DNA extracted from the sediment of one lake in the 63°N region (W1) was of insufficient quantity to perform further analysis. The negative control yielded insufficient DNA for library preparation. Libraries were prepared with the NEBNext® Ultra™ II FS DNA Library Prep Kit for Illumina (New England Biolabs, US). All nucleic acid concentrations and libraries were quantified using a Qubit dsDNA High Sensitivity Assay Kit (ThermoFisher, US) on a Qubit 3.0 Fluorometer (ThermoFisher, US). Library quality was confirmed on a Bioanalyzer HS DNA chip (Agilent, US) before pooling at equimolar concentrations into a single multiplexed sample. Samples were sequenced on a NextSeq 500 using a High Output Kit v2 (300 cycles, paired-end) (Illumina, Inc, US). Negative and positive controls revealed no significant contamination. Sequencing yielded an average of 37 (standard error 2.25;

SE) million reads per sample, after quality filtering using Fastp (Chen et al., 2018), with a percentage of 92 (SE 0.001) and 87 (SE 0.002) of bases, respectively. Microbial data are available in the European Nucleotide Archive at EMBL-EBI with access number PRJEB36558.

We used the *hgcA* gene as a genetic marker for microbial Hg^{II} methylation and *merA* and *merB* as genetic markers for Hg^{II} reduction and MeHg demethylation. We assessed gene abundance using GraftM, identifying gene clades (i.e., representative monophyletic groups) in shotgun metagenomics data and assigning taxonomic classifications based on phylogenetic placements into gene trees built from reference sequences (Boyd et al., 2018). GraftM gene-specific packages were created using curated reference sequences of *hgcA* (*n*=243; Gionfriddo et al., 2020), *merA* (*n*=219; Boyd & Barkay, 2012), and *merB* (*n*=359; Mistry et al., 2021). We used the microbial housekeeping gene 16S rRNA to normalize *hgcA, merA,* and *merB* gene abundances, providing an estimated proportion of Hg^{II} methylators, Hg^{II}-reducing, and MeHg demethylating microbes, respectively, within each site. 16S rRNA sequences were identified using the default gene package provided by GraftM. We expected the ratios of *hgcA, merA*, and *merB* relative to 16S to represent the gene's proportional presence in the microbial communities.

2.2.5 Statistical methods

We conducted analyses in RStudio® utilizing R version 3.6.1 (R Core Team, 2022). We used permutational analysis of variance (perANOVA) tests to examine the variability among waterbody type and region for MeHg concentrations, THg concentrations, and MeHg to THg ratio (hereafter %MeHg, a proxy for net MeHg formation; Bravo & Cosio, 2020), including an interaction parameter, with *lmPerm* (Wheeler & Torchiano, 2016). We used the same method to examine variability in additional water chemistry parameters among waterbody type and region, including concentrations of DOC, Fe, S, pH, and EC. The interaction parameter tested the hypothesis that the region would influence lake or stream characteristics.

Linear regressions were used to estimate the strength and direction of the relationship between water chemistry variables and MeHg, exploring water chemistry parameters that have been previously shown to covary with MeHg, including DOC concentrations and composition, pH, Fe, THg, and S (Bravo & Cosio, 2020; Lavoie et al., 2019). Data were log-transformed if Shapiro-Wilk tests indicated non-normality in the distribution of the residuals. Path analysis was used to

examine potential direct (DOC concentrations) and indirect drivers (permafrost region, peatland coverage, catchment size) influencing MeHg concentrations in lakes and streams with the *piecewiseSEM* package (Lefcheck, 2016; St. Pierre et al., 2019); further details are described in Section A.2.3.

To compare *hgcA* and *merAB* gene diversity across the transect, we estimated Aitchison distance matrices between each pairwise combination of sites for the abundances of the clades with DEICODE (Bolyen et al., 2019; Martino et al., 2019) and tested if gene proportions and diversity varied across permafrost extent using perANOVA and permutational multivariate analysis of variance (perMANOVA), respectively.

2.3 Results and discussion

2.3.1 Variability of THg and MeHg in lakes and streams

Lakes and streams had high variability across the transect in both filtered and unfiltered THg and MeHg concentrations, with MeHg concentrations varying by more than two orders of magnitude (Figure 2.2). MeHg concentrations and %MeHg were higher in streams than lakes ($p<0.05$, n streams=47, lakes=25), while differences were absent for THg concentrations ($p>0.05$). Unfiltered MeHg concentrations (0.47±0.77 ng MeHg L^{-1} in streams, 0.19±0.23 ng MeHg L^{-1} in lakes, mean±1SD) were higher than those typically measured in Arctic water bodies (≤0.1 ng MeHg L^{-1}; Chételat et al., 2015) and exceeded Canadian water quality guidelines at one stream in the 67°N region (4.81 ng MeHg L^{-1}, Figure 2.2B; Canadian Council of Ministers of the Environment, 2003). Most of the MeHg and THg was in the dissolved form, which has the potential to be more bioavailable than particle-bound forms (Le Faucheur et al., 2014), with 86±13% of MeHg and 81±18% of THg in dissolved form in streams and 70±18% of MeHg and 75±21% of THg in lakes. The %MeHg (18±18% in streams, 10±11% in lakes, unfiltered) was also relatively high throughout the transect (Figure 2.2B, C) compared to European streams (Bravo, Kothawala, et al., 2018) and eastern Arctic lakes (Richardson et al., 2021) and of similar magnitude to productive Arctic thaw ponds (MacMillan et al., 2015). The high MeHg concentrations and %MeHg observed in this study are consistent with the numerous fish consumption advisories in the Interior Plains (Evans et al., 2005).

Both filtered and unfiltered concentrations of THg, MeHg, and %MeHg varied among the regions along the latitudinal transect (p<0.05), but only THg concentrations had a consistent latitudinal trend with the highest values in the northernmost continuous permafrost zone (Figure 2.2). The northernmost region (68°N) had especially high proportions of particulate THg, potentially connected to distinct landscape characteristics, including less widespread peatlands and thinner organic soils (Figure 2.1A; Zoltai & Tarnocai, 1974). This study's latitudinal trend in THg contrasts those found in other regions. For example, in streams in Russia and lakes in the eastern Canadian Arctic, the highest THg concentrations were found in the sporadic and discontinuous permafrost zones, respectively (Lim et al., 2019; Richardson et al., 2021). The same lakes studied here displayed a strong latitudinal pattern of increasing methane emissions and an increasing carbon dioxide sink with decreasing latitude and permafrost extent (Kuhn, Thompson, et al., 2021), in contrast to our findings of no direct association between climate or permafrost conditions and differences in MeHg and %MeHg among regions. Further assessment of regional catchment characteristics and environmental conditions were needed to understand the variability across the transect, e.g., the low MeHg concentrations and %MeHg in the 63°N region.

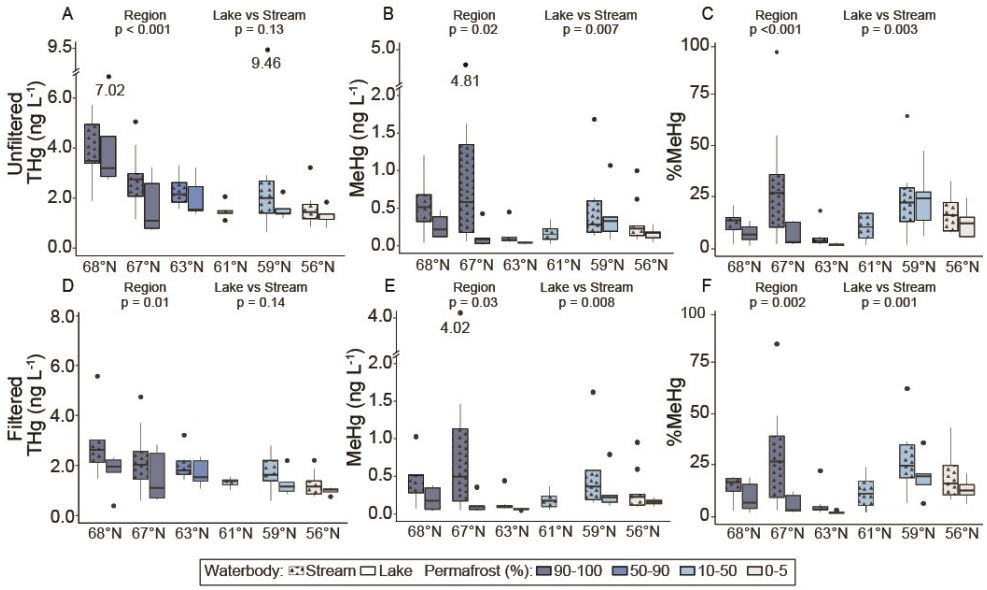

Figure 2.2. Total mercury (THg) and methylmercury (MeHg) concentrations in surface waters vary amongst regions across the permafrost transect. Box plots of the median, first, and third quartiles, whiskers of 1.5 times the interquartile range, and outliers of A) unfiltered THg, B) unfiltered MeHg, and C) proportion of THg as MeHg across the study regions (%MeHg) as a proxy for net methylation, D) filtered THg, E) filtered MeHg, F) %MeHg of filtered THg as MeHg; box plots are separated into lake and stream, and lakes were not sampled at 61°N. The p-values from testing the variability of waterbody type and region with permutational analysis of variance (perANOVA) are displayed above each boxplot, and Table A.2.2 has further details from the perANOVAs.

2.3.2 Drivers of MeHg and %MeHg in lakes and streams

The regions sampled across the continental permafrost transect had distinct water chemistry characteristics. Some parameters exhibited latitudinal trends, with Fe concentrations increasing and pH decreasing towards northern sites (Figure 2.1B–C). Other parameters were regionally distinct, such as concentrations of DOC, S, and EC (Figure 2.1D–F). Widespread permafrost was generally associated with low EC and pH, likely indicating low hydrological connectivity with deeper groundwater sources (Frey & McClelland, 2009). Regions with lower permafrost coverage had more variable concentrations of DOC, ions, and nutrients, suggesting that land cover, surficial geology, and topography of the sampled regions influenced the connectivity to groundwater discharge and groundwater-fed fen peatlands (Frey & McClelland, 2009; Gordon et al., 2016; Kuhn, Thompson, et al., 2021). Lakes and streams at 59°N, a region with low permafrost extent, had particularly high indicators of groundwater connectivity, i.e., EC and S (Frey & McClelland, 2009; Kuhn, Thompson, et al., 2021). There was also a consistent trend of higher Fe concentrations, pH, and EC in streams than in lakes (Figure 2.1).

Relationships varied between MeHg concentrations and water chemistry parameters among streams and lakes (Figure 2.3). Concentrations of MeHg increased with DOC concentrations and A_{254} in both streams and lakes, but streams had higher MeHg concentrations than lakes at similar levels of DOC and A_{254} (Figure 2.3A–B). A_{254} was a better predictor of MeHg concentrations for streams based on R^2 compared to DOC and $SUVA_{254}$ (Figure 2.3A–B; Figure A.2.2), suggesting higher absolute quantities of aromatic carbon may drive MeHg transport vs. higher concentrations of the total DOC pool or higher percent aromaticity. Slopes of THg and MeHg against DOC have been explored in many aquatic environments, and we found differences in the strength of relationships among lakes and streams using untransformed data (THg-DOC: lake slope=-0.038 ng mg^{-1}, R^2=0.13, p=0.04; stream slope=0.040 ng mg^{-1}, R^2=0.07, p=0.05; MeHg-DOC: lake slope=0.006 ng mg^{-1}, R^2=0.15, p=0.03; stream slope=0.050 ng mg^{-1}, R^2=0.51, p<0.001). DOC concentrations explained ≤15% of the variability in lake MeHg concentrations and lake/stream THg concentrations, while stream MeHg-DOC had the strongest relationship. These results suggest a decoupling of THg and organic matter input in lakes and a stronger linkage between MeHg and DOC concentrations in streams, as has been observed in other wetland-influenced catchments (Branfireun et al., 2020; Lavoie et al., 2019).

Stream and lake DOM also differed in their chemical composition. Stream DOM was relatively more aromatic and dominated by humic acids (associating with higher humification index, $SUVA_{254}$, and PARAFAC Component 2; see Figure A.2.3, Figure A.2.4, Table A.2.3), which can facilitate binding with MeHg (Klapstein & O'Driscoll, 2018) and reduce MeHg bioavailability (Tsui & Finlay, 2011). In contrast, lake DOM had lower aromaticity and was relatively more influenced by amino acids (associating with higher biological index and PARAFAC Component 4; see Figure A.2.3, Figure A.2.4, Table A.2.3), which can stimulate MeHg production in lake sediments (Klapstein & O'Driscoll, 2018). Therefore, DOM in streams was likely associated with terrestrially derived sources, while lake DOM may have been relatively more influenced by autochthonous, algal DOM production, littoral vegetation exudates, or selective photochemical degradation of humic DOM (Kellerman et al., 2015; Tank et al., 2011), as has been observed in other Canadian ecozones (Aukes et al., 2021). The dominance of terrestrial sources in streams aligns with findings from Hg stable isotopes in a headwater peatland catchment, where aqueous Hg was primarily derived from dry deposition on vegetation (Woerndle et al., 2018).

Lake and stream water chemistry indicated peatlands as primary sources of DOM and MeHg. Concentrations of MeHg in streams increased with lower pH and higher concentrations of Fe and THg (Figure 2.3C–E), suggesting that MeHg was delivered to streams in runoff generated from peatlands with acidic and reducing conditions (Bourbonniere, 2009; St. Louis et al., 1994). For lakes, we found that MeHg concentrations increased with groundwater indicators (i.e., EC, Cl, K, Na, S, SO_4^{-2}-S; Figure A.2.5, Figure 2.3F; Frey & McClelland, 2009; Kuhn et al., 2021). These relationships may point to groundwater-rich lakes as high *in situ* MeHg production sites with the exchange of MeHg from sediment to the water column, potentially due to the supply of SO_4^{-2}-S for sulfate-reducing bacteria (Bravo & Cosio, 2020). However, we also found that higher concentrations of SO_4^{-2}-S and MeHg were associated with a lower proportional abundance of the *hgcA* (Hg^{II} methylating) gene in lake sediments (Figure A.2.5, Figure 2.3H). Although the relationship between the abundance of the *hgcA* gene and *in situ* biological methylation is unclear, these results suggest that its potential activity may have been decreased at higher MeHg and SO_4^{-2}-S concentrations. As groundwater-rich fens are abundant in the Interior Plains (Ecosystem Classification Group, 2009; Quinton et al., 2009), they are potentially important external MeHg sources for these lakes, as fens readily convey water in their channels (Quinton et al., 2009) and have been previously identified as Hg^{II} methylation hotspots in boreal sites (Fahnestock et al.,

2019; Gordon et al., 2016; Poulin et al., 2019; Tarbier et al., 2021). Lakes that receive high DOM inputs from their surrounding catchment, as is typical for peatland lakes in the Interior Plains (Olefeldt, Turetsky, et al., 2013; Pugh et al., 2021), have also previously been shown to have high MeHg concentrations but low rates of *in situ* methylation (Branfireun et al., 2020; Bravo et al., 2017).

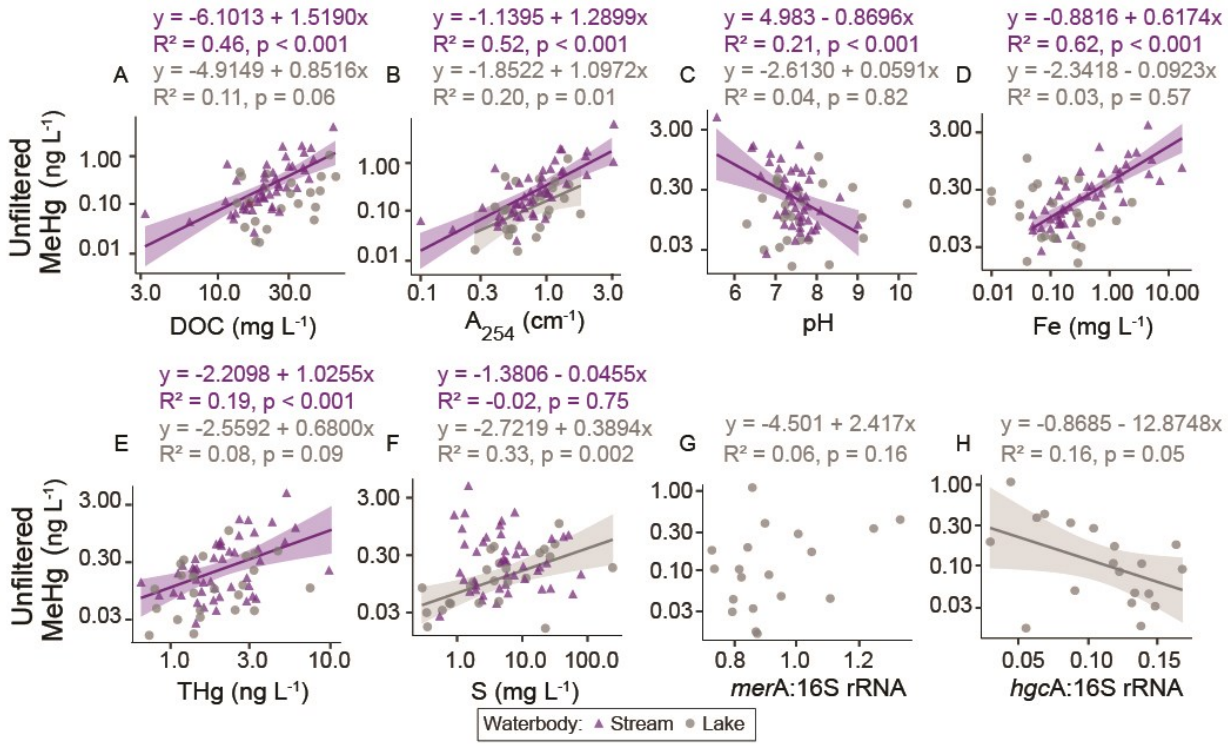

Figure 2.3. Relationships between unfiltered methylmercury (MeHg) concentrations and chemical and microbial parameters of surface waters. Regression of unfiltered MeHg concentrations of surface waters separated into lakes (n=25) and streams (n=47) with A) dissolved organic carbon (DOC) concentrations, B) absorbance at 254 nm (A_{254}), C) pH, concentrations of D) iron (Fe), E) unfiltered total mercury (THg), F) sulfur (S), and genes in lake sediments (n=19), normalized by 16S rRNA, G) *merA*:16S rRNA for Hg^{II} reduction, and H) *hgcA*:16S rRNA for Hg^{II} methylation. The regression of MeHg with *mer*B:16S rRNA for MeHg demethylation is in Figure A.2.6. Model formula, adjusted R^2 values, and p-values of the regressions are displayed, a 95% confidence interval surrounds the best-fit line if statistically significant, and the axes are on a log scale except for the x-axis of C), G), and H).

Lake and stream %MeHg increased with DOC concentrations. Stream DOC concentrations were higher in smaller catchments with greater peatland extent, whereas lake DOC concentrations were higher in warmer climates with less permafrost (Figure 2.4). The link between DOC concentrations and %MeHg is not universal, e.g., it was not observed in European streams (Bravo, Kothawala, et al., 2018), but has previously been observed in boreal regions, e.g., among lakes within the Mackenzie River Basin (Evans et al., 2005). Corresponding patterns of increasing stream DOC

concentrations with greater catchment peatland cover and smaller catchment size have been documented in other boreal regions (Kothawala et al., 2014; Mattsson et al., 2005). The lack of a relationship between DOC and catchment area and peatland cover for lakes in this study may be due to the generally smaller and less variable catchment sizes of lakes (0.05–13 km^2) compared to streams (0.14–37,000 km^2; Table 2.1), as well as uncertainty with our method to assess peatland cover in small lake catchments as using the national digital elevation model may not capture the extent of smaller wetlands or uplands within the landscape because of their relatively fine-scale spatial resolution. Lower permafrost extent has been connected with higher DOC concentrations in other boreal regions (Frey & Smith, 2005) and within the study region (Olefeldt et al., 2014). Increased DOC concentrations are also projected in peatland-rich catchments as permafrost thaw advances and hydrological connectivity increases (Frey & Smith, 2005; Hugelius et al., 2020).

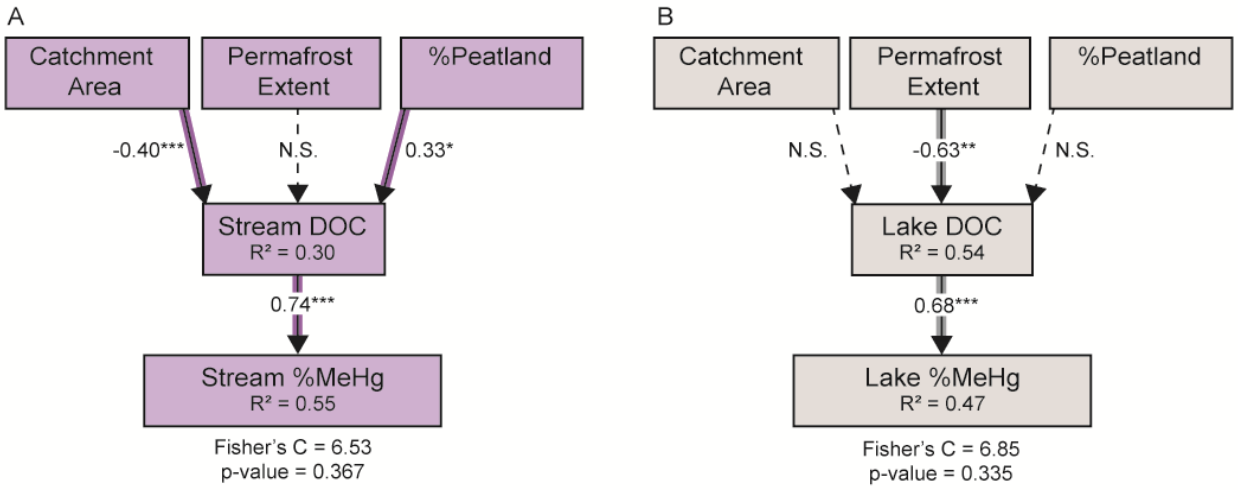

Figure 2.4. Association of the proportion of THg as MeHg (%MeHg) as a proxy for net methylation with catchment characteristics and dissolved organic carbon (DOC). Path analysis representing connections between unfiltered %MeHg, catchment area, permafrost extent, %peatland (proportion of catchment with slope <1°), and DOC concentrations for A) streams (n=47) and B) lakes (n=25). Numbers beside arrows are standardized path coefficients. A solid and colored arrow indicates a statistically significant relationship, while a dashed arrow with N.S. (non-significant) indicates an insignificant relationship. Asterisks indicate the significance of the relationship (*p<0.05, ** p<0.01, *** p<0.001), and R^2 is the proportion of the variance explained by the model for each response variable. The model fit is indicated with Fisher's C statistic that evaluates Shipley's test of directed separation, and p>0.05 shows no missing relationships amongst unconnected variables; the p-value of the stream model was 0.367 and was 0.335 for the lake model (Lefcheck, 2016; Shipley, 2000).

2.3.3 Gene abundance and diversity of *hgcA* and *merAB* in lake sediments

Peatland lakes generally had a greater abundance of microbial genes associated with reducing rather than methylating Hg^{II}. The microbial communities in lake sediments had a ~ nine-fold

greater abundance of gene sequences for Hg^{II} reduction than Hg^{II} methylation, based on *merA* and *hgcA* genes, respectively (Figure 2.5A). These results may be unsurprising given that Hg^{II} methylators are relatively low in abundance in nature. When present, methylators are expected to constitute <5% of the bulk microbial community (Christakis et al., 2021; Christensen et al., 2019; Podar et al., 2015). The *merA* gene is more ubiquitous and was found in ~ 8% of microbial genomes in public databases (Christakis et al., 2021). By contrast, the gene for MeHg demethylation, *merB*, had the lowest abundance compared to *hgcA* and *merA* (Figure 2.5A). The proportion of *merB* in microbial communities is expected to be lower than for *merA*, as it is present in only 2% of genomes in public databases (Christakis et al., 2021). Furthermore, gene duplication could contribute to greater relative proportions of *merA* than *merB* (Christakis et al., 2021). Nevertheless, our data suggest that detoxification potentially occurs via *merA* over the *merB* pathway. With permafrost thaw, emission of Hg^0 may be a dominant pathway of Hg mobilization from permafrost regions (Schaefer et al., 2020), and direct measurements of thermokarst ponds in Tibet suggest a 15% increase in annual Hg^0 emissions in the past decades (Ci et al., 2020). The abundances of *merA* demonstrate that microbial communities in lake sediments have the potential to cause aquatic Hg losses through Hg^0 emissions.

The proportions and diversity of *hgcA, merA*, and *merB* did not vary across the transect (Table A.2.4 and Table A.2.5, respectively). Although we observed a negative relationship between MeHg concentrations and *hgcA* gene abundances (Figure 2.3H), we found no significant relationships between MeHg concentrations and *merA* proportions (Figure 2.5A, Figure 2.3G) or *merB* proportions (Figure A.2.6B). One explanation for this result is that gene abundance may not always translate into activity. Still, the decreasing *hgcA* gene abundance at high MeHg concentrations may be speculatively connected to an inhibitive effect from high concentrations of externally delivered SO_4^{-2}-S alongside MeHg (Figure A.2.5), as high concentrations of SO_4^{-2} have been observed to limit methylation in lakes (Gilmour et al., 1992; Shao et al., 2012). However, the association between MeHg and SO_4^{-2}-S concentrations in lake surface waters and the proportion of *hgcA* in sediments would need confirmation through gene activity analyses with additional potential influence from Hg^{II} bioavailability and environmental conditions (Bravo & Cosio, 2020).

We identified 69, 83, and 48 clades with *hgcA, merA*, and *mer*B, respectively, known to taxonomic reference sequences. These included phyla of previously known Hg^{II} methylators, Hg^{II}-reducing,

and MeHg demethylating microbes (Christakis et al., 2021; Christensen et al., 2019; McDaniel et al., 2020). Many abundant sequences were unclassified or classified only at the domain level (Figure 2.5B–D), indicating that the communities studied here may harbor novel representatives of Hg-cycling microbes. When comparing water chemistry parameters against clades in lake sediments, we found that the abundance of some *hgcA*-containing classes was lower in lakes with higher ion concentrations (Figure A.2.7A), potentially linked to external MeHg contributions discussed above. However, an increased abundance of putative methylators within the phylum Acidobacteriota (Bravo, Peura, et al., 2018; McDaniel et al., 2020; Xu et al., 2019) was strongly related to MeHg concentrations (R^2=0.59; p<0.001), suggesting a potential contribution by some resident bacteria to levels of MeHg. For *merA*-containing classes, abundance tended to increase with concentrations of MeHg and decrease with Fe concentrations (Figure A.2.7B). These relationships could reflect a detoxification mechanism involving Hg^{II} reduction from abiotically demethylated MeHg (Barkay & Gu, 2021; Christakis et al., 2021) and may explain the predominance of *merA* compared to *merB* genes (Figure 2.5). Still, the abundance of several classes with *merB* increased with concentrations of MeHg (Figure A.2.7C), suggesting resident bacteria may be involved in demethylation to some degree. Tracking the activity of Hg-cycling microbes in future studies may reveal under-explored mechanisms of aquatic Hg losses in the Interior Plains and would elucidate the importance of biotic versus abiotic drivers.

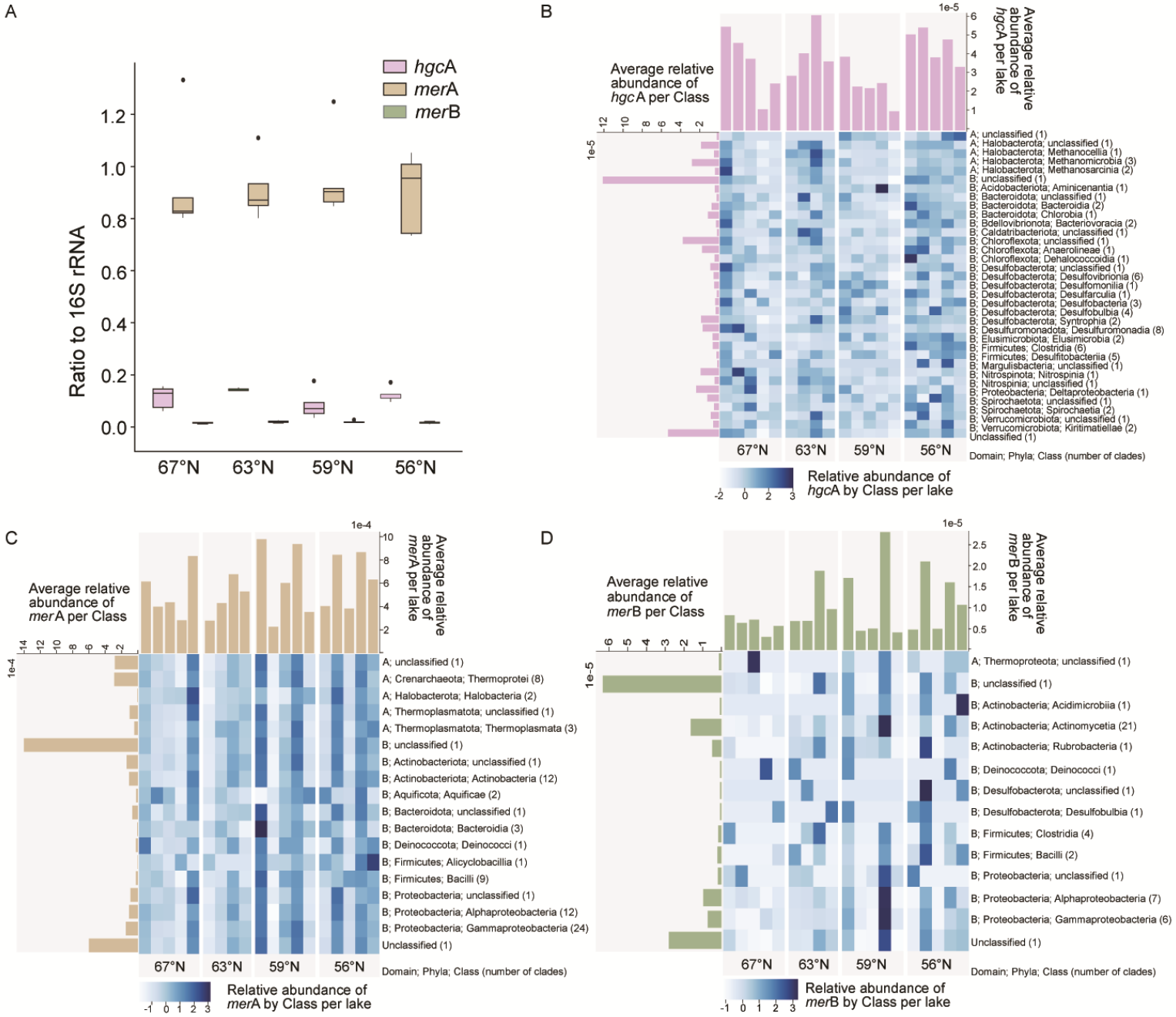

Figure 2.5. Relative abundances and distribution among identified clades of Hg^{II} methylating (*hgcA*), Hg^{II} reducing (*merA*), and MeHg demethylating (*merB*) genes in microbial communities of 19 lake sediments along a permafrost transect on the Interior Plains, western Canada. A) Box plot of the median, first and third quartiles, and outliers for ratios of Hg-cycling genes (*hgcA*, *merA*, *merB*) in lake sediments to 16S rRNA across the permafrost transect. The heatmaps display the z-score normalized relative abundance of B) *hgcA*, C) *merA*, and D) *merB* genes by clade in lake sediments across the permafrost transect. Upper bar plots represent the average relative abundance of the gene in a given sample, and regions are indicated by breaks in grey shading. The left bar plots represent the average relative abundance of the gene by clade. The domain is identified as A for archaea and B for bacteria. The relative abundance values represented in plots B)–D) indicate the gene count per number of reads.

2.3.4 Photodemethylation in the water column of lakes

By modeling the rate of UV MeHg photodemethylation based on a representative photon flux density for each site and measured DOC and MeHg concentrations (Lehnherr & St. Louis, 2009), we found that the maximum depth of photodemethylation increased towards northern sites in line with lower DOC concentrations (Figure 2.6). The depth-specific photodemethylation rates approached zero at 0.3–0.7 m in the continuous permafrost zone at 68°N in comparison to 0.05–0.2 m at the two southern regions of 56°N and 59°N. Modeled areal fluxes of UV photodemethylation ranged from 0.29 to 9.23 ng MeHg m^{-2} d^{-1} (Figure 2.6D), with the highest rates in the northernmost region. Modeled daily areal UV photodemethylation fluxes were comparable to lakes in boreal Ontario (1–20 ng MeHg m^{-2} d^{-1}; (Lehnherr & St. Louis, 2009; Sellers et al., 2001) Alaska (5–13 ng MeHg m^{-2} d^{-1}; Hammerschmidt et al., 2006) and Nunavut (2–33 ng MeHg m^{-2} d^{-1}; Lehnherr, St. Louis, Emmerton, et al., 2012). While a mass balance would be required to contextualize areal fluxes of photodemethylation in the lakes, the daily rates represent an average of 1.0±0.5% of the total MeHg in these lakes (concentration×volume); thus, photodemethylation is likely an important MeHg sink in the studied lakes. If climate change and permafrost thaw lead to increased DOC concentrations in surface waters as predicted (Frey & Smith, 2005; Hugelius et al., 2020; Olefeldt et al., 2014), photodemethylation rates may decrease and thus reduce the MeHg sink capacity of lakes in the continuous permafrost zone (Klapstein et al., 2018; Lehnherr & St. Louis, 2009).

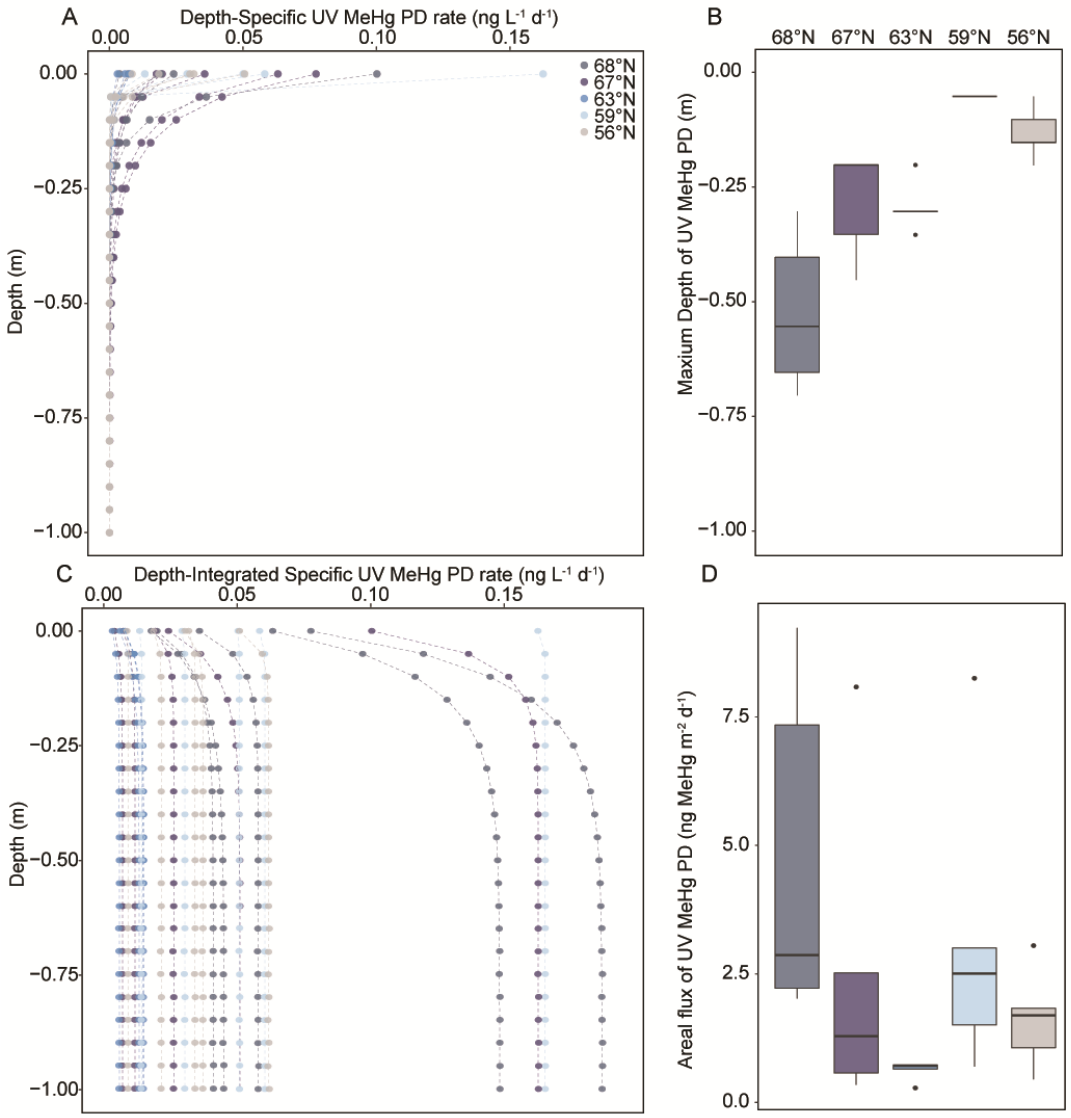

Figure 2.6. Modeled ultraviolet methylmercury photodemethylation (UV MeHg PD) in the water column of 25 lakes on a permafrost transect. A) Depth-specific rates per 5 cm of UV-A + UV-B light-mediated MeHg PD (Lehnherr & St. Louis, 2009). B) Box plot of the median, first and third quartiles, and outliers of maximum depth of UV MeHg PD across the study regions; maximum depth was defined at the depth where PD rate approached the asymptote of zero. Lakes were not sampled at 61°N. C) Depth-integrated UV MeHg PD rates, calculated to 1 m depth by summing depth-specific rates to the specified depth. D) Box plot of the median, first and third quartiles, and outliers of maximum depth of areal UV MeHg PD flux across the study regions; areal fluxes were calculated by summing daily flux per 5 cm "slice" of lake water column to the depth equivalent to 1% of surface rate (Lehnherr & St. Louis, 2009).

2.3.5 MeHg concentrations under current and future climates

Peatlands were indicated to be the dominant sources of MeHg to streams across the transect, as stream MeHg concentrations increased with acidic, reduced conditions and humic DOM associated with peatland runoff (Bourbonniere, 2009). The %MeHg in streams also increased with

peatland catchment coverage. Although permafrost thaw and thermokarst expansion in peatlands create local hotspots for MeHg production (Fahnestock et al., 2019; Gordon et al., 2016; Poulin et al., 2019; Tarbier et al., 2021), we did not find elevated MeHg concentrations in streams of the rapidly thawing discontinuous and sporadic permafrost zones. Thermokarst wetlands, however, occupy a minor fraction of peatlands (Gibson et al., 2021) and may not have a detectable influence on downstream MeHg concentrations, and the variability of stream catchment size potentially precluded the detection of a direct permafrost influence. As the export of peatland-derived aromatic DOC is expected to increase with permafrost thaw (Frey & Smith, 2005; Hugelius et al., 2020; Olefeldt et al., 2014), continued research at different spatial and temporal scales is needed to understand the potential for permafrost thaw to increase downstream delivery of MeHg from peatlands.

Small peatland lakes had lower concentrations of MeHg and lower %MeHg than streams at similar concentrations of DOC and A_{254}; alongside the pattern of %MeHg decreasing with increased stream catchment size, the abundant peatland lakes in the Interior Plains may act as MeHg sinks. Further work examining methylation and demethylation rates may confirm whether these lakes act as landscape-scale sinks of MeHg. Potential drivers of MeHg degradation in lakes include biotic demethylation (Boyd & Barkay, 2012) and UV photodemethylation (Lehnherr, St. Louis, Emmerton, et al., 2012). In this study, we modeled areal fluxes of UV photodemethylation ranging up to 9.2 ng MeHg m^{-2} d^{-1}. If climate change and permafrost thaw increase the delivery of both DOM and MeHg from peatlands, our study suggests that this could affect the sink capacity of lakes by decreasing potential UV photodemethylation given the highest modeled rates in the continuous permafrost zone.

This study provides insight into the importance of regional biogeochemical factors that influence MeHg concentrations in lakes and streams of the Interior Plains during the summer period. As our study was based on a synoptic survey during moderate to low flow conditions, it cannot give estimates of annual catchment MeHg yields as concentrations can markedly fluctuate during high-flow periods such as spring freshet (Mitchell et al., 2008c) or summer storms (Coleman Wasik et al., 2015). Still, the summer sampling conditions of this study prevail for the majority of the ice-free season. We show that both terrestrial delivery of MeHg into aquatic ecosystems and solar degradation of MeHg in lakes of the Interior Plains of boreal Canada is likely to be linked to

changes in the delivery and downstream degradation of peatland DOM as permafrost thaws. Post-thaw factors that dictate groundwater dynamics and inputs of DOM, ions, and nutrients into aquatic environments (e.g., land cover shifts, landscape position, and surficial geology; Frey & McClelland, 2009; Gibson et al., 2021; Gordon et al., 2016) will in turn influence MeHg production and downstream delivery. Therefore, continued monitoring of MeHg in surface waters (Figure 2.7) and fish of the Interior Plains and additional work on the mass balance budgets of peatland catchments is recommended to enable the detection of changes associated with permafrost thaw and assess potential impacts on the physical and cultural health of Northern Indigenous communities (Wheatley & Wheatley, 2000).

Figure 2.7. Field team for Chapter 2, sampling lakes near Teetł'it Zheh (Fort McPherson, NWT). Left to right: Andrew Koe (Teetłit Gwich'in Band Council), McKenzie Kuhn (Univerisity of Alberta), Maya Frederickson (University of Alberta), Johanna Winder (Cambridge University), and Lauren Thompson (University of Alberta).

3. Landscape drives variability in concentrations and yields of mercury, methylmercury, and dissolved organic carbon in boreal catchments

Abstract

Climate change and permafrost thaw may impact the mobilization of terrestrial dissolved organic carbon (DOC), mercury (Hg), and neurotoxic methylmercury (MeHg) into aquatic ecosystems; thus, understanding processes that control solute export in northern catchments is needed. We monitored solute chemistry for three years (2019–2021) at a peatland catchment (Scotty Creek) and mixed catchment (Smith Creek) in the Dehcho, within the discontinuous permafrost zone of boreal western Canada. The peatland catchment had higher DOC and MeHg, but lower total Hg concentrations (mean ± standard deviation; 19±2.6 mg DOC L^{-1}; 0.09±0.03 ng MeHg L^{-1}; 1.1±0.3 ng THg L^{-1}) than the mixed catchment (12±4.4 mg DOC L^{-1}; 0.08±0.04 ng MeHg L^{-1}; 3.1±2.2 ng THg L^{-1}). Solute concentrations increased with discharge at the mixed catchment, suggesting transport limitation and the flushing of near-surface, organic-rich flow paths during wet periods. In contrast, solute concentrations in the peatland catchment were not primarily associated with discharge. Instead, MeHg concentrations, MeHg:THg, and MeHg:DOC increased with water temperature, suggesting production limitation and enhanced Hg methylation during warmer periods. Mean open water season DOC and MeHg yields were greater and more variable from the peatland than the mixed catchment (1.1–6.6 vs. 1.4–2.4 g DOC m^{-2}; 5.2–36 vs. 6.1–10 ng MeHg m^{-2}). Crucial storage thresholds controlling runoff generation likely drove greater inter-annual variability in solute yields from the peatland catchment. Our results suggest increasing temperatures and shifting runoff patterns driven by climate change will alter concentrations and yields of THg, MeHg, and DOC.

3.1 Introduction

Boreal rivers are important conduits of terrestrially-derived dissolved organic carbon (DOC) that co-transport mercury (Hg) and neurotoxic methylmercury (MeHg) to downstream freshwater environments and the ocean (Fink-Mercier, Lapierre, et al., 2022; Kirk & St. Louis, 2009; Zolkos et al., 2020). Monitoring total Hg (THg) and MeHg concentrations and yields in high-latitude catchments is a research priority for northern communities as permafrost thaw exposes previously frozen Hg and carbon to biogeochemical and hydrological processes (Dastoor et al., 2022; St. Pierre et al., 2018). Within the Interior Plains of boreal western Canada, extensive peatlands in the discontinuous permafrost zone are increasingly warming, burning, and thawing (Gibson et al., 2018, 2021; Wright et al., 2022); complete permafrost loss is projected by 2050 (Chasmer & Hopkinson, 2017). As MeHg biomagnifies and bioaccumulates in food webs, local increases in THg and MeHg concentrations may threaten the food security of northern Indigenous communities while enhanced export of THg and MeHg may accumulate in downstream waterbodies and marine ecosystems (Basu et al., 2022; Houde et al., 2022; Moslemi-Aqdam et al., 2023).

Anoxic, acidic, DOC-rich conditions support the microbial production (methylation) of inorganic divalent Hg^{II} into MeHg, making peatlands ideal methylation sites (Bravo & Cosio, 2020; Gordon et al., 2016; Poulin et al., 2019). High methylation efficiency is linked to the presence of bioavailable Hg^{II} and labile dissolved organic matter (DOM), while aromatic DOM has been identified as a transport vector of MeHg in boreal surface waters (Bravo et al., 2017; Mangal et al., 2022; Shanley et al., 2022). Permafrost peatlands have accumulated large Hg stores bound to organic matter (Lim et al., 2020; Schuster et al., 2018), and thawed fens and bogs are hotspots of MeHg production across the global boreal-Arctic (Gordon et al., 2016; Poulin et al., 2019; Tarbier et al., 2021). However, few studies have examined concentrations and export of MeHg in northern rivers (Jonsson et al., 2022), and it remains unclear how strongly local hotspots of MeHg production influence the chemistry of catchment outlets.

The species (i.e., THg or MeHg), fraction (i.e., dissolved or particulate), and concentrations of Hg drive biotic uptake, where elevated concentrations of dissolved MeHg lead to greater uptake (Blanchfield et al., 2021; Gagnon & Fisher, 1997). Peatland-dominated catchments predominantly deliver dissolved Hg species bound with DOC (Emmerton et al., 2022; Kirk & St. Louis, 2009), with a higher proportion of MeHg to THg (%MeHg) than sediment-laden rivers carrying

particulate-bound Hg species (St. Pierre et al., 2018; Staniszewska et al., 2022). Discharge and changing water sources can drive variability in solute concentrations, where concentration-discharge metrics identify chemodynamic (i.e., high variability in response to discharge) or chemostatic (i.e., low variability or non-systematic in response to discharge) behavior and thus the hydrological or biogeochemical controls on a solute (Basu et al., 2010; Pohle et al., 2021). Where a non-systematic response to discharge is observed, additional factors may alter the chemistry of water sources over time, such as temperature; elevated temperatures can stimulate the production of both MeHg and DOC (Mattsson et al., 2015; Yang et al., 2016). The presence of discontinuous permafrost in the Interior Plains influences the connectivity of catchment water sources (Wright et al., 2022) and thus may contrast concentration trends of THg and MeHg observed in other boreal regions, which have shown the highest concentrations during summer and the stronger response of THg than MeHg to changing discharge (Fink-Mercier, Lapierre, et al., 2022; Lam et al., 2022).

Export of THg and MeHg has been quantified primarily in large Arctic rivers, carrying 37–44 Mg THg and 0.8–2.5 Mg MeHg into the Arctic Ocean annually, where contributions from sub-catchments vary depending on land cover and hydrology (Soerensen et al., 2016; Sonke et al., 2018; Zolkos et al., 2020). The yields of THg, MeHg, and DOC (i.e., annual solute mass delivered per unit area) in boreal catchments can exhibit high seasonal variability tied to either hydrological or biogeochemical controls. Spring freshet, driven by snowmelt, often dominates seasonal hydrographs and the annual yields of DOC and Hg in northern regions, despite its short period (i.e., days to weeks; Burd et al., 2018; Gandois et al., 2021; Schelker et al., 2011). Conversely, summer storms can drive high-intensity exports of terrestrially-derived THg and DOC from deeper soil layers and mobilize MeHg produced during warmer summertime conditions (Kirk & St. Louis, 2009; Schelker et al., 2011; Shanley et al., 2022). Runoff generation in peatland-dominated catchments is controlled by significant storage thresholds where runoff is generated when a storage threshold is exceeded. However, low runoff occurs during dry periods when the landscape retains water (Goodbrand et al., 2019). The dry climate of the Interior Plains lends additional sensitivity to runoff generation as even small variability in the balance between precipitation and evapotranspiration can drive large relative variations in annual runoff (Burd et al., 2018). However, unique amongst peatland-dominated regions of the boreal-Arctic, the Interior Plains has significant increases in annual basin runoff and runoff ratios in the absence of increasing precipitation, suggesting that ongoing permafrost thaw is altering runoff regimes (Mack et al.,

2021). Therefore, understanding the relationships between solute concentrations, yields, and changing runoff is essential in the rapidly-warming Interior Plains.

Here, we aimed to quantify the inter- and intra-annual variability in THg, MeHg, and DOC concentrations and yields from three years of water chemistry observations from two sub-arctic catchments with differing land cover composition in the Interior Plains (boreal Western Canada). To meet this goal, we monitored solute concentrations during the open-water season, coupled with DOM composition metrics and analysis of concentration-discharge relationships. We expected the peatland catchment to be chemostatic due to consistent contributions from peatlands, with potential for a signal of summertime MeHg production peaks, and deliver consistently high concentrations of MeHg and DOC as observed in other boreal peatland catchments. In contrast, we anticipated chemodynamic behavior from the catchment with a mixed landscape of mountain, forest, and peatlands with terrestrial solute flushing during high flow events and a greater contribution of particle-bound Hg. Our findings will reveal processes that control the concentrations and exports of THg, MeHg, and DOC to predict the influence of current and future climate-driven changes, such as permafrost thaw, on solute delivery in the Interior Plains.

3.2 Materials and methods

3.2.1 Study catchments

Samples were collected at the outlets of Scotty Creek and Smith Creek catchments in the Dehcho region, Northwest Territories (Figure 3.1); Scotty Creek is within the sporadic discontinuous permafrost zone (10–50% permafrost), while Smith Creek has extensive discontinuous permafrost (50–90% permafrost; Brown et al., 2002). The catchments are located in the homelands of Łíídlı̨ Kų́ę́ First Nation and Pehdzeh Ki First Nation, respectively. Scotty Creek is a 129 km^2 catchment located within the Taiga Plains Mid-Boreal Ecoregion, and Smith Creek is a 154 km^2 catchment that intersects the Taiga Plains Mid-Boreal Ecoregion, Taiga Cordillera Low Subarctic Ecoregion, and Boreal Cordillera High Boreal Ecoregion (Ecosystem Classification Group, 2009, 2010), with both catchments draining into the Mackenzie River. The regional climate is characterized by long, cold winters and short summers, although Scotty Creek is warmer and wetter than Smith Creek based on mean annual air temperature (-2.5 and -4.7°C, respectively) and mean annual precipitation (415 and 350 mm, respectively; Fick & Hijmans, 2017). The surficial geology of

Scotty Creek is characterized by thin-thick tills and fine-grained glaciolacustrine deposits from glacial retreat that support peatland development, with a bedrock of shale, limestone, and dolomite formed during the Devonian period (Aylsworth et al., 2000; Wheeler et al., 1996). Smith Creek has surficial geology of glaciolacustrine deposits, thick tills, and some areas of exposed shale, limestone, and dolomite bedrock within the Franklin mountains (Aylsworth et al., 2000; Wheeler et al., 1996). Vegetation cover at both sites includes mixed-wood forests of trembling aspen (*Populus tremuloides*) and white spruce (*Picea glauca*) in the uplands with peatlands in the lowlands (Ecosystem Classification Group, 2009, 2010). Peatlands in this region are mosaics of relatively dry permafrost peat plateaus that support black spruce (*Picea mariana*), Labrador tea (*Rhododendron groenlandicum*), and lichens alongside wetter permafrost-free wetlands: bogs with *Sphagnum* mosses and fens with varying vegetation of sedges and shrubs (Quinton et al., 2009). The land cover composition varies between the sites; Scotty Creek is low-relief and peatland-dominated, while Smith Creek is steeper and predominantly forested with peatlands in the southwest portion of the catchment (Figure 3.1; Table 3.1). We henceforth refer to Scotty Creek as the "Peat" catchment and Smith Creek as the "Mixed" catchment.

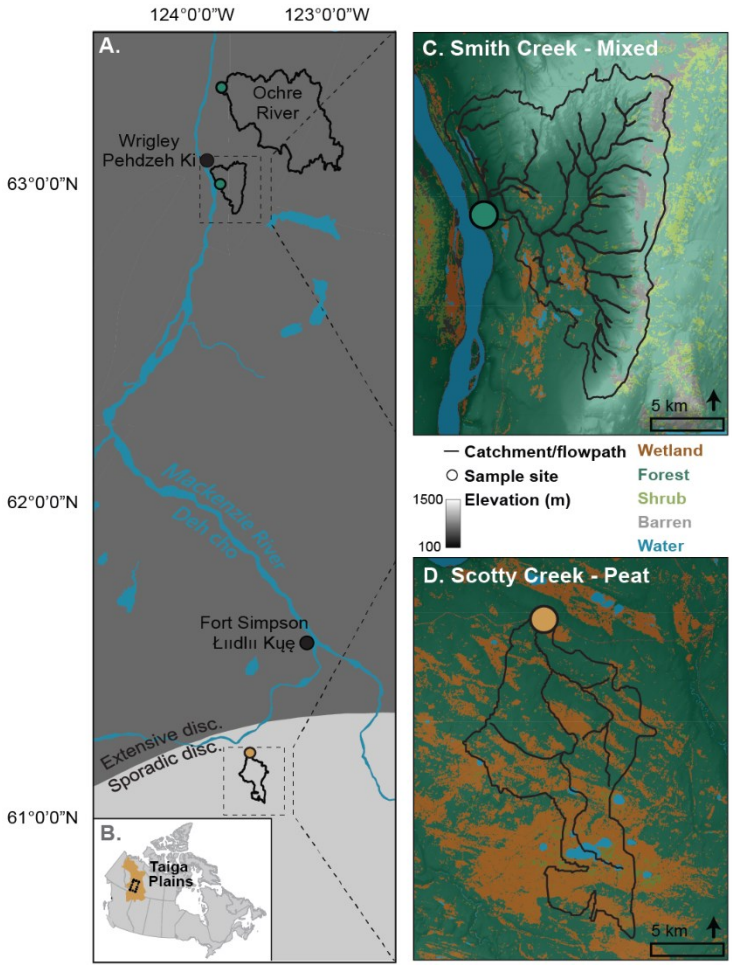

Figure 3.1. Study catchments. A) Study site locations in relation to permafrost zones (Brown, Ferrians, Melnikov, et al., 2002) and nearby communities, B) location within Canada and the Taiga Plains, C) Smith Creek – mixed catchment, and D) Scotty Creek – peatland catchment, with flow paths and elevation (Natural Resources Canada, 2013, 2022) overlaid by land cover (Hermosilla et al., 2022).

We quantified the Smith Creek catchment characteristics with the slope and hydrology toolsets on ArcGIS 10.8 using the Canadian Digital Elevation Model (Natural Resources Canada, 2013) with corrections in low-lying areas with the National Hydro Network (Natural Resources Canada, 2022). The Scotty Creek catchment boundaries were obtained from the National Hydro Network (Natural Resources Canada, 2022). We further summarized simplified land cover characteristics in Table 3. 1; the numeric classification used by Hermosilla et al. (2022) corresponds to land cover types as follows: Wetland=class 80+81; Forest=210+220+230; Shrub=40+50+100; Barren=32+33; Water=20.

Table 3.1. Site and sampling characteristics at A) Scotty Creek and B) Smith Creek. Catchment characteristics are from Natural Resources Canada (2013, 2022) and Hermosilla et al. (2022). The total annual rainfall and mean±SD values of annual air temperature (15 m height) were taken from meteorological stations at the sites. The water chemistry of grab samples includes total mercury (THg), methylmercury (MeHg), dissolved organic carbon (DOC) concentrations, specific absorbance at 254 nm ($SUVA_{254}$), pH, and electrical conductivity (EC). ND=no data.

Site characteristics	A) Scotty Creek – Peat			B) Smith Creek – Mixed		
Monitoring location	61.415739, -121.45535			63.173589, -123.337311		
Permafrost zone	Sporadic discontinuous			Extensive discontinuous		
Catchment area (km^2)	129			154		
Mean slope (degrees)	0.6			10.1		
Mean elevation (m)	274			382		
Wetland (%)	41			4		
Forest (%)	54			86		
Shrub (%)	2			3		
Barren (%)	0			6		
Water (%)	3			1		
Sampling characteristics	2019	2020	2021	2019	2020	2021
Total rainfall (mm)	259	474	245	305	323	304
Air temperature (°C)	-0.9	-2.1	1.4	-2.9	-4.4	-3.1
Monitoring start	Mar 24	Jun 11	Jun 25	Mar 24	Jun 5	Jun 30
Monitoring end	Sep 29	Sep 24	Oct 5	Sep 28	Oct 22	Sep 16
Bulk THg (ng L^{-1})	1.21±0.33	1.09±0.29	1.05±0.25	3.57±2.80	2.56±1.55	3.00±1.56
Filtered THg (ng L^{-1})	0.93±0.31	ND	ND	1.19±1.14	ND	ND
Bulk MeHg (ng L^{-1})	0.09±0.04	0.09±0.02	0.08±0.02	0.08±0.07	0.07±0.02	0.11±0.04
Filtered MeHg (ng L^{-1})	0.08±0.04	ND	ND	0.05±0.01	ND	ND
DOC (mg L^{-1})	18.1±2.2	21.6±1.5	20.3±1.4	14.1±4.9	11.9±3.5	10.9±2.1
$SUVA_{254}$ (L mg^{-1} C m^{-1})	3.4±0.2	3.6±0.2	3.4±0.5	3.5±0.7	3.3±0.3	3.3±0.1
pH	7.6±0.3	7.5±0.2	7.4±0.4	8.1±0.1	8.1±0.1	8.1±0.1
EC (µS cm^{-1})	188±24	157±21	211±31	553±197	659±219	736±116

3.2.2 Sample collection and analysis

Sample collection was initiated in 2019, where water samples were taken ~monthly during the ice-free season (~ April–September) for Hg, MeHg, DOC, DOM characterization, nutrients, and major ions (University of Alberta & Dehcho-AAROM, 2022). Dehcho Aboriginal Aquatic Resources and Ocean Management program members collected samples from 2020 to 2021. We collected unfiltered (2019 to 2021) and filtered (2019 only) samples from the edge of the rivers for total Hg (THg) (2×125 mL) and MeHg (2×250 mL) analysis following the clean hands-dirty hands protocol (St. Louis et al., 1994). All samples were collected in certified pre-cleaned glass amber bottles (Environmental Supply Company, Inc., Durham, NC, US). Filtered THg and MeHg samples were

obtained by filtering one of the two samples through pre-cleaned Nalgene 0.45 µm cellulose nitrate filter towers within 24 hours. The filtrate was then transferred to a new bottle. All THg and MeHg samples were preserved with 0.2% and 0.4% trace-metal grade hydrochloric acid, respectively.

Hg samples were analyzed in the Canadian Association for Laboratory Accreditation-certified Biogeochemical Analytical Service Laboratory (University of Alberta). Water samples were analyzed for THg concentrations on a Tekran 2600 Mercury Analyzer (Tekran Instruments Corporation, Scarborough, ON, Canada). Water samples were analyzed for MeHg using isotope dilution, distillation, and analyses on a Tekran 2700 Methylmercury Analyzer (Tekran Instruments Corporation, Scarborough, ON, Canada) coupled to an Agilent 7900 inductively coupled plasma-mass spectrometer (ICP-MS; Agilent Technologies, Inc., Santa Clara, CA, US).

We measured each site's physical parameters, nutrients, major ions, and DOM characteristics. Electrical conductivity (EC), pH, and water temperature were measured on-site with calibrated PT1 and PT2 Ultrapens (Myron L Company, Carlsbad, CA, US). We collected two additional filtered (0.7 µm Grade GF/F, Whatman) 60 mL water samples in acid-washed amber glass bottles, one of which was preserved with 0.6 mL of 2M HCl for dissolved organic carbon (DOC) and metal analysis, while the other sample remained non-acidified for nutrient analysis, DOM absorbance, and fluorescence spectroscopy. All water samples were kept cool in transit to the laboratory and remained refrigerated until analyses.

The Natural Resources Analytical Laboratory (University of Alberta) analyzed samples for DOC, metals, and nutrients. A TOC-L combustion analyzer with a TNM-L module (Shimadzu Corporation, Kyoto, Japan) measured DOC and total dissolved nitrogen (TDN) concentrations. Colorimetry (Thermo Gallery Plus Beermaster Autoanalyzer, Thermo Fisher Scientific, Waltham, MA, US) determined concentrations of chloride (Cl), nitrate (NO_3-N), nitrite (NO_2-N), ammonium (NH_4-N), orthophosphate (PO_4-P), and sulfate (SO_4^{-2}-S). Concentrations of sodium (Na), potassium (K), calcium (Ca), manganese (Mn), iron (Fe), copper (Cu), zinc (Zn), magnesium (Mg), phosphorus (P), and sulfur (S) were measured by inductively coupled plasma optical emission spectroscopy (ICP-OES, iCAP6300 Duo, Thermo Fisher Scientific, Waltham, MA, US).

We assessed the DOM aromaticity of grab samples using the specific ultraviolet absorbance ($SUVA_{254}$) at 254 nm, where $SUVA_{254}$ values increase with DOM aromaticity (Weishaar et al.,

2003). The absorbance of DOM was measured from 200 to 700 nm (UV-1280, UV-VIS Spectrophotometer, Shimadzu Corporation, Kyoto, Japan) and corrected with Milli-Q water blanks. We calculated $SUVA_{254}$ after correcting decadal absorbance at 254 nm (A_{254}, cm^{-1}) for interference by Fe (Weishaar et al., 2003). We used an Aqualog fluorometer (Horiba Ltd., Kyoto, Japan) to measure DOM fluorescence emission-excitation matrix spectra (EEMs). Samples were scanned from excitation wavelengths of 230–500 nm at 5 nm increments and emission wavelengths of 210–620 nm at 2 nm increments. Corrections for excitation and emission, inner filter effects, and Raman signal calibration were applied before analysis. We used R (R version 4.1; R Core Team, 2022) package *staRdom* (Pucher et al., 2019) to analyze the biological index (BIX) and humification index (HIX) and characterized the DOM pool into components with parallel factor analysis (PARAFAC) using MATLAB toolbox drEEM (Mathworks, US) following protocol from Oliver et al. (2017). We identified five unique components (Figure A.3.1) that were validated through half-split analysis and found multiple matches for each component on the online fluorescence database, OpenFluor (Murphy et al., 2014). The maximum fluorescence of excitation and emission in Raman units (Fmax) was used to calculate the percent contribution of each component to total fluorescence, as the fluorophores' actual structure is unknown (Oliver et al., 2017). Table A.3.1 summarizes the characteristics of the absorbance and fluorescence analyses. We used the R package *vegan* (Oksanen et al., 2022) to perform a principle component analysis (PCA) to examine relationships among the absorbance and fluorescence indices from grab samples at both rivers. We used the PCA's first principle component (PC1) scores to indicate aromatic quality.

3.2.3 Continuous data collection

In 2019, Smith Creek was instrumented with HOBO water level loggers (HOBO MX2001, Onset Computer, Bourne, Ma, US), recorded hourly, and both the peatland catchment and mixed catchment were instrumented with Spectro::lysers (s::can, Vienna, Austria) to measure UV-visible absorbance, recorded on 3-12 hour intervals depending on sunlight conditions and duration between site visits. The Spectro::lyser measured decadal absorbance (cm^{-1}) between 200 and 700 nm at 2.5 nm intervals and was turbidity-corrected at 255 nm by subtracting the average wavelength between 550 and 700 nm from the Spectro::lyser spectra (Burd et al., 2018); 255 nm is presumed proportional to 254 nm. An autosampler (Teledyne ISCO, Lincoln, NE, US) collected

~daily water samples to analyze UV-visible absorbance, fluorescence, and DOC. Spectro::lyser and autosampler data were checked by comparing them to grab samples (Table A.3.2). Spectro::lyser data were gap-filled with autosampler data on occasions where debris was caught in the measurement window, or there was insufficient solar panel charge. Due to COVID-19 constraints, no continuous absorbance measurements were taken from 2020 to 2021, although water level loggers were installed at Smith Creek. Discharge data from the peatland catchment was acquired from Water Survey Canada records (Environment and Climate Change Canada, 2021), while we estimated discharge from hourly water depth records at the mixed catchment, converted using a stage rating curve and velocity-area calculations from monthly field measurements in 2019 (Turnipseed & Sauer, 2010). Any data gaps in discharge for mixed catchment were filled based on a regression derived from discharge records of the nearby Ochre River (Figure 3.1); see Table A.3.3 for details on the Ochre River catchment characteristics and gap-filling regression (Environment and Climate Change Canada, 2021). Environmental data (mean annual air temperature at 15 m height and total rainfall) were taken from meteorological stations within the peatland catchment and mixed catchment (Sonnentag, 2022; Sonnentag & Quinton, 2022).

3.2.4 Concentration-discharge analysis

To compare flow annually and between the study catchments, we calculated runoff (mm d^{-1}) by dividing the daily discharge rate by catchment area. To examine the response of Hg, MeHg, and DOC concentration to discharge, we determined chemodynamic (where solute concentration varies in response to discharge) or chemostatic (a non-systematic or limited variation in solute concentration in response to discharge) relationships between solutes and discharge (Pohle et al., 2021). We calculated β, the log-log slope between discharge and the solute. We used β as an indicator of transport limitation ($\beta>0$), where solute sources are present on the landscape and become connected as discharge increases), source limitation ($\beta<0$), where finite solutes are depleted or mixed with more dilute waters), or chemostasis ($\beta=0$; Koger et al., 2018; Musolff et al., 2015). In order to determine the stability or variability of the solute concentration relative to discharge, we plotted β against the ratio of coefficients of variation of solute concentration over discharge ($CV_C/CV_Q=[\mu_Q\sigma_C]/[\mu_C\sigma_Q]$), where μ_C and μ_Q are mean values of concentration and discharge, respectively, and σ_C and σ_Q are standard deviations. In the case of $\beta\approx0$, the solute concentrations may vary little with discharge or exhibit large but non-systematic variability.

Chemostatic behavior was defined as $-0.2<\beta<0.2$ and $CV_C/CV_Q<0.5$ (Koger et al., 2018; Musolff et al., 2015). We additionally examined three high-flow events per river (via identification of the inflection point on the hydrograph and confirming a >10% increase in discharge) in spring, early summer, and late summer of 2019. The flushing index ($FI=[C_{Qpeak,norm}]-[C_{Qinitial,norm}]$) was calculated to indicate whether flushing or diluting was observed during the rising limb. We identified the direction of hysteresis, where clockwise hysteresis indicates flushing (i.e., higher concentrations during the rising limb than the falling limb), anticlockwise hysteresis indicates a delayed transport response, and no hysteresis indicates an intermediate response (Gandois et al., 2021; Pohle et al., 2021; Shogren et al., 2021; Vaughan et al., 2017).

3.2.5 Flux estimates

We modeled daily THg, MeHg, and DOC fluxes from measured concentrations and discharge using a web-based tool (Park et al., 2015) developed using the USGS constituent-load modeling software LOADEST (Runkel et al., 2004), spanning April–September 2019, 2020, and 2021. Daily constituent fluxes were calculated from daily river discharge measurements based on a calibration regression model developed from paired concentration and discharge data; one outlier MeHg concentration value was removed from the mixed catchment regression model. A regression derived from Spectro::lyser A_{254} was used to predict daily DOC concentrations for a subset of our observations (2019) to use within the LOADEST DOC models to ensure hard-to-capture high-flow events were included in our modeling framework (Figure A.3.2). To contextualize the 2019–2021 yields, we included historical discharge data (2006–2021) in the LOADEST solute flux models from the peatland catchment, and the mixed catchment river discharge was estimated as described above from the Ochre River record**.** Concentration-discharge relationships can vary over time, so we examined possible scenarios and ranges in Hg, MeHg, and DOC fluxes between 2006 and 2021 rather than directional trends. We used the Adjusted Maximum Likelihood Estimator (AMLE) calibration regressions and selected the model based on the lowest Akaike Information Criterion (AIC) using the default model (Model 0), and those without a linear time function (acceptable models=1, 2, 4, 6). Models are nested within Equation 1, where *ln Q* is the *ln Q* minus the center of *ln Q*, *dtime* is the decimal time minus the center of decimal time, *Q* is discharge in ft^3 s^{-1}, and flux is in mass d^{-1}. The LOADEST output model coefficients and fit (R^2) are in Table A.3.4.

$$\ln \text{load} = a0 + a1 \ln Q + a2 \ln Q^2 + a3 \sin(2\pi \text{dtime}) + a4 \cos(2\pi \text{dtime}) \quad (1)$$

We obtained yields from the sum of daily fluxes within the yearly sampling period normalized to the catchment area. The spring period was defined as April 1 to the end of high freshet flows, while the summer period was defined from the end of freshet to September 30 (Burd et al., 2018).

3.3 Results

3.3.1 Meteorological conditions and hydrology

The mean annual air temperature over the three years was higher at both sites than long-term averages (Table 3.1). In 2020, the highest total rainfall occurred at both sites, especially at the peatland catchment, which had 474 mm. Total rainfall in 2019 and 2021 was lower and varied little at both sites. Cumulative runoff from the spring and summer of 2019 to 2021 at the peatland catchment was 61, 311, and 142 mm, respectively, while the mixed catchment totaled 87, 146, and 86 mm (Figure 3.2, Table A.3.5). Summer runoff, occurring in response to storm events rather than snowmelt, was greater than spring freshet in 2019 and 2020 at both catchments, while freshet dominated the seasonal hydrographs in 2021 at 79% of runoff at the peatland catchment and 51% of runoff at the mixed catchment. During the monitoring period, the mixed catchment exhibited similar runoff patterns as the nearby gauged Ochre River (Table A.3.3). While the mixed catchment does not have long-term hydrometric data, we utilized the long-term record at Ochre River to compare its variability with the peatland catchment (2006–2021; Table A.3.6). The longer-term records showed cumulative runoff in the peatland catchment to exhibit far greater variability (mean±1 standard deviation [SD]: 164±91 mm y^{-1}; coefficient of variation [CV] 56) compared to the proxy for the mixed (236±42 mm y^{-1}; CV 18).

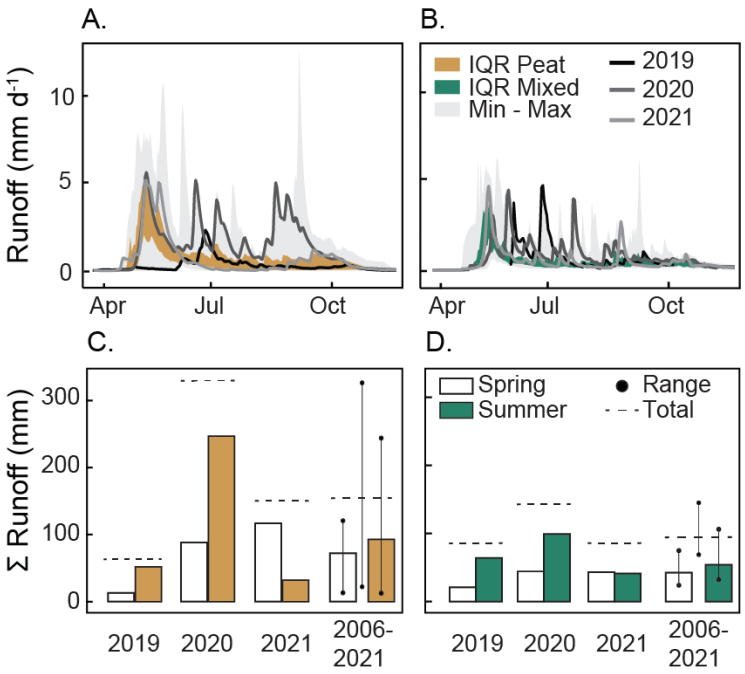

Figure 3.2. Catchment runoff trends. Comparison of 2019–2021 hydrographs with the historical record from 2006 to 2021 at A) Scotty Creek – Peat, and B) Smith Creek – Mixed, with Smith Creek's pre-2019 record predicted from Ochre River discharge; see Table A.3.3. Historical runoff data maintained by the Water Survey of Canada. C)–D) Cumulative runoff is separated by spring and summer (April to September 2019–2021). The mean partitioning and range of runoff from 2006 to 2021 were from discharge records of Scotty Creek, and Ochre River records were used to predict pre-2019 discharge at Smith Creek. The spring period is defined between April 1 and the end of high freshet flows, and summer is defined between the end of freshet to September 30. Smith Creek flow record in 2019 ranges from May 27 to Sept 28; cumulative runoff is based on this period. IQR=interquartile range.

3.3.2 Characterizing catchment water chemistry and DOM composition

Relative to the mixed catchment, the peatland catchment had lower EC (190±32 vs. 620±200 µS cm^{-1}), pH (7.5±0.3 vs. 8.1±0.1), and THg concentrations (1.13±0.30 vs. 3.13±2.17 ng THg L^{-1}), with higher concentrations of DOC (19.5±2.6 vs. 11.9±4.3 mg DOC L^{-1}) and MeHg (0.09±0.03 vs. 0.08±0.04 ng MeHg L^{-1}; Figure 3.3; Table 3.1). When comparing the DOM composition between the two catchments, we found the peatland catchment had higher $SUVA_{254}$, humification index values, and higher contributions of humic-like PARAFAC component C1 (Figure 3.4; Figure A.3.1; Table A.3.1). By contrast, the DOM composition at the mixed catchment spanned a wider range of aromaticity than the peatland catchment (Figure 3.4). In 2019, the proportion of bulk THg as MeHg (%MeHg) was higher at the peatland catchment than at the mixed catchment (8.1±3.5 vs. 3.4±1.8 %MeHg), as was the dissolved fraction of MeHg and THg (peatland

catchment: dissolved MeHg=88±11%; dissolved THg=77±16%; mixed catchment: dissolved MeHg=71±22%; dissolved THg=57±17%).

We sampled a groundwater spring in the mixed catchment in July of 2021 and found low concentrations of DOC (1.22 mg L^{-1}), THg (0.91 ng L^{-1}), and MeHg (0.03 ng L^{-1}) with high EC (1600 µS cm^{-1}), ions (266 mg Na L^{-1}; 179 mg Ca L^{-1}; 188 mg SO_4^{-2}-S L^{-1}), but similar pH to stream measurements (7.8). By comparison, peatland (i.e., peat plateaus, bogs, and fens) porewater sampled at both catchments in 2021 had high mean DOC (44.0±11.7 mg L^{-1}), THg (19.10±10.50 ng L^{-1}), and MeHg concentrations (0.32±0.29 ng L^{-1}) with low values of EC (56±29 µS cm^{-1}) and pH (5.1±0.8) (Thompson et al., 2022).

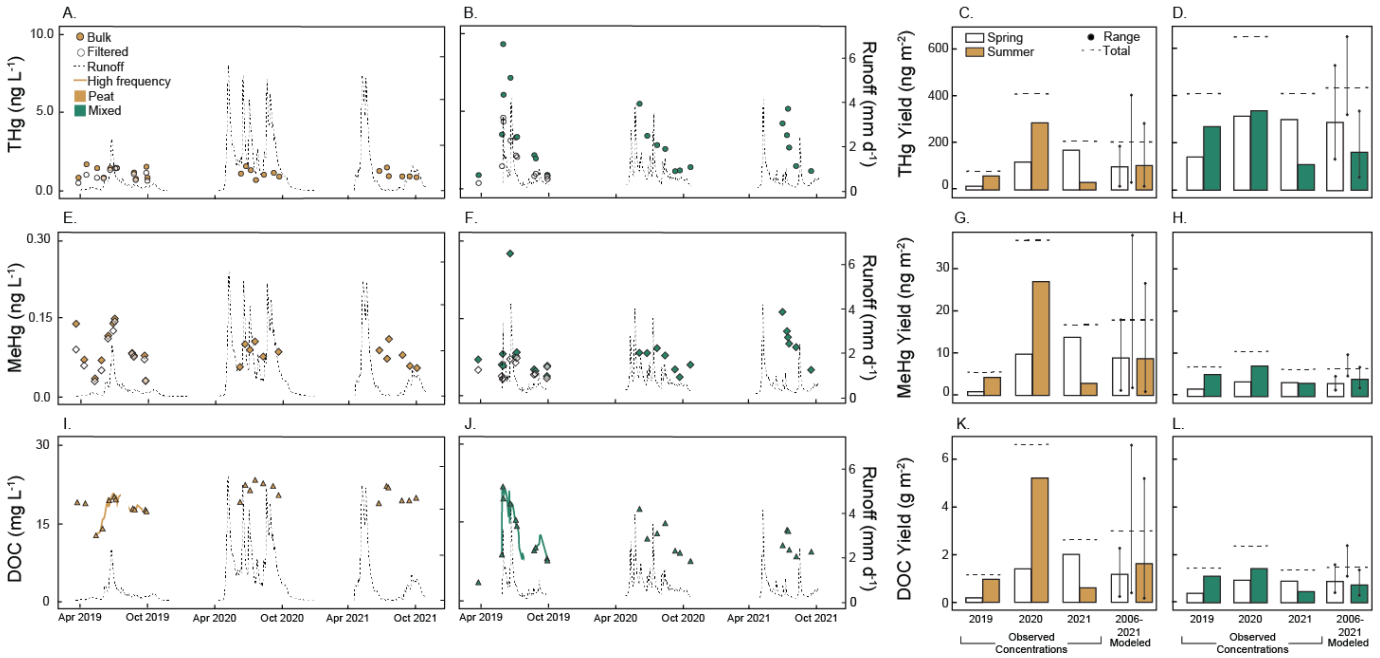

Figure 3.3. Seasonal solute concentrations and yields. Concentrations of filtered (2019) and concentrations and yields of bulk (2019–2021) A)–D) total mercury (THg), E)–H) methylmercury (MeHg), and I)–L) dissolved organic carbon (DOC) in Scotty Creek – Peat and Smith Creek – Mixed. Yields of bulk THg, MeHg, and DOC from April to September 2019–2021 are normalized by catchment area and displayed by season. The mean partitioning and range of solute yields from 2006 to 2021 were modeled from discharge records of Scotty Creek, and Ochre River records were used to predict pre-2019 discharge at Smith Creek.

Due to COVID-19 constraints, early spring sampling occurred only in 2019; at the peatland catchment, MeHg and DOC concentrations were relatively high in March 2019, temporarily declined, increased through early summer, and declined through late summer. By contrast, THg, MeHg, and DOC concentrations at the mixed catchment were relatively low in spring, increased

with early summer high flows, and showed a consistent decline towards late summer (Figure 3.3). DOM composition varied through the year, with changing aromaticity associated with flow conditions and sampling months (Figure 3.4).

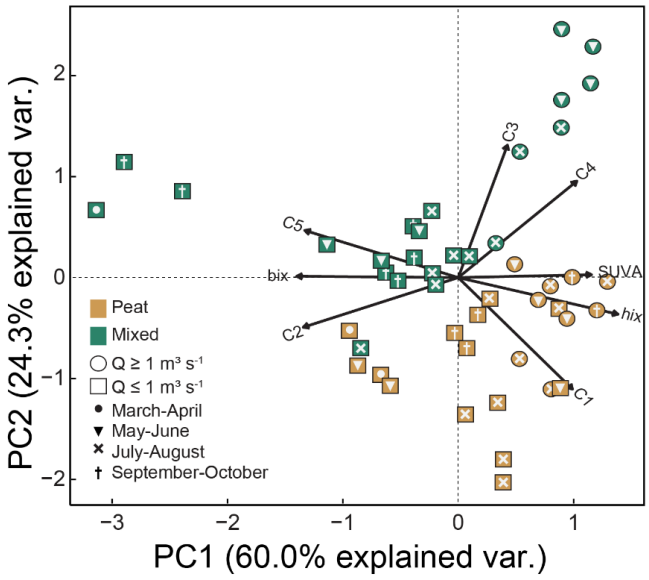

Figure 3.4. Seasonal dissolved organic matter (DOM) composition. Principle component analysis (PCA) with shapes indicating high (discharge, Q≥1 m^3 s^{-1}) and low (Q≤1 m^3 s^{-1}) flow periods as well as the month of the year in Scotty Creek – Peat and Smith Creek – Mixed. DOM indices are described in Table A.3.1, and PCA loadings are in Table A.3.7. C1–C5=parallel factor analysis components, SUVA=specific ultraviolet absorbance at 254 nm, hix=humification index, bix=biological index.

3.3.3 Concentration-discharge relationships

Low-flow, early-season samples at the peatland catchment were associated with a microbial humic-like peak (C2, Figure 3.4), lower concentrations of DOC, and higher EC values (Figure A.3.3). In contrast, higher flow periods were associated with higher $SUVA_{254}$ and HIX regardless of the season (Figure 3.4). However, flow-related differences were more pronounced for the mixed catchment. Two distinctive regimes were present in the mixed catchment: low flows had higher EC and Na and lower DOC and THg concentrations (Figure A.3.3) with microbial/protein-like DOM composition during early and late season sampling (microbial humic-like C2 and protein-like C5; Figure 3.4). In comparison, high flows had lower EC and higher DOC (Figure A.3.3) with aromatic, terrestrial DOM composition corresponding with humic-like components in early to mid-summer samples (C3 and C4; Figure 3.4).

We observed chemostatic relationships of THg, MeHg, and DOC at the peatland catchment and chemodynamic flushing responses to increased discharge at the mixed catchment when inputting all grab samples from the monitoring period (Figure 3.5). We plotted the log-log slope of concentration-discharge (β) and the relative stability of the response (coefficients of variation of solute concentration over discharge, CV_C/CV_Q). From regressions of untransformed THg, MeHg, and DOC concentrations against discharge for the peatland catchment, only DOC significantly increased with discharge (R^2=0.26, p<0.001), as observed in the paired high-low discharge analysis (Figure A.3.3). At the mixed catchment, THg concentrations responded most strongly to discharge (R^2=0.68, p<0.001), followed by DOC (R^2=0.47, p<0.001), in contrast to no statistically significant response of MeHg to discharge, which is reflected by its higher CV_C/CV_Q value in Figure 3.5A.

We found that changes in flow influenced the fraction of Hg species, where the proportion of particulate MeHg increased with discharge at the mixed catchment. Interestingly, the proportion of particulate Hg significantly decreased with discharge at the peatland catchment and did not significantly vary with discharge at the mixed catchment (Figure A.3.4).

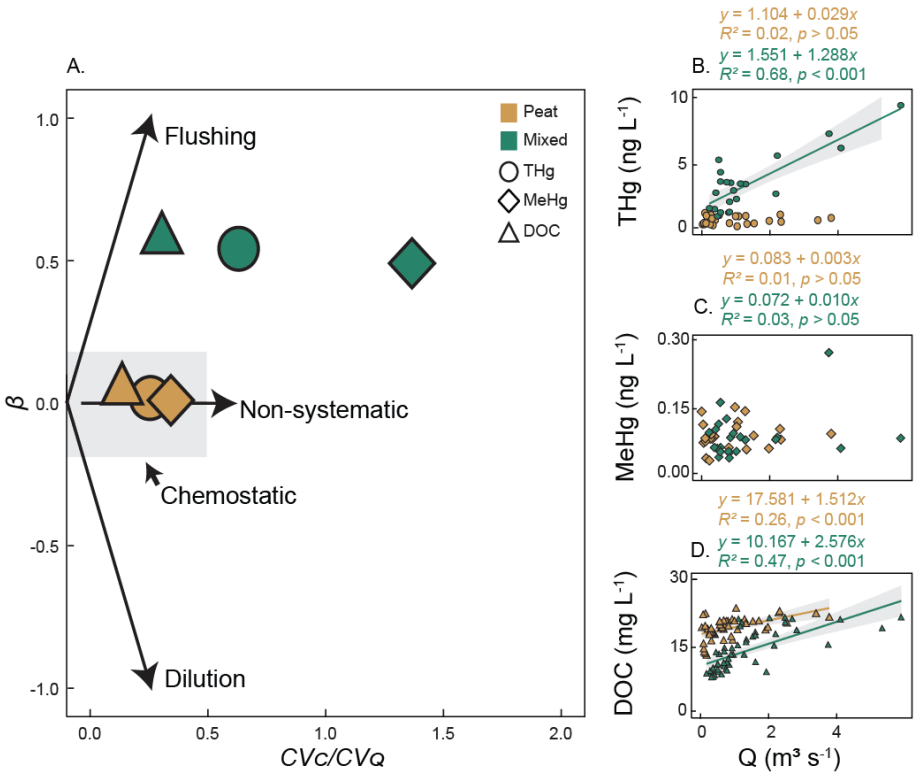

Figure 3.5. Concentration-discharge relationships, 2019-2021. Evaluation of relative chemostatic or chemodynamic behavior in Scotty Creek – Peat, and Smith Creek – Mixed, for observations of bulk total mercury (THg; n=24, 24, respectively), methylmercury (MeHg; n= 23, 24), and dissolved organic carbon (DOC; n=53, 52) by plotting A) the log-log slope between discharge and the analyte (β) vs. coefficients of variation of analyte concentration over

discharge (CV_C/CV_Q), and B)–D) untransformed concentration and discharge (Q) values with model formula, adjusted R^2 values, and p-values of the regressions and a 95% confidence interval surrounding the best-fit line if statistically significant ($p<0.05$).

As biogeochemical processes governing the chemistry of stream water sources shift through the year, we selected three flow events in 2019 where A_{254} (DOC proxy; Figure A.3.2) was monitored at high-frequency (Figure 3.6). Corresponding to spring, early summer, and late summer, event-scale analysis of concentration-discharge metrics showed variability throughout the 2019 monitoring period in the response of DOM to changing flow conditions.

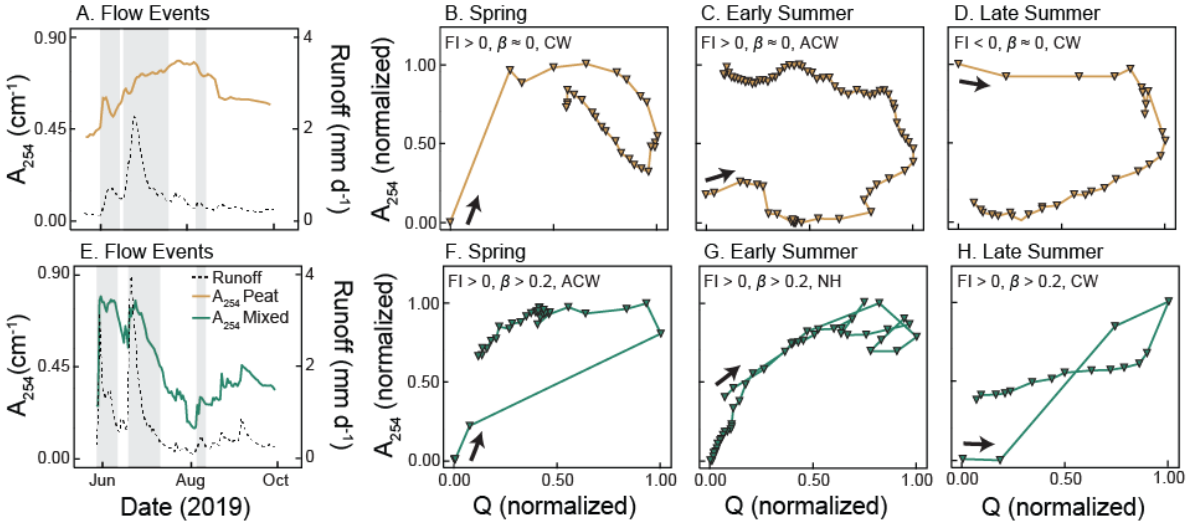

Figure 3.6. Event-scale concentration-discharge relationships, 2019. High-frequency monitoring of absorbance at 254 nm (A_{254}) in 2019 plotted with runoff at A)–D) Scotty Creek – Peat and E)–H) Smith Creek –Mixed. Shading identifies the timeframe of the A_{254}–discharge (Q) hysteresis plots, normalized per high flow event, during spring, early summer, and late summer of 2019. The arrow indicates the start of the high-flow event. FI=flushing index, β=log-log slope between discharge and A_{254}, CW=clockwise hysteresis, ACW=anticlockwise hysteresis, and NH=no hysteresis.

At the peatland catchment, FI and hysteresis response of A_{254} to discharge varied through the open-water season despite β of the full-season and event-scale analyses falling within the chemostatic threshold ($-0.2>\beta<0.2$). In spring and early summer, FI>0 indicated A_{254} enrichment, although the response was quicker in spring (clockwise hysteresis) than in early summer (anticlockwise hysteresis). By contrast, rapid A_{254} dilution was observed in late summer (FI<0, clockwise hysteresis).

In all three events at the mixed catchment, we observed FI>0 and $\beta>0.2$, indicating consistent enrichment of A_{254} and transport limitation (Figure 3.6). However, the hysteresis responses at each event differed; in spring, anticlockwise hysteresis indicated a slow response from either low

connectivity or distant sources. During early summer, a lack of hysteresis indicated an intermediate response due to variable sources and pathways. In late summer, A_{254} at the mixed catchment exhibited a clockwise response as an indication of a fast response from near sources or high connectivity. Throughout the open water season, we thus observed an increasingly quick enrichment of A_{254} in response to increased discharge at the mixed catchment (Figure 3.6).

3.3.4 Biogeochemical drivers of THg and MeHg concentrations

DOC concentrations were associated more strongly with MeHg concentrations at the peatland catchment and THg concentrations at the mixed catchment (Figure 3.7). DOM composition additionally had varying associations with Hg forms in the rivers. Filtered THg and MeHg concentrations at the peatland catchment and THg concentrations (bulk and filtered) at the mixed catchment increased with PC1 scores (Figure 3.7), corresponding to increasing aromatic quality. Both bulk and filtered MeHg increased with A_{254} at the peatland catchment (bulk MeHg-A_{254}: R^2=0.20, p=0.01; filtered MeHg-A_{254}: R^2=0.62, p=0.002), while bulk and filtered THg increased with A_{254} at the mixed catchment (bulk THg-A_{254}: R^2=0.76, p<0.001; filtered THg-A_{254}: R^2=0.87, p<0.001). When examining relationships with PARAFAC components at the peatland catchment, filtered MeHg concentrations decreased with a microbially derived, humic-like component (C2) and increased with a terrestrial-humic component (C4), while filtered THg concentrations likewise decreased with the microbially derived C2 and increased with terrestrial-humic components (C1, C4; Figure A.3.5). In contrast, at the mixed catchment, bulk and filtered THg concentrations decreased with a microbially derived, humic-like component (C2) and increased with fulvic-like and terrestrial-humic components (C3, C4; Figure A.3.5).

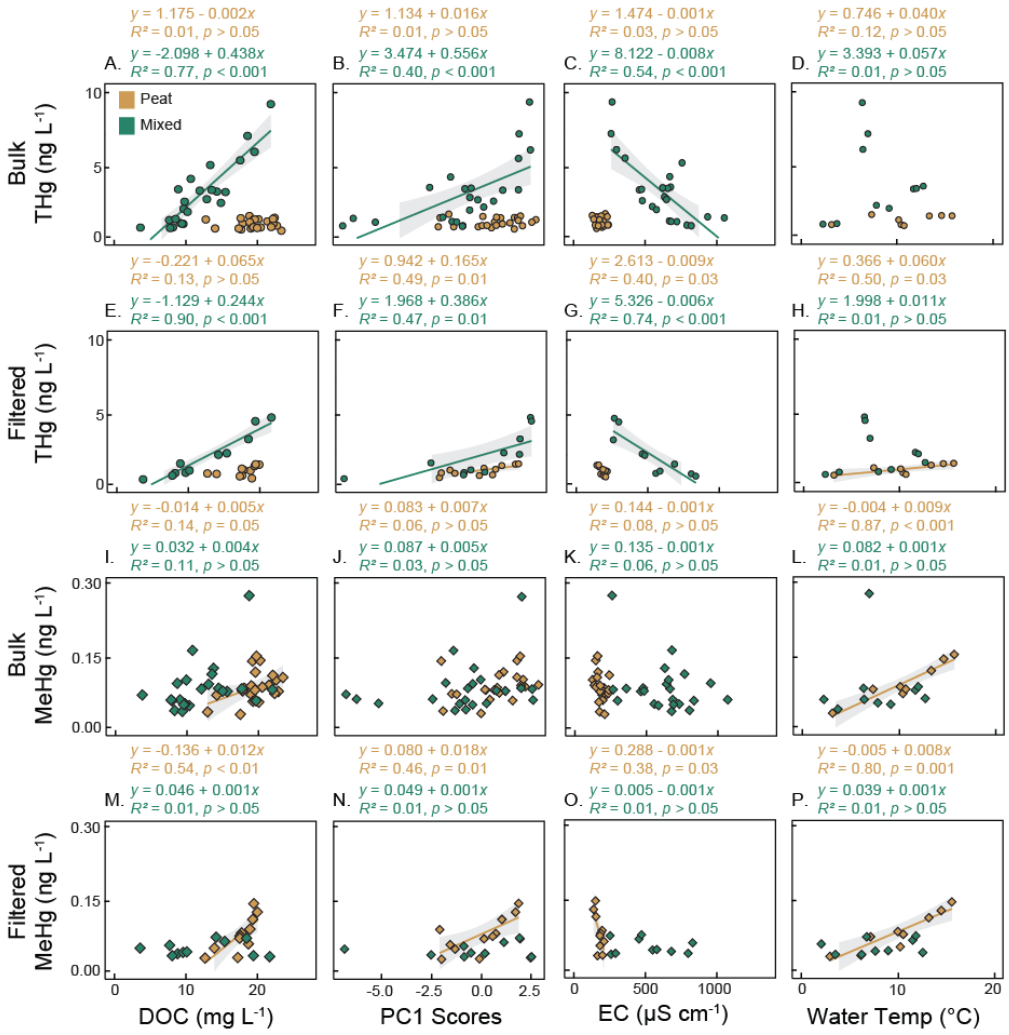

Figure 3.7. Relationships between geochemical parameters and mercury (Hg) forms. Regressions of dissolved organic carbon (DOC), scores of principle component 1 (PC1) from principal component analysis on absorbance and fluorescence indices (Figure 3.4), electrical conductivity (EC), and water temperature in Scotty Creek – Peat, and Smith Creek – Mixed, against A)–D) bulk total Hg (THg; n=24, 24 respectively), E)–H) filtered THg (n=11, 11), I)–L) bulk methylmercury (MeHg; n=24, 23), and M)–P) filtered MeHg (n=11, 11) separated by the site. Water temperature data are from May to September 2019. The model formulas, adjusted R^2 values and p-values of the regressions are displayed, and a 95% confidence interval surrounds the best-fit line if statistically significant (p<0.05).

Increasing EC corresponded to decreasing concentrations of filtered THg and MeHg at the peatland catchment and bulk and filtered THg at the mixed catchment (Figure 3.7). However, EC exhibited a much narrower range at the peatland catchment (129–244 µS cm^{-1}) than at the mixed catchment (263–1064 µS cm^{-1}). In addition, EC significantly decreased with increasing discharge at both sites (R^2=0.41, p<0.001 at peatland catchment; R^2=0.64, p<0.001 at mixed catchment).

Bulk and filtered MeHg increased with the water temperature at the peatland catchment, as did filtered THg (Figure 3.7), with no significant relationships for the same parameters at the mixed

catchment. We further explored indicators of MeHg production (Figure A.3.6), finding strong increases in bulk and filtered %MeHg, MeHg:DOC, and MeHg:A_{254} with the water temperature at the peatland catchment. Conversely, bulk %MeHg decreased with the water temperature at the mixed catchment, while MeHg:DOC and MeHg:A_{254} did not significantly relate to water temperature at the mixed catchment.

3.3.5 Yields of THg, MeHg, and DOC

Cumulative spring and summer yields from 2019 to 2021 of bulk THg ranged from 76–406 ng THg m^{-2} at the peatland catchment and 405–645 ng m^{-2} at the mixed catchment (Figure 3.3, Table A.3.5). Cumulative bulk MeHg yields ranged from 5.21–36.3 ng MeHg m^{-2} at the peatland catchment and 6.06–10.0 ng MeHg m^{-2} at the mixed catchment, while cumulative DOC yield ranged from 1.16–6.63 g DOC m^{-2} at the peatland catchment and 1.37–2.37 g DOC m^{-2} at the mixed catchment. At both sites, 2021 was the only year spring solute yields comprised ≥half of the cumulative yield.

We used the 2006 to 2021 discharge record from the peatland catchment and mixed catchment (2019–2021: measured; 2006–2018: predicted from the mixed catchment proxy) to estimate scenarios of yield magnitude and seasonal partitioning for the rivers (Figure 3.3, Table A.3.5). At the peatland catchment, the mean cumulative yields were estimated to be 209 ng THg m^{-2}, 18 ng MeHg m^{-2}, and 3.0 g DOC m^{-2}. The mean partitioning was roughly equal between freshet and summer yields, albeit with substantial variation. From 2006 to 2021, spring freshet delivered between 15% and 80% of the cumulative solute yields at the peatland catchment. At the mixed catchment, mean cumulative yields from 2006 to 2021 were estimated to be 443 ng THg m^{-2}, 6.6 ng MeHg m^{-2}, and 1.5 g DOC m^{-2}. Spring freshet yields of THg and DOC at the mixed catchment typically outsized summer yields from longer-term estimates, while MeHg was evenly divided or had higher summer yields.

3.4 Discussion

Few studies have monitored stream chemistry and quantified yields of Hg forms in small to mid-sized catchments in permafrost regions. To understand processes that the concentrations and yields of THg, MeHg, and DOC in the face of climate change, we conducted three years of open-water

season sampling within the discontinuous permafrost zone of boreal western Canada, focusing on a peatland catchment and a mixed-landscape catchment. Below, we discuss temporal variabilities of concentrations and yields from the two catchments and link the processes likely responsible for driving variability to climate change and permafrost thaw.

3.4.1 Comparing catchment water chemistry and DOM composition

Overall, the water chemistry and DOM composition in the peatland catchment were characteristic of wetland sources (Bourbonniere, 2009), with higher DOM aromaticity and concentrations of MeHg and DOC and lower pH and EC than the mixed catchment. The water chemistry and DOM composition exhibited greater variability in the mixed catchment. Notably, we found much higher EC and THg concentrations with a greater particulate fraction of Hg forms relative to the peatland catchment. The THg and MeHg concentrations in the peatland catchment and mixed catchment were relatively low but within previously observed ranges for boreal streams in Canada (0.46–20.46 ng THg L^{-1}; 0.03–4.82 ng MeHg L^{-1}; Fink-Mercier, Lapierre, et al., 2022; Lam et al., 2022; Thompson et al., 2023).

We found stronger associations of MeHg-DOM in the peatland catchment, while THg-DOM was strongly correlated in the mixed catchment. Global assessments have found THg-DOM relationships to be typically stronger than MeHg-DOM in surface waters (Lavoie et al., 2019; Wu et al., 2022), although robust coupling, with some seasonal variability, has been observed between MeHg and aromatic DOM in boreal streams (Fink-Mercier, del Giorgio, et al., 2022; Mangal et al., 2022).

3.4.2 Hydrological influences on catchment water chemistry

In the peatland catchment, discharge had no consistent influence on MeHg or THg concentrations, although higher discharge had a moderately positive effect on DOC concentrations and aromaticity. The widespread peatlands were likely responsible for the muted influence of discharge on MeHg, THg, and DOC concentrations. Channel fens constitute much of the stream network in the peatland catchment (Haynes et al., 2022) and are likely to act as biogeochemical reactor sites for MeHg, THg, and DOC in addition to conveying water. Regardless of flow conditions, solutes from other land covers would then move through the fen network, where they are degraded or

transformed and mixed with internal sources, thus reducing the overall variability in solute concentrations delivered to the outflow (Olefeldt & Roulet, 2012; Poulin et al., 2019; Tarbier et al., 2021; Figure 3.8). A Siberian watershed influenced by peatlands likewise exhibited overall chemostatic DOC behavior, with a narrow range of DOC concentrations when considering all observations, whereas event-scale analyses elucidated seasonal shifts in hysteresis loops and flushing relationships (Gandois et al., 2021).

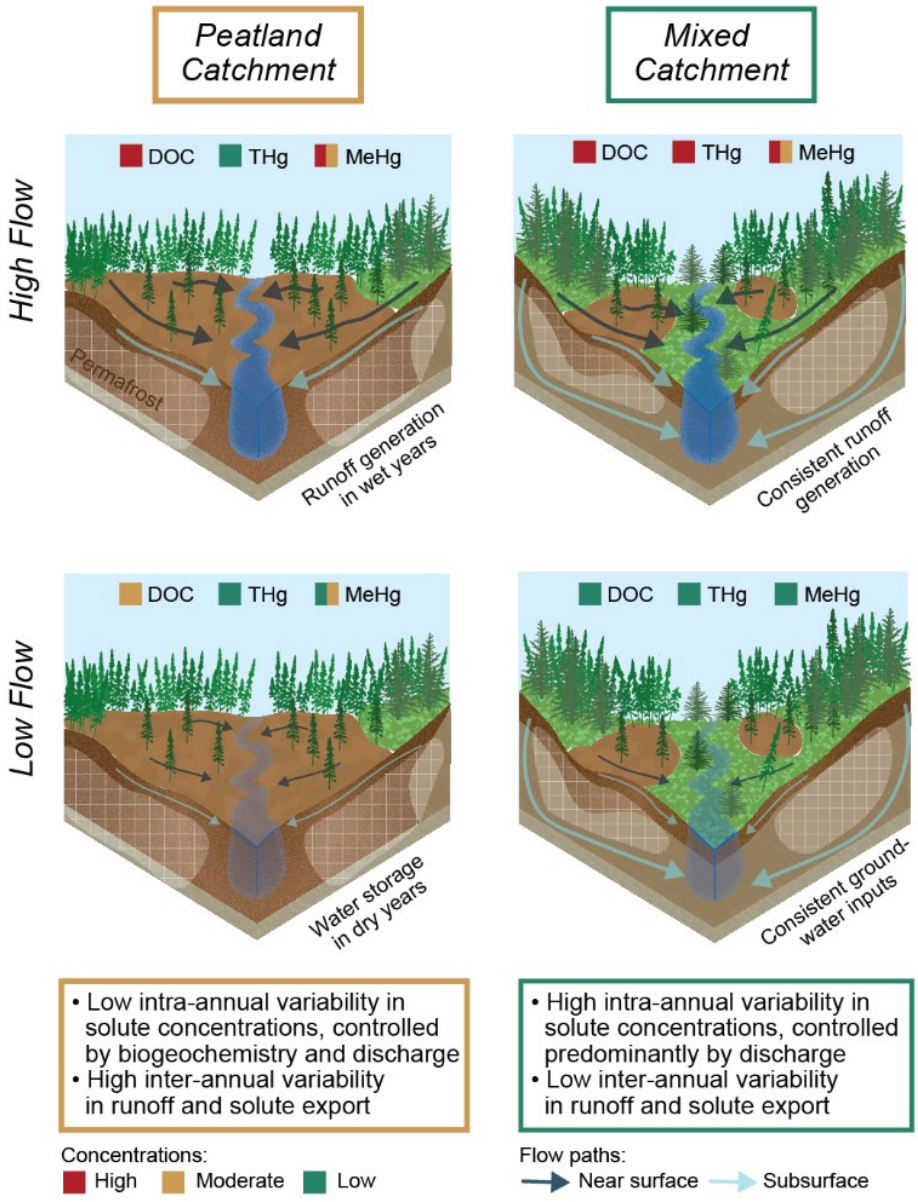

Figure 3.8. Conceptual diagram showing the hydrologic pathways and relative concentration trends of Scotty Creek – peatland catchment compared to Smith Creek – mixed catchment during high and low flow periods. DOC=dissolved organic carbon, THg=total mercury, MeHg=methylmercury.

Examining event-scale patterns of water chemistry from different times of the year can provide further insight into shifting water sources and MeHg mobilization. While MeHg is difficult to monitor at high temporal frequency, we found that dissolved MeHg strongly correlated with A_{254} in the peatland catchment, and we measured A_{254} at high frequency through 2019. The modest and late snowmelt of 2019 rapidly enriched A_{254} at the start of the freshet in the peatland catchment. We interpret this enrichment to signal a shift from groundwater contributions with lower DOM to DOM influenced by surficial organic soils, in contrast to A_{254} dilution during freshet from a strong precipitation signal previously observed elsewhere (Burd et al., 2018; Gandois et al., 2021). A subsequent high-flow event lasting nearly a month through early summer showed slower A_{254} enrichment through anticlockwise hysteresis. Commonly observed in boreal catchments, anticlockwise hysteresis suggests an initial source close to the river (e.g., riparian zones) supplied DOM, followed by increasing contributions from peatlands with higher DOC and MeHg concentrations (Gordon et al., 2016; Shogren et al., 2021; Thompson et al., 2022). The rapid dilution of DOM in response to a late summer high-flow event suggested the initial mobilization of nearby high DOM sources and lower DOM contributions after peak flows, possibly due to increasing groundwater influence during late summer (Burd et al., 2018) that likely delivered lower MeHg concentrations. Given the correlation between dissolved MeHg and A_{254}, high-frequency tracking of A_{254} can plausibly inform MeHg co-transport in peatland-influenced streams where it is not practical to frequently sample MeHg (Thompson, 2021).

The chemodynamic flushing relationship between solute concentrations and discharge at the mixed catchment revealed consistent transport limitation of THg and DOC, with a less systematic response from MeHg. During low flow periods, groundwater contributions likely controlled the high EC and low concentration inputs of THg, MeHg, and DOC (Figure 3.8); DOM adsorption in mineral soils can lead to low DOC concentrations and less aromatic DOM quality (Kaiser & Kalbitz, 2012; Kothawala et al., 2012). With permafrost thaw, high-latitude catchments across the Interior Plains are expected to have increased groundwater interaction with surface waters (Wright et al., 2022). We believe that periods of high flow led to increased hydrological connectivity of organic-rich and riparian soils that contributed higher THg and DOC (Figure 3.8), as shown from chemodynamic flushing responses that aligned with DOC behavior in organic-rich tundra (Shogren et al., 2021) and heterogeneous catchments across Scotland (Pohle et al., 2021).

Event-scale behavior of DOM at the mixed catchment investigated through high-frequency A_{254} monitoring showed DOM enrichment in response to increased flow. In addition, we found increasingly rapid enrichment throughout the summer, which may be linked to enhanced connectivity from high antecedent moisture conditions in the early summer event and the seasonal evolution of subsurface flow paths due to the deepening of the active layer in organic soils (Lafrenière & Lamoureux, 2019). These findings likely reflect patterns of THg concentrations that correlated well with A_{254} in the mixed catchment. Overall, the high-frequency sampling indicated consistent transport limitation during the open water period at the mixed catchment in contrast to the peatland catchment.

In the mixed catchment, erosion was a potential contributor to sediment-bound THg and MeHg. The proportion of particulate MeHg increased with discharge; while THg did not linearly increase with discharge, the catchment had a consistently high particulate fraction of THg relative to the peatland catchment. In catchments with readily erodible sediments, sediment supply has been identified as an important control on concentrations and fluxes of THg and MeHg (e.g., St. Pierre et al., 2018; Staniszewska et al., 2022). The mountainous regions of the mixed catchment could thus deliver sediments, and associated metals, to the catchment outlet.

3.4.3 Biogeochemical influences on catchment water chemistry

Stream water temperature, a likely proxy of metabolic activity in peatlands, was indicated to influence the mobilization of MeHg in the peatland catchment. As such, MeHg is likely to be production-limited in the peatland catchment. In 2019, MeHg concentrations increased with rising water temperature, as did %MeHg, MeHg:DOC, and MeHg:A_{254}, suggesting enhanced microbial methylation (Bravo & Cosio, 2020; Shanley et al., 2022). In addition, filtered MeHg concentrations strongly increased with DOC concentrations and terrestrially-derived DOM; these results provide further evidence of wetlands as environments where MeHg concentrations strongly associate with aromatic DOC (Branfireun et al., 2020; Lavoie et al., 2019). We inferred that higher intensity MeHg co-transport with aromatic DOM (i.e., higher MeHg:A_{254}) occurred during warm summer periods of high MeHg production. During low flow, early-season periods, lower intensity co-transport occurred when DOM quality at the peatland catchment was less aromatic. Therefore, seasonality must be considered when interpreting A_{254} as a proxy for MeHg concentrations (as

referenced previously). Boreal Quebec streams had similar trends, where MeHg:DOC strengthened and increased seasonally with warmer temperatures (Fink-Mercier, del Giorgio, et al., 2022). Production limitations within the mixed catchment may still be present, but other catchment processes (e.g., transport limitation and flushing) were likely more influential.

3.4.4 Drivers of inter- and intra-annual variability in catchment solute yields

Low inter-annual variability in solute concentrations at the peatland catchment was contrasted by high inter-annual variability in runoff and solute yields. A particularly high-flow year at the peatland catchment (2020) resulted in a ≥400% increase in cumulative runoff and yields of THg, MeHg, and DOC relative to a low-flow year (i.e., 2019). The predominance of peatlands likely contributed to this variability, where high runoff generation occurred upon the exceedance of storage thresholds, but low runoff occurred during dry periods when the landscape retains water (Goodbrand et al., 2019). By contrast, the cumulative runoff and solute yields varied by less than two-fold at the mixed catchment, reflecting the lower inter-annual variability in longer-term runoff trends inferred from the nearby gauged Ochre River. Consistent runoff generation at the mixed catchment can be connected to the steeper topographic relief and groundwater inputs from deep flow paths with long residence times that explain the lower inter-annual runoff variability (Utting et al., 2013).

We found freshet solute yields to be variable, despite the importance of spring freshet highlighted in previous studies of northern catchments (Burd et al., 2018; Gandois et al., 2021; Zolkos et al., 2020). The continental climate can result in variable precipitation during winter and summer; the freshet versus summer runoff balance depends on snow cover and summer storms. This variability was highlighted at both sites by the occurrence of summer storms in 2020 that contributed to high summer yields (52–79% of cumulative yields) in comparison to the high freshet yields in 2021 (51–84% of cumulative yields) likely driven by above-average snow pack and high antecedent moisture from the previous year (Sonnentag & Quinton, 2022).

Our work provides data on THg, and MeHg yields from small-medium northern catchments, which are limited in permafrost regions. Permafrost thaw will have very different impacts on THg and MeHg in streams, depending on the type of thaw, land cover, and climate (Tank et al., 2020). In our study catchments, ongoing permafrost thaw in peatlands is expanding the coverage of

thermokarst bogs and fens (Gordon et al., 2016; Haynes et al., 2022), but we observed modest concentrations and yields of THg, MeHg, and DOC compared to other boreal-Arctic catchments across Canada (Table 3.2).

Table 3.2. Comparison of mean bulk total mercury (THg), methylmercury (MeHg), and dissolved organic carbon (DOC) yields and ratios. Data are from this study (2006-2021) and other Canadian boreal-Arctic rivers listed by catchment area.

Site	Area (km^2)	THg (ng m^{-2} y^{-1})	MeHg (ng m^{-2} y^{-1})	DOC (g m^{-2} y^{-1})	MeHg:THg (ng ng^{-1})	THg:DOC (ng g^{-1})	MeHg:DOC (ng g^{-1})	Citation
Thaw slump, Peel River tributary SE†	5.5×10^{0}	3.8×10^{5}	1.8×10^{3}	1.8×10^{0}	4.7×10^{-3}	2.1×10^{5}	1.0×10^{3}	St. Pierre et al. (2018); Zolkos et al. (2019)
Chinusaw, QC	4.4×10^{1}	1.2×10^{3}	7.5×10^{1}	7.8×10^{0}	6.0×10^{-2}	1.6×10^{2}	9.6×10^{0}	Fink-Mercier, Lapierre, et al. (2022); de Melo et al. (2022)
Peatland-dominated Scotty Creek, NWT*	1.3×10^{2}	2.1×10^{2}	1.8×10^{1}	3.0×10^{0}	8.6×10^{-2}	7.0×10^{1}	6.0×10^{0}	This study
Mixed-landscape Smith Creek, NWT*	1.5×10^{2}	4.4×10^{2}	6.6×10^{0}	1.5×10^{0}	1.5×10^{-2}	2.9×10^{2}	4.4×10^{0}	This study
Old Crow, YU	1.4×10^{3}	9.0×10^{2}	1.0×10^{1}	2.1×10^{0}	1.1×10^{-2}	4.3×10^{2}	4.8×10^{0}	Staniszewska et al. (2022)
Nottaway, QC	5.5×10^{4}	2.9×10^{3}	6.4×10^{1}	7.1×10^{0}	2.2×10^{-2}	4.1×10^{2}	9.0×10^{0}	Fink-Mercier, Lapierre, et al. (2022); de Melo et al. (2022)
Churchill, MB	2.8×10^{5}	1.3×10^{2}	1.4×10^{1}	1.4×10^{0}	1.1×10^{-1}	9.3×10^{1}	1.0×10^{1}	Kirk & St. Louis, (2009); Liu et al. (2022)
Mackenzie, NWT	1.8×10^{6}	2.0×10^{3}	1.1×10^{1}	1.0×10^{0}	5.6×10^{-3}	1.9×10^{3}	1.1×10^{1}	Emmerton et al. (2013); Liu et al. (2022)

†Calculated from spot discharge measurements and grab sample concentrations

*Cumulative spring-summer yields, missing autumn and winter

Land cover and climate could partially explain the relatively low yields of THg, MeHg, and DOC (Table 3.2). The yields and yield ratios (i.e., MeHg:THg, THg:DOC, and MeHg:DOC) of the peatland catchment were most similar to the Churchill River (Kirk & St. Louis, 2009), a large wetland-influenced river system. The mixed catchment had solute yields and yield ratios in between the wetland-influenced Churchill and the more sediment-laden Old Crow and Mackenzie rivers (Emmerton et al., 2013; Kirk & St. Louis, 2009; Staniszewska et al., 2022), which aligns with mixed-landscape contributions from peatlands, mountains, and uplands. Both the peatland and mixed catchments had lower solute yields than the Eastern James Bay rivers of variable size (Chinusaw and Nottaway rivers), likely explained by a much wetter regional climate than the dry Interior Plains (Fink-Mercier, Lapierre, et al., 2022; de Melo et al., 2022). The most dramatic yields of THg and MeHg were observed downstream of retrogressive thaw slumps in the Peel Plateau, related to steep relief, high ice content within the widespread permafrost, and erodible Pleistocene tills (St. Pierre et al., 2018; Tank et al., 2020).

3.4.5 Changing climate and hydrology in the Interior Plains

Continued permafrost thaw and rising temperatures may result in enhanced production of MeHg from Hg^{II} in thaw wetlands (Gordon et al., 2016; Poulin et al., 2019; Tarbier et al., 2021) and mobilization of DOC (Frey & Smith, 2005; Olefeldt et al., 2014). Increased downstream transport of MeHg and DOC has negative implications for water treatment processes (Matilainen et al., 2010) and the toxicity of country food (Basu et al., 2022). Therefore, continued and expanded monitoring of small and mid-sized catchments that contribute terrestrial Hg and DOC to large Arctic rivers and, eventually, the ocean will be required in the coming years. In addition, understanding lateral DOC transport will be necessary for evaluating the carbon sink-source strength of thawing landscapes (Hugelius et al., 2020; Vonk et al., 2019). The ongoing sampling of the peatland catchment will be particularly essential, as the catchment suffered an intense wildfire in October 2022 (Lamberink, 2022) with potential impacts on runoff generation, MeHg production, and solute loads (Ackley et al., 2021; Burd et al., 2018; Nelson et al., 2021).

Our study suggests that climate change could influence MeHg yields by reducing limitations on production (i.e., via potential increases in temperature-driven Hg^{II} methylation) and transport (i.e., by increasing runoff), especially in peatland-dominated catchments. We showed runoff to be a primary driver of solute yields, with particularly variable runoff at the peatland catchment that reflects the runoff-regulating function of peatlands. Increasing solute yields may be expected with increasing streamflow regimes in peatland-dominated catchments of the Interior Plains due to landscape change and permafrost thaw (Mack et al., 2021). Moreover, despite current interannual runoff stability at the mixed catchment, chemodynamic increases of THg and DOC concentrations from increased flows imply a heightened sensitivity of solute yields to enhanced summer precipitation and streamflow predicted in high latitudes (Lafrenière & Lamoureux, 2019).

3.5 Conclusions

We used a three-year dataset to show that MeHg, Hg, and DOC concentrations and yields in two northern catchments underlain by discontinuous permafrost were governed by the hydrology and biogeochemical processes of their contributing landscapes. Variability in the water chemistry of the peatland catchment was not primarily driven by discharge, with a signal of summertime Hg^{II} methylation as MeHg concentrations increased with water temperature. Instead, high inter-annual

variability in runoff and solute yields was likely driven by peatland hydrological function shifting from water storage in drier periods to runoff generation in wetter periods. By contrast, the chemodynamic solute flushing in the mixed catchment reflected shifts from groundwater influence during low flows to the predominance of peatland and riparian zone inputs during high flows. During the sampling period, annual runoff and solute yields varied little at the mixed catchment. With ongoing permafrost thaw and changes to temperature and precipitation, THg, MeHg, and DOC yields will likely be sensitive to shifting runoff patterns and biogeochemical controls on DOC and MeHg production.

4. Enhanced methylmercury formation in thawing permafrost peatlands of northwestern Canada

Abstract

Permafrost thaw in northern peatlands may enhance the production of methylmercury (MeHg), a bioaccumulative neurotoxin that poses hazards to human health. Here we demonstrate that the rates of microbial methylation of inorganic mercury (Hg) to MeHg in northern peatland complexes vary across distinct thermokarst wetlands (i.e., nutrient-poor bogs and nutrient-rich fens) that develop after the thawing of permafrost peatlands. From the analysis of potential methylation rates (k_m) and chemistry of soil and porewater in twelve wetlands across a 500 km latitudinal gradient in northwestern Canada, we observed higher, but more variable, MeHg concentrations and k_m in thermokarst wetlands compared to intact permafrost peatlands. Methylation rates were not associated with the abundance of MeHg production genes (*hgcAB*) which did not vary among wetlands or across the latitudinal gradient. Instead, Hg methylation potential increased with higher water table, labile organic matter, higher pH, and key terminal electron acceptors (sulfate and iron). We expect enhanced methylation with continued permafrost thaw, with soil %MeHg (MeHg:THg) increasing by a predicted 65% at a landscape scale in northwestern Canada by 2100. Wetland trophic status, groundwater connectivity, and hydrological functioning will likely control MeHg production and export in the changing North.

4.1 Introduction

Ongoing permafrost thaw in northern peatlands leads to drastic shifts in environmental conditions, which may enhance the microbial production (methylation) of the neurotoxin methylmercury (MeHg) from mercury (Hg) stored in peat soils (Jonsson et al., 2022). Plants and organic matter in remote environments accumulate Hg from atmospheric deposition, including the uptake of gaseous elemental Hg^0 from distant sources and minor contributions of divalent inorganic Hg^{II} (Obrist et al., 2017). Rapid permafrost thaw in northern peatlands of northwestern Canada is leading to the collapse of relatively dry permafrost plateaus (Wright et al., 2022), developing favorable environments for Hg^{II} methylation, a predominantly anaerobic process, in subsequently formed thermokarst wetlands (i.e., bogs and fens) with waterlogged conditions (Fahnestock et al., 2019; Gordon et al., 2016; Poulin et al., 2019; Tarbier et al., 2021). In addition, enhanced hydrological connectivity with permafrost thaw and thermokarst wetland development (Connon et al., 2014) may increase the transport of solutes such as MeHg to downstream aquatic environments (Varty et al., 2021). As MeHg bioaccumulates and biomagnifies in aquatic food webs, understanding changes to MeHg production and export in landscapes affected by permafrost thaw is essential for northern Indigenous communities that consume fish as a healthy and culturally significant food source (Basu et al., 2022).

Peat plateaus, bogs, and fens fall on a trophic gradient of nutrient and vegetation species richness (plateau≤bog<poor fen<moderate-rich fen) (Vitt & Chee, 1990), with distinctive biogeochemical characteristics that may control Hg^{II} methylation efficiency. Enhanced methylation may occur in anoxic environments with bioavailable Hg^{II}, abundant terminal electron acceptors (TEAs, i.e., sulfate [SO_4^{2-}] or ferric iron [Fe^{III}]), and labile dissolved organic matter (DOM) (Bravo & Cosio, 2020). Peat plateaus typically have dry near-surface conditions with highly aromatic DOM pools. Thermokarst bogs are wetter, DOM-rich environments fed by precipitation and solutes of surrounding wetlands and uplands. Only fens receive groundwater inputs that can deliver TEAs and nutrients from the weathering of mineral sediments that supports richer vegetation and more labile DOM, with water tables near the ground surface (Bourbonniere, 2009; Poulin et al., 2019; Vitt & Chee, 1990).

Crucially, microbes with *hgcAB* genes facilitate methylation as *hgcA* is a methyl carrier, and *hgcB* is an electron donor for corrinoid cofactor reduction (Parks et al., 2013). Key microbial Hg^{II}

methylators in wetlands include SO_4^{2-}-reducing bacteria (Gilmour et al., 1992), Fe-reducing bacteria (Fleming et al., 2006), and methanogens (Gilmour et al., 2013; Hamelin et al., 2011) as identified by the presence of *hgcAB* genes or methylation experiments that inhibit specific guilds.

Tracing links between DOM quantity and composition, TEAs, and microbial communities can provide valuable information on the trajectory of MeHg production in rapidly thawing northern peatlands. Here, we investigated MeHg production in thawing peatlands by analyzing the chemistry of soil and porewater, *hgcAB* gene abundance, and potential Hg^{II} methylation rates (k_m). We sampled twelve wetlands of varying nutrient richness and groundwater connectivity that span >500 km of the Taiga Plains in northwestern Canada (Figure 4.1), a region undergoing rapid warming and landscape change (Wright et al., 2022). Permafrost in the region formed epigenetically, where organic matter accumulation initiated after the last glacial maximum (~ 8500 cal yr bp), and permafrost aggradation occurred centuries to millennia later (~ 1800 cal yr bp at 59°N, Heffernan et al., 2020; ~ 5000 cal yr bp at 61°N, Pelletier et al., 2017). Although organic matter in peat plateaus may not be particularly labile upon thaw due to millennia of decomposition prior to permafrost aggradation, thermokarst development results in soil inundation and shifts the vegetation community towards higher productivity and lability of organic matter inputs (Halsey et al., 1995; Heffernan et al., 2020; Zoltai, 1993). We expected low potential methylation rates in peat plateaus with drier, nutrient-poor conditions, intermediate methylation rates in bogs, and highest methylation rates in fens from productive conditions with groundwater-mediated delivery of TEAs and nutrients, with labile DOM pools.

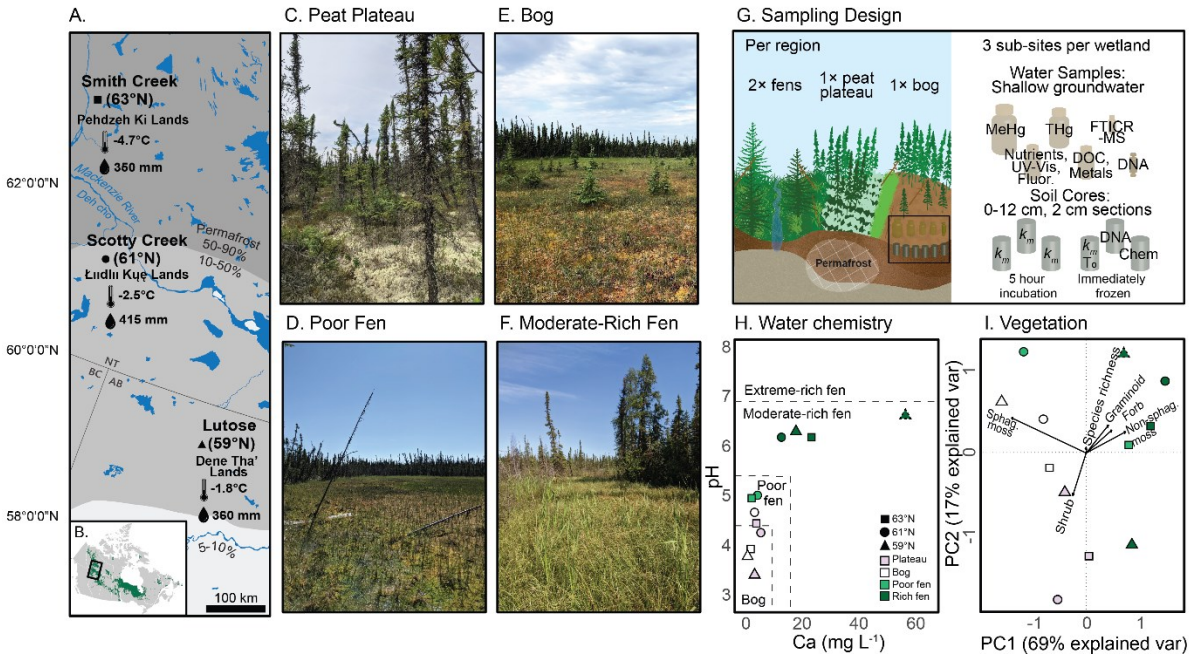

Figure 4.1. Study sites and sampling design. A) Study site locations relative to permafrost zones (Brown, Ferrians, Heginbottom, et al., 2002), with mean annual air temperature and total annual precipitation (Fick & Hijmans, 2017), B) study region within Canada with an overlay of >25% peatland extent (Hugelius et al., 2020), photographic examples of wetland sites including C) peat plateau (63°N), D) poor fen (63°N), E) bog (61°N), and F) moderate-rich fen (59°N), G) sampling design across regions and wetlands, H) site classification based on pH and calcium (Ca; Alberta Environment and Sustainable Resource Development, 2015; Bourbonniere, 2009) and I) vegetation composition. MeHg=methylmercury, THg=total mercury, FTICR-MS=Fourier transform ion cyclotron mass spectrometry, Fluor=fluorescence spectroscopy, DOC=dissolved organic carbon, k_m=potential Hg^{II} methylation rates, chem=soil chemistry. Photos: L. Thompson.

4.2 Materials and methods

4.2.1 Study Sites

Samples were collected in July 2021 at three regional peatland sites: Lutose (59°N), Scotty Creek (61°N), and Smith Creek (63°N). The regions span ~500 km of the sporadic to extensive discontinuous permafrost zones (Brown, Ferrians, Heginbottom, et al., 2002) of northern Alberta and the southern Northwest Territories (Figure 4.1, Table A.4.1). The sites are located in the homelands of Dene Tha' First Nation, Łíídlıı Kų́ę First Nation, and Pehdzeh Ki First Nation, respectively. The region has a continental climate with cold winters and short, warm summers, with mean annual air temperature ranging from -4.7 to -1.8°C and mean annual precipitation ranging from 360 to 415 mm (Fick & Hijmans, 2017). At each peatland site, we sampled one peat plateau (permafrost present) and three permafrost-free wetlands spanning a trophic gradient: one bog, one nutrient-poorer fen, and one nutrient richer-fen (Figure 4.1). The nutrient status of the

wetlands (Figure 4.1) was characterized based on the pH and calcium (Ca) concentrations of porewater and vegetation composition (Alberta Environment and Sustainable Resource Development, 2015; Bourbonniere, 2009). While we targeted relatively richer and poorer fens at each region, the 59°N fens were generally richer than the 61°N and 63°N fens (Figure 4.1H). We completed vegetation surveys using 0.5×0.5m quadrats at four to ten randomly selected locations within each wetland, where we determined species composition, percent cover, and calculated species richness. Generally, sphagnum mosses were dominant in bogs, fens had greater brown moss and graminoid cover, and peat plateaus had greater shrub/tree coverage (Figure 4.1I). Table A.4.2 contains a vegetation species list, while Figure A.4.1 displays the geochemistry of porewater and soil for each sampled wetland.

4.2.2 Water sampling and analysis

We collected shallow groundwater samples from three locations per wetland by hand or with a peristaltic pump with Teflon tubing. A 10×10 cm section of soil from a microtopographic hollow was removed to ~20 cm depth and allowed to fill with water and settle from disturbance for ≥1 hour. Water table depth was then measured from the ground surface. Total Hg (THg) and MeHg samples were collected in certified pre-cleaned glass amber bottles (Environmental Supply Company, Inc., Richmond, VA, US) and preserved with 0.2% and 0.4% trace-metal grade hydrochloric acid (HCl), respectively. Hg samples were analyzed in the Canadian Association for Laboratory Accreditation-certified Biogeochemical Analytical Service Laboratory (BASL, University of Alberta). Water samples were analyzed for THg concentrations on a Tekran 2600 Mercury Analyzer (Tekran Instruments Corporation, Knoxville, TN, US) following EPA Method 1631, calibrated with a 9-point standard curve (0–40 ng L^{-1}) daily with Brooks Rand $HgCl_2$ standards (R^2>0.999). Water samples were analyzed for MeHg with EPA Method 1630 using isotope dilution, distillation, and analysis on a Tekran 2700 Methylmercury Analyzer (Tekran Instruments Corporation, Knoxville, TN, US) coupled to an Agilent 7900 inductively coupled plasma-mass spectrometer (ICP-MS; Agilent Technologies, Inc, Santa Clara, CA, US). Samples were spiked with isotopically enriched $Me^{201}Hg$ as an internal standard to correct for MeHg loss or formation during analysis, with $Me^{202}Hg$ quantified as the ambient tracer. Blanks with reagents were analyzed alongside samples.

We measured each subsite's physical parameters, nutrients, major ions, and DOM characteristics. Electrical conductivity (EC) and pH were measured on-site with a calibrated Elite PCTS sensor (Thermo Fisher Scientific, Waltham, MA, US). We collected two filtered (0.45 µm polyethersulfone membrane; Sartorius AG, Göttingen, Germany) 60 mL water samples in acid-washed amber glass bottles. One sample was preserved with 0.6 mL of 2M HCl for dissolved organic carbon (DOC) concentration and metal analysis, while the other sample remained non-acidified for nutrient analysis and DOM composition (absorbance and fluorescence spectroscopy). We collected an additional 15 mL of filtered (0.45 µm) water at each sub-site in acid-washed glass vials, where 5 µL of concentrated HCl were added, and samples were covered with aluminum foil before analysis for DOM composition with Fourier transform ion cyclotron resonance mass spectrometry (FTICR-MS). All water samples were kept cool in transit to the laboratory, and nutrient samples were immediately frozen until analysis.

To collect a microbial community sample in porewater, we connected a 0.22 µm Sterivex filter (MilliporeSigma, Burlington, MA, US) to the peristaltic pump and ran the pump until the filter clogged, noting the volume of filtered water (minimum=25 mL). After extracting all water from the filter, the Sterivex unit was frozen to -20°C in the field and later transferred to -80°C until analysis (see 4.2.4 Microbial Analysis).

The Natural Resources Analytical Laboratory (University of Alberta) analyzed samples for DOC, total dissolved nitrogen (TDN), nutrients, and metals. A TOC-L combustion analyzer with a TNM-L module (Shimadzu, Japan) measured DOC and TDN concentrations. Colorimetry (Thermo Gallery Plus Beermaster Autoanalyzer, Thermo Fisher Scientific, US) determined concentrations of chloride (Cl), nitrate (NO_3-N), nitrite (NO_2-N), ammonium (NH_4-N), phosphate (PO_4-P), and sulfate (SO_4^{2-}S). Concentrations of sodium (Na), potassium (K), calcium (Ca), manganese (Mn), iron (Fe), copper (Cu), zinc (Zn), magnesium (Mg), phosphorus (P), and sulfur (S) were measured by inductively coupled plasma optical emission spectroscopy (ICP-OES, iCAP6300, Duo, Thermo Fisher Scientific, Waltham, MA, US).

We assessed the aromaticity of the DOM using the specific ultraviolet absorbance at 254 nm ($SUVA_{254}$), where $SUVA_{254}$ values increase with DOM aromaticity (Weishaar et al., 2003). The absorbance of DOM was measured from 200 to 700 nm (UV-1280, UV-VIS Spectrophotometer,

Shimadzu Corporation, Kyoto, Japan) and corrected with Milli-Q water blanks. We calculated $SUVA_{254}$ after correcting decadal absorbance at 254 nm (A_{254}, cm^{-1}) for interference by Fe (Weishaar et al., 2003). We used an Aqualog fluorometer (Horiba Scientific, Kyoto, Japan) to measure DOM fluorescence emission-excitation matrix spectra (EEMs); DOM composition indices were calculated, including fluorescence index (McKnight et al., 2001; FI), humification index (Ohno, 2002; HIX), and biological index (Huguet et al., 2009; BIX) (Table A.4.3).

The molecular composition of DOM in the wetlands was analyzed via FTICR-MS at the Trent University Water Quality Center. Samples were solid phase extracted (Priority PolLutant cartridge, Agilent Technologies, Inc, Santa Clara, CA, US) prior to analysis to concentrate the DOM and remove impurities (i.e., salts and ions) that inhibit electrospray ionization (Dittmar et al., 2008). We used a 7 T Bruker Solarix XR FTICR-MS (Bruker, Billerica, MA, US) housed in the Trent University Water Quality Center to characterize DOM using parameters from Mangal et al. (2020). We used Bruker DataAnalysis (v. 4.4) for baseline corrections, background noise subtractions, and formula assignment and normalized compound classes to the total number of assigned formulae before calculating weighted intensity abundances. Compound classes (Kellerman et al., 2015) and FTICR-MS indices (Koch & Dittmar, 2006; Riedel et al., 2012) are described in Table A.4.3. To identify molecular level correlations between intensity-weighted FTICR-MS derived DOM molecules and MeHg concentrations, we used Spearman's rank correlation similar to Mangal et al. (2020) with an in-house script in R (Version 4.0.4). Only significant ($p<0.05$) molecules were reported, and the *wPerm* package was used at 999 permutations to minimize type I errors. Correlations were plotted in a Van Krevelen space to relate the compositional properties of DOM to MeHg concentrations.

4.2.3 Soil sampling and analysis

At each subsite, we collected soil cores from a microtropographic hollow with 5 cm diameter Lexan core tubes to a depth of 12 cm. We sampled adjacent hollows from which water samples were collected to ensure the presence of representative porewater. Three separate cores for soil chemistry analysis and microbial composition were combined at 2 cm intervals into sterile Ziplock bags, homogenized, and frozen at -20°C in the field.

Soil samples were dried for 24 hours at 55°C, ground first through a 40-mesh sieve, and then ground to a fine powder using a ball mill (Tungsten carbide grinding tools; MM400, Restch, Germany) to measure elemental contents and the degree of peat decomposition (humification). We measured humification through Fourier-transform infrared (FTIR) spectroscopic analysis at the University of Münster Institute of Landscape Ecology. Samples were prepared from 2 mg dry weight of powdered soil, ground with 200 mg of potassium bromide, and pressed into pellets for analysis. FTIR spectra were scanned between 4000 to 650 cm^{-1} with a resolution of 2 cm and 32 scans per sample on an FTIR spectrometer (Varian 660, Agilent Technologies, Inc, Santa Clara, CA, US). We subtracted a potassium bromide background from the spectra and performed baseline correction. The spectra were preprocessed using the R package *ir* (Teickner, 2021). We used R package *irpeat* (Teickner & Hodgkins, 2021) to compute humification indices by dividing intensity at 1420/1090 cm^{-1} (relative presence of phenolic and aliphatic structures to polysaccharides), 1510/1090 cm^{-1} (relative presence of aromatic C=C or C=O of amides to polysaccharides), 1630/1090 (relative presence of aromatics and aromatic or aliphatic carboxylates to polysaccharides), and 1720/1090 (relative presence of carboxylic and aromatic esters to polysaccharides) (Harris et al., 2020; Teickner et al., 2022). Concentrations of carbon (C) and nitrogen (N) were analyzed by catalytic combustion using an elemental analyzer (EA 3000, Eurovector, Italy). Concentrations of other major elements (data: Thompson et al., 2022) were analyzed from 500 mg of ground, powered sample pressed into a 13 mm pellet and used wavelength dispersive X-ray fluorescence spectroscopy (WD-XRF; ZSX Primus II, Rigaku, Japan). The WD-XRF was calibrated with certified reference materials, including peat, plant, and sediment, in addition to in-house working standards (Teickner et al., 2022).

We determined potential gross rates of Hg^{II} methylation (k_m) and MeHg demethylation (k_d) by conducting in-situ assays of enriched Hg stable-isotope tracers (Lehnherr, St. Louis, & Kirk, 2012; Varty et al., 2021). Three intact soil cores were collected from 0 to 12 cm depth with 5 cm diameter Lexan core tubes with silicone-filled injection ports every 1 cm. Solutions of enriched $^{198}Hg^{II}$ and $Me^{199}Hg$ spike diluted in filtered porewater (0.45 μm) and equilibrated for one hour were injected from the surface at 1 cm intervals from water table depth to 12 cm depth. Injections added 77.88 ng $^{198}Hg^{II}$ and 0.257 ng $Me^{199}Hg$ each 1-cm interval (3.96 ng $^{198}Hg^{II}$ cm^{-3}; 0.013 ng $Me^{199}Hg$ cm^{-3}). After five hours of incubation in the extraction hole, 2 cm soil sections were collected, stored in whirl-pack bags, and frozen within an hour of collection. A blank soil core was collected

alongside the assays, sectioned, bagged, amended with $^{198}Hg^{II}$ and $Me^{199}Hg$ spike, and immediately frozen until analysis at -20°C.

We freeze-dried and homogenized the isotope assay soil samples before analysis at the Biogeochemical Analysis Service Laboratory (BASL) at the University of Alberta. THg concentrations of isotope tracers were determined via microwave digestion of a 0.20 g dry-weight sample with 12 mL reverse aqua regia (9 mL of concentrated nitric acid and 3 mL of concentrated HCl). Bromine chloride (BrCl) oxidized digest solution was analyzed on a Tekran 2600 (Tekran Instruments Corporation, Knoxville, TN, US) coupled with an Agilent 7900 ICP-MS (Agilent Technologies, Inc, Santa Clara, CA, US) with a stream of argon carrier gas to quantify individual isotopes. MeHg concentrations of isotope tracers were determined on 0.12 g dry weight of solid samples (+45 g MilliQ water) amended with 500 µL of 50% sulfuric acid and 200 µL 20% potassium chloride, in addition to an internal standard ($Me^{201}Hg$) to correct for procedural recovery. Samples were distilled at 147°C for approximately three hours. The distillate was ethylated with sodium tetraethyl borate, followed by purge and trap of volatile Hg species on Tenax trap thermally desorbed and separated using a GC glass column, packed with 15% OV-3 Chromosorb (60/80 mesh). MeHg species were detected on a Tekran 2700 (Tekran Instruments Corporation, Knoxville, TN, US) coupled with an Agilent 7900 ICP-MS (Agilent Technologies, Inc, Santa Clara, CA, US). Blanks, duplicates (<10% RSD), spikes (recovery range: 93-110%, mean: 103%), and reference material (Hg: MESS-4 [National Research Council Canada, Ottawa, ON, Canada]; within certified concentrations, 90 ± 40 ng Hg g^{-1}; MeHg: SQC1238 [Sigma-Aldrich, St. Louis, MO, US], within certified concentrations of 10.00 ± 0.35 ng MeHg g^{-1}) ensured quality control.

Soil THg (inorganic + organic Hg) and MeHg concentrations were calculated using the isotopic signal from $^{202}Hg^{II}$ and $Me^{202}Hg$ concentrations. In addition, a subset of non-spiked soil chemistry samples was analyzed for MeHg concentrations at Stockholm University as described by Tarbier et al. (2021); Figure A.4.2 shows a strong agreement between the contrasting methods. We used first-order kinetics to calculate k_m as the proportion of added ^{198}Hg methylated to $Me^{198}Hg$, divided by incubation time (5 hours). k_d was calculated by first-order decay kinetics (k_d=-1/t $\ln[MeHg_t/MeHg_0]$), where t=incubation duration, $MeHg_0$=starting concentration, and

$MeHg_t$=ending concentrations. No demethylation was detected during the incubation period in several samples.

4.2.4 Microbial analysis

Microbial analysis was undertaken by the Ecosystems and Global Change group at Cambridge University. DNA was extracted from Sterivex samples with a previously established phenol-chloroform method (Nercessian et al., 2005), scaling the volumes of all chemicals used to 600 µL of cetyltrimethylammonium bromide. DNA was extracted from 0.3 g of soil with the DNeasy Powersoil Pro Kit (QIAGEN N.V., Venlo, The Netherlands). A dsDNA High Sensitivity Assay Kit (Thermo Fisher Scientific, Waltham, MA, US) determined the quantity of DNA in each extracted sample on a Qubit 3.0 Fluorometer.

We used quantitative PCR (qPCR) to estimate the abundance of *hgcAB* genes, essential for Hg^{II} methylation, and 16S rRNA, a housekeeping gene to normalize *hgcAB* abundance. We amplified the ORNL-HgcAB-uni-F/ORNL-HgcAB-uni-R primer pair to determine the abundance of *hgcAB* genes (Christensen et al., 2016) and the primer pair 515F-Y/926R to determine the presence of 16S rRNA (Parada et al., 2016). qPCR was conducted on CFX Connect Real-Time PCR Detection System (Bio-Rad, Hercules, CA, US), using Luna® Universal qPCR Master Mix (New England Biolabs, Ipswich, MA, US). The qPCR cycles for *hgcAB* involved initial denaturation at 95°C (2 min); 5 cycles of touchdown at 95°C (30 s), 68°C (dropping 2°C per 30 s cycle), 72°C (30 s); 40 cycles of 95°C (30 s), 55°C (30 s), and 72°C (60 s); final extension at 72°C (5 min) (Bae et al., 2019; Gionfriddo et al., 2020). qPCR cycles for 16S rRNA included initial denaturation at 95°C (3 min); 40 cycles of 95°C (45 s), 50°C (45 s), 68°C (90 s); final extension at 68°C (5 min) (Parada et al., 2016). Abundances were then estimated from a standard curve generated for each qPCR run by relating log-transformed gene abundance to quantification cycle (Ct) values with linear regression (*hgcAB* R^2: 0.9955–0.9981; 16S R^2: 0.9942–0.9977). Cell cultures of *Geobacter sulfurreducens* PCA (American Type Culture Collection no. 51573) from the Leibniz-Institute DSMZ-German Collection of Microorganisms and Cell Cultures were extracted as a positive control to generate standard curves for 16S and *hgcAB* genes. Amplified *G. sulfurreducens* were purified using Monarch® DNA Gel Extraction Kit Protocol (NEB #T1020, New England Biolabs, Ipswich, MA, US) and diluted in a 10-times series from 10^8 copies to 10^4 copies for each gene.

4.2.5 Statistical analyses

Statistical analyses were performed in RStudio® utilizing R version 4.2.0 (R Core Team, 2022). We used principle component analysis (PCA) to assess variation in vegetation composition and DOM composition among the wetland porewater with the R package *vegan* (Oksanen et al., 2022). We used the *lmPerm* R package for permutational analysis of variance (perANOVA) tests to examine the variation of THg concentrations, MeHg concentrations, the MeHg to THg ratio (%MeHg), *hgcAB* gene abundance, and k_m values in soil (factors: wetland class, region, depth) and porewater (factors: wetland class, region) (Wheeler & Torchiano, 2016). Relationships between geochemical variables, dissolved organic matter composition, and methylation potential were explored with the *vegan* R package's redundancy analysis (RDA) (Oksanen et al., 2022). We used the mean values per wetland from the porewater (triplicates) and soil (0-12 cm depth) for the RDA.

4.3 Results and discussion

4.3.1 Increases in MeHg concentrations and methylation potential in thermokarst wetlands

The thermokarst wetlands had higher soil %MeHg (a proxy for net methylation), k_m, MeHg concentrations, and lower THg concentrations than the peat plateaus (Figure 4.2). As inferred from soil MeHg concentrations, %MeHg, and k_m, methylation potential increased with trophic status (plateau < bog < fen). We found THg, MeHg, %MeHg, and k_m varied significantly among regions and wetland class; among regions, differences were likely driven by higher values observed at the rich fens at 59°N. Only THg concentrations significantly varied with depth in these near-surface samples, with a general decline in concentrations. The abundance of Hg^{II} methylation genes, *hgcAB* normalized by 16S rRNA, showed no significant differences among the region, wetland class, or depth in peat (p>0.05). Potential k_d varied among wetland classes without a clear relation to wetland trophic status, and no demethylation was detected in several samples (Figure A.4.3).

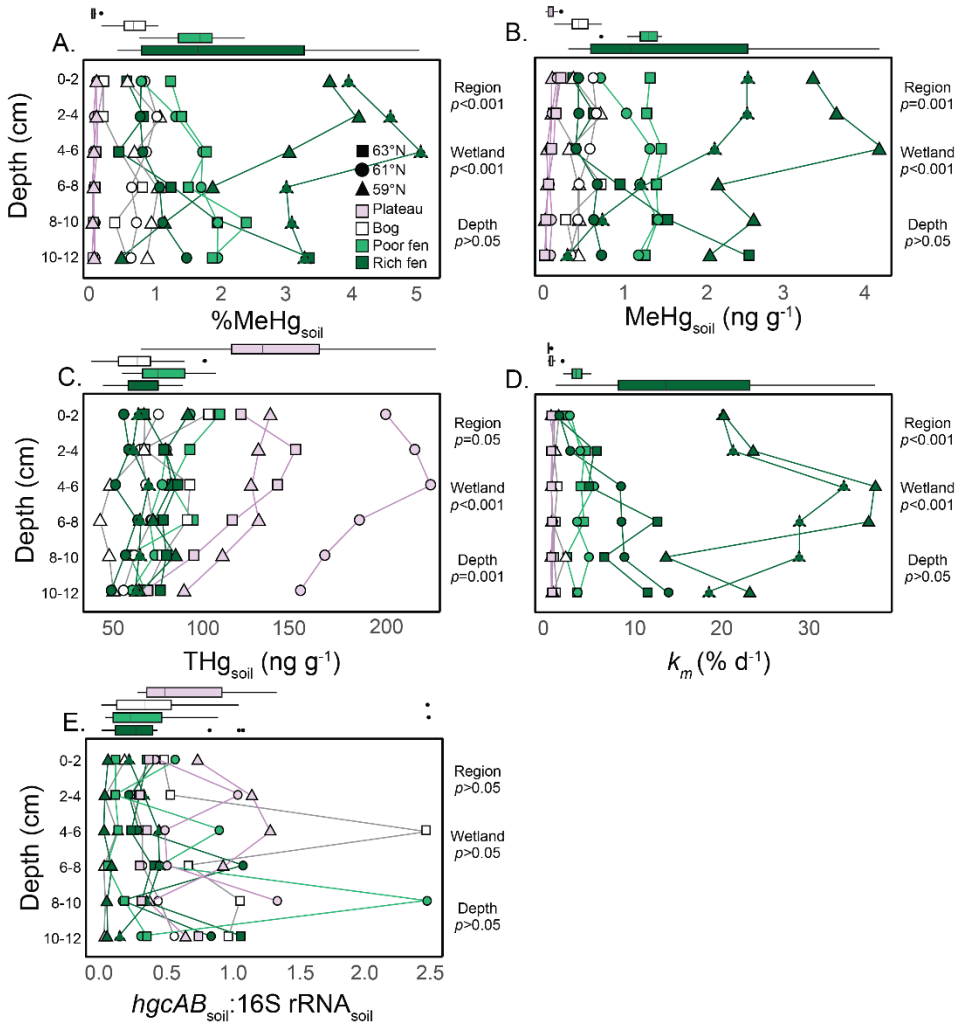

Figure 4.2. Higher and more variable methylation potential in soils of thermokarst wetlands than in peat plateaus. Soil profiles from 0–12 cm depth for A) %MeHg (methylmercury to total mercury concentration ratio, [MeHg]/[THg]), concentrations of B) MeHg and C) THg, D) potential methylation rate (k_m), and E) *hgcAB* genes in soil normalized by 16S rRNA; values are mean of triplicate samples grouped by wetland classification. Fens are separated by moderate-rich and poor classification, with two moderate-rich fens at 59°N; the relatively richer fen at 59°N has a dashed border. The *p*-values from testing the region, wetland class, and depth variability with permutational analysis of variance (perANOVA) are displayed beside the plots, and boxplots of the median, first, and third quartiles, whiskers of 1.5 times the interquartile range, and outliers grouped by wetland classification are above each plot.

We found a close agreement between short-term MeHg production potential (k_m) and the longer-term balance of net methylation (%MeHg) in soil. Soil k_m was a significant predictor of MeHg concentrations and %MeHg (Figure A.4.4, R^2=0.54 and 0.58, respectively, p<0.001), and although several samples had no detected demethylation, k_m/k_d patterns among wetland classes (Figure A.4.3B) roughly aligned with %MeHg. Observed results suggest that enriched isotope tracers may predict longer-term methylation activity despite seasonal variability (Tjerngren et al., 2012; Varty

et al., 2021) and the potential for the bioavailability of added tracers to differ compared to natural conditions (Jonsson et al., 2012).

The abundance of *hgcAB* genes did not drive methylation potential in the studied wetlands. We found *hgcAB* gene abundances in soils to poorly predict %MeHg, concentrations of MeHg and THg, and k_m (Figure A.4.5), as observed in other environments (Christensen et al., 2019). While *hgcAB* was ubiquitous across wetland classes, we observed some of the lowest normalized *hgcAB* abundances in samples with higher net methylation (inferred from %MeHg, MeHg concentrations, and k_m; Figure A.4.5). Given the variation in methylation efficiency across wetland classes, investigating metatranscriptomics could reveal higher gene expression in the sites with higher net methylation, despite a smaller proportion of microbes with the *hgcAB* genes. For example, samples from permafrost peatlands in Sweden showed higher *hgcA* expression in fens than bogs, with no *hgcA* transcripts in permafrost peatlands (McDaniel et al., 2020), aligning with our results for k_m, %MeHg, and MeHg concentrations in soil samples. MeHg production requires a synergy of Hg bioavailability and microbial methylation capacity (Peterson et al., 2023), where the availability of Hg^{II} for uptake in microbes is controlled by complexation with DOM and S species (Bravo & Cosio, 2020). We suggest Hg bioavailability and environmental conditions as limiting factors for methylation efficiency in the wetlands due to the widespread presence of *hgcAB* in contrast to variable net methylation across wetland classes.

4.3.2 Potential downstream MeHg mobilization

We studied porewater concentrations of MeHg and THg to further link soil MeHg production potential to downstream MeHg mobility and the hydrological functioning of thermokarst wetlands. We found that thermokarst wetland porewaters had higher %MeHg and concentrations of MeHg and THg than peat plateau porewaters (Figure 4.3), falling within the range of previously reported concentrations (Fahnestock et al., 2019; Gordon et al., 2016; Poulin et al., 2019). Still, concentrations were variable within individual wetlands and within wetland classes. As observed in the soil samples, *hgcAB* genes in porewater, normalized by 16S rRNA, showed no significant differences among region or wetland class and poorly predicted patterns of %MeHg and concentrations of THg and MeHg (Figure A.4.5).

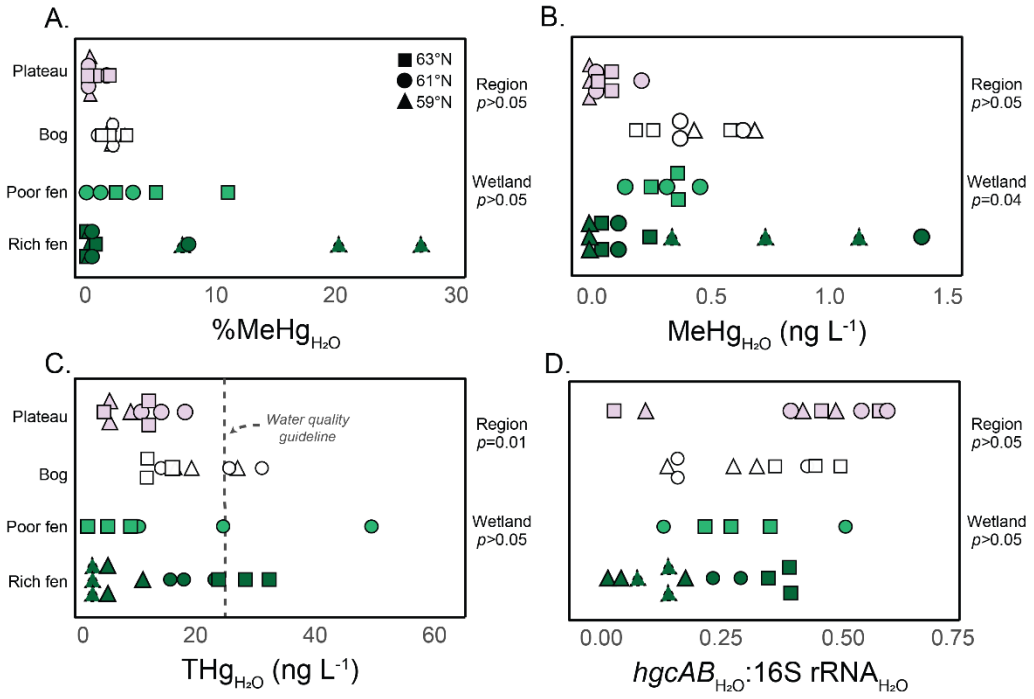

Figure 4.3. Higher and more variable methylmercury concentrations in thermokarst wetland porewaters than in peat plateaus. A) %MeHg (methylmercury to total mercury concentration ratio, [MeHg]/[THg]), concentrations of B) MeHg and C) THg, and D) *hgcAB* genes in porewater normalized by 16S rRNA; values show triplicate samples of shallow groundwater, grouped by wetland classification. Fens are separated by moderate-rich and poor classification, with two moderate-rich fens at 59°N; the relatively richer fen at 59°N has a dashed border. The *p*-values from testing the region and wetland class variability with permutational analysis of variance (perANOVA) are displayed beside each dot plot. Canadian water quality guidelines for protecting aquatic life (26 ng THg L^{-1}) are displayed in panel C (Canadian Council of Ministers of the Environment, 2003).

A longer water residence time in bogs may explain the consistently higher porewater MeHg and THg concentrations relative to fens. Due to low hydrological conductivity, water entering deeper layers of isolated bogs is stored until removal by groundwater recharge, while near-surface porewater of bogs may infrequently discharge into channel fens during high flow events (Hayashi et al., 2004). By contrast, fens integrate external water sources, including groundwater inputs, and have a shorter water residence time than bogs (Hayashi et al., 2004; Quinton et al., 2003). Furthermore, as fens convey water and solutes through catchments, porewater MeHg and THg concentrations may be continually flushed in addition to supporting higher soil methylation efficiency. Flow networks of fens also feed into and out of small peatland lakes, where MeHg photodemethylation, Hg^{II} photoreduction, or sedimentation can influence downstream export (Thompson et al., 2023).

However, recent work showed an absence of elevated aquatic MeHg and THg concentrations downstream of northwestern Canada's most rapidly thawing peatlands (Thompson et al., 2023). Indeed, we found the wetland porewater concentrations measured in this study were far higher than the THg and MeHg concentrations measured during three years of monitoring the drainage outlets of 61°N (1.13±0.30 ng THg L^{-1}, 0.09±0.03 ng MeHg L^{-1}) and 63°N (3.14±2.13 ng THg L^{-1}, 0.08±0.05 ng MeHg L^{-1}; Thompson et al., Under review). Continued monitoring of rivers and wetlands is required to determine the impacts of expanding thermokarst wetlands on downstream aquatic environments.

4.3.3 Geochemical drivers of methylation

As we found thermokarst wetlands to have high variability in k_m and MeHg concentrations, we used an RDA (Figure 4.4A) to determine how redox conditions and DOM quantity and composition are associated with methylation potential. We inferred DOM composition through a PCA of optical and FTICR-MS indices (Figure A.4.6; Table A.4.4). Trophic status effectively indicated overall methylation potential, increasing towards the RDA's first axis and aligning with predictor variables indicative of groundwater connectivity. High trophic status fens had the highest methylation efficiency among wetland classes, which contrasts observations elsewhere that found poor-intermediate fens to be optimum Hg^{II} methylation hotspots, with dampening of net production in very nutrient-poor or nutrient-rich sites (Poulin et al., 2019; Tjerngren et al., 2012). Fens were associated with higher concentrations of TEAs, higher pH due to the buffering capacity of carbonate bedrock (Bourbonniere, 2009), greater vegetation species richness, and graminoid cover that supports larger pools of labile DOM (Haynes et al., 2017). Peat plateaus had lower pH and TEA availability, higher soil carbon-to-nitrogen ratio (C/N), and higher concentrations of DOC with more aromatic quality, while bogs fell between fens and plateaus.

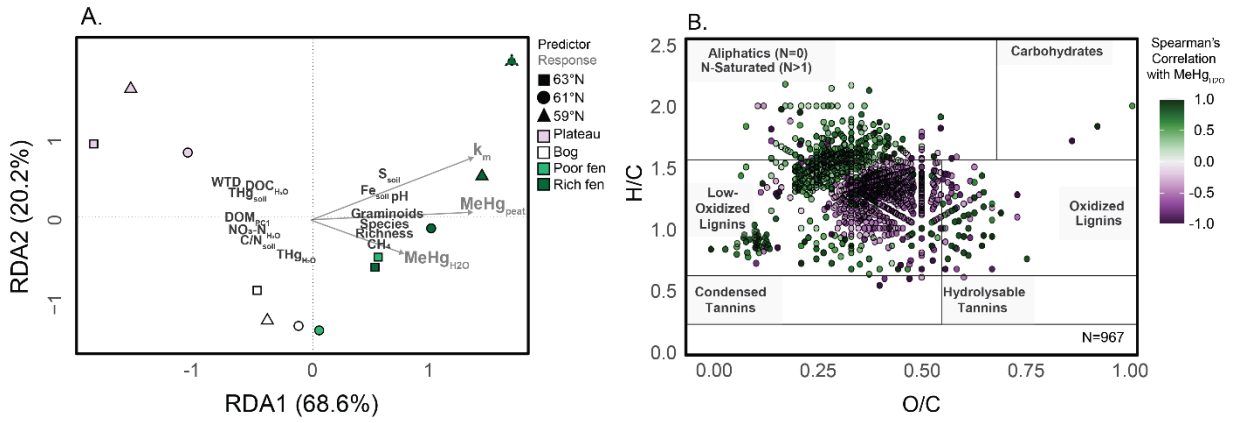

Figure 4.4. Influence of wetland biogeochemistry and dissolved organic matter (DOM) composition on methylmercury (MeHg) concentrations and methylation potential. A) Redundancy analysis (RDA) ordination for MeHg concentrations in soil and porewater, as well as potential methylation rates (k_m) in soil. Predictors include water table depth (WTD), dissolved organic carbon (DOC), PC1 scores from a PCA of dissolved organic matter indices (DOM_{PC1}; Figure A.4.6), total mercury (THg), carbon to nitrogen ratio (C/N), nitrate-as-nitrogen (NO_3-N), sulfur (S), iron (Fe), pH, vegetation species richness, and percent graminoid cover (graminoids). Subscripts indicate whether the parameter was measured in soil or porewater (H_2O). Fens are separated by moderate-rich and poor classification, with two moderate-rich fens at 59°N; the relatively richer fen at 59°N has a dashed border. B) Relationships between DOM compound classes and MeHg concentrations in wetland porewaters. Van Krevelen plot of oxygen/carbon (O/C) and hydrogen/carbon (H/C) wherein each data point represents the strength of significant correlations (Spearman's Rank, $p<0.05$ after 999 permutations) between the relative intensity of a specific DOM molecule with MeHg concentrations in porewaters. Biomolecular compound classes are denoted by boxed regions (Kim et al., 2003).

We found that methylation potential was dependent on the abundance of different TEAs. Lower soil MeHg concentrations were associated with higher porewater NO_3-N concentrations which could be connected to suppressed methylation in favor of enhanced denitrification, as NO_3 is a more energetically favorable TEA than Fe^{III} or SO_4^{2-} (Lescord et al., 2019; Todorova et al., 2009). Recent work in peatlands of northwestern Canada found both peat plateaus and thermokarst bogs to be nitrous oxide sinks from active denitrification (Schulze et al., 2023), which may partially explain lower k_m and %MeHg in bogs.

Higher potential k_m was associated with higher concentrations of S and Fe in soil, which can control Hg^{II} speciation and methylation (Bravo & Cosio, 2020). SO_4^{2-} and Fe^{III} are TEAs that can stimulate the activity of Hg^{II} methylators, SO_4^{2-}-reducing and Fe-reducing bacteria (Fleming et al., 2006; Gilmour et al., 1992). Experimental additions of S have also led to higher MeHg solubility in peat porewaters (Åkerblom et al., 2020). We observed high k_m values and MeHg concentrations in soil and porewater at the richest 59°N fen, with the highest porewater SO_4^{2-} and soil S concentrations (13.7 mg SO_4^{2-}-S L^{-1}; 7.4 mg S g^{-1}). While high SO_4^{2-} concentrations and SO_4^{2-}-reduction rates can

eventually inhibit methylation from the subsequent sulfide production, creating less bioavailable Hg-S complexes (Gilmour et al., 1998), such inhibitive effects were not apparent in the fens. Notable groundwater discharge at 59°N may explain the high trophic status of regional fens due to surrounding high-elevation areas and sporadic permafrost cover that permits deep subsurface flow paths.

Sites that had higher porewater MeHg concentrations also had higher methane emissions, measured concurrently via chamber fluxes at each wetland (Harris et al., In prep.). The activity of methanogens and syntrophs (i.e., syntrophy between secondary fermenters and methanogens) are pathways of mineralizing organic matter via fermentation products and mediate MeHg production under strongly reducing conditions with depletion of more energetically favorable TEAs (Schmidt et al., 2016). MeHg concentrations in northern pond waters have similarly correlated with dissolved methane (Lehnherr, St. Louis, & Kirk, 2012; MacMillan et al., 2015).

Lower porewater MeHg concentrations were associated with greater water table depth. As Hg^{II} methylation is a predominantly anaerobic process associated with Fe and SO_4^{2-} reduction and methanogenesis (Bravo & Cosio, 2020), higher oxygen availability may dampen the activity of methylating microbes. While oxygenated environments can stimulate Hg^{II} methylation through the regeneration of favorable TEAs, which has been linked to water table fluctuations (Coleman Wasik et al., 2015; Haynes et al., 2017), we found overall low net methylation in peat plateaus, which had deeper water tables, while bogs and fens had water tables close to or above the soil surface at the time of sampling. However, oxygen shuttling in aerenchyma tissues to regenerate TEAs that sustain Fe and SO_4^{2-} reduction may partially explain the association of higher soil MeHg with higher graminoid cover and greater species richness (Haynes et al., 2017; Mitchell et al., 2008a).

4.3.4 Role of DOM in methylation and transport

We found that porewater MeHg concentrations were strongly associated with non-aromatic and high hydrogen/carbon (H/C) DOM, suggesting that DOM composition plays an important role in Hg^{II} methylation. Characteristic of peatlands (Bourbonniere, 2009), DOC concentrations in the wetlands were generally high (Figure A.4.1, range: 26 to 93 mg DOC L^{-1}), although we found higher MeHg concentrations were associated with relatively lower DOC concentrations and aromaticity. In finer detail, we examined the relationship between MeHg concentrations and DOM

in porewater (Figure 4.4B). We used a Van Krevelen diagram to plot oxygen/carbon (O/C) and hydrogen/carbon (H/C) of intensity-weighted FTICR-MS derived DOM molecules that significantly (p<0.05) correlated with porewater MeHg concentrations (Kim et al., 2003; Mangal et al., 2022). We found a positive relationship between concentrations of MeHg with higher H/C and lower O/C compounds and a corresponding negative relationship between MeHg with lower H/C and higher O/C compounds (Figure 4.4B). The same pattern was observed when isolating each wetland class (Figure A.4.7).

While this correlative approach does not directly measure DOM-Hg binding or complexation, we found a striking association between MeHg concentrations in porewater and molecules characterized as unsaturated aliphatic/N-saturated, which are likely to be bioavailable (Mangal et al., 2022). Autochthonous, labile DOM can facilitate Hg^{II} methylation (Bravo et al., 2017; Herrero Ortega et al., 2018; Lei et al., 2019) and MeHg uptake in biota (French et al., 2014; Lescord et al., 2018). We observed rich fens to have fresher, microbially-derived DOM (Figure A.4.1, Figure A.4.6), potentially fueling MeHg production. Greater DOM processing typically occurs in fens (Bourbonniere, 2009; Gandois et al., 2019; Olefeldt, Roulet, et al., 2013), and vascular plants such as graminoids can deliver labile DOM through root exudates (Haynes et al., 2017). However, in reducing conditions, anaerobic microbes preferentially consume compounds with high nominal oxidation state of carbon (NOSC) values, which leads to the enrichment of low NOSC substrates (Lin et al., 2021; Pracht et al., 2018). As the DOM compounds in the higher H/C and lower O/C regions had lower NOSC values, as did richer fens (Figure A.4.8), the DOM may not solely represent a substrate for methylation and could be representative of processing under reducing conditions. The correlation between MeHg and DOM in these regions could thus indicate how low redox conditions lead to higher overall MeHg production and solubility in wetlands.

In contrast, lower MeHg concentrations were associated with more oxidized, lignin-like DOM. Highly aromatic DOM can bind with Hg^{II}, inhibiting its bioavailability and, thus, Hg^{II} methylation (Bravo et al., 2017; Chiasson-Gould et al., 2014; French et al., 2014). Peat plateaus had the highest concentrations of aromatic DOM amongst wetland classes (Figure A.4.1, Figure A.4.6), likely produced from millennial-aged soil in drier, oxygen-rich conditions that can enhance microbial respiration and DOM production (Tanentzap et al., 2021) but reduce methylation potential.

Our findings indicate DOM aromaticity controls MeHg production in wetlands differently than downstream export as a vector. Here, MeHg production in wetlands was associated with aliphatic, bioavailable DOM as previously recorded in boreal lakes (Bravo et al., 2017; Herrero Ortega et al., 2018; Lei et al., 2019) and peatlands (Mitchell et al., 2008a). However, aromatic DOM facilitated the co-transport of MeHg in rivers draining the studied wetlands (Thompson et al., 2023, Under review) and in other boreal streams (Mangal et al., 2022; Shanley et al., 2022). Considering the role of fens as biological reactors and integrators of catchment water sources, aromatic DOM flowing through fens from peat plateaus and bogs could carry MeHg for longer-range transport to downstream waters.

4.3.5 Effects of continued permafrost thaw on near-surface methylation capacity of the landscape

Taken together, patterns of MeHg and methylation potential in the porewater and soils of wetlands in northwestern Canada support previous observations of Hg^{II} methylation hotspots in thawing permafrost peatlands (Figure 4.5A; Fahnestock et al., 2019; Gordon et al., 2016; Poulin et al., 2019; Tarbier et al., 2021). To project how ongoing permafrost thaw will impact the landscape-scale production of MeHg in the Taiga Plains ecozone, we utilized the Boreal-Arctic Wetland and Lake Dataset (BAWLD), a methane-specific land cover product (Kuhn, Varner, et al., 2021; Olefeldt et al., 2021), for its current wetland cover distribution and projected wetland cover in 2100 based on Shared Socio-economic Pathway (SSP) 4.5 (Kuhn et al., In prep.). Currently, peatland complexes across the Taiga Plains are comprised of 61% peat plateaus, 17% bogs, and 23% fens (Table A.4.5). By 2100, with continued permafrost thaw, the distribution of peatland complexes is expected to shift drastically due to widespread losses of peat plateau cover and subsequent expansion of bog and fen cover (SSP4.5 mid-scenario: 28% plateaus, 35% bogs, 37% fens; Table A.4.5).

Many factors driving Hg^{II} methylation in wetlands observed here and elsewhere (Poulin et al., 2019; Tarbier et al., 2021) are consistent with the biogeochemical drivers of methane emissions (Kuhn, Varner, et al., 2021), and methanogens are notable methylators in boreal waters (Bravo, Peura, et al., 2018). We harmonized our observations with the BAWLD wetland classes predominant within the Taiga Plains (consistent bog class; fen class=combined poor fen and moderate-rich fen; permafrost bog class=peat plateau). We then assessed the current net

methylation potential of the landscape using a representative range (first, second, and third quartile) of %MeHg observed in the top 12 cm of soil for each wetland class multiplied by their fractional distribution in peatland complexes across the Taiga Plains. Future scenarios of wetland class distributions based on SSP4.5 (Kuhn et al., In prep.) informed future net methylation potential (Figure 4.5B), with details on uncertainties in Table A.4.5.

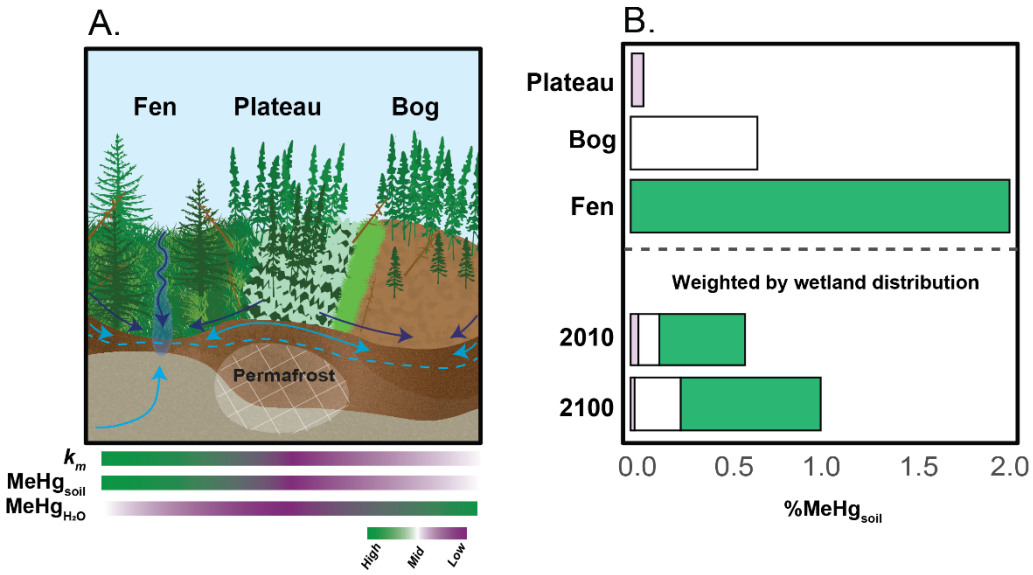

Figure 4.5. Shifting methylmercury production in thawing permafrost peatlands of northwestern Canada. A) Hydrology and relative methylation efficiency of peat plateaus, bogs, and fens in the Interior Plains. Subscripts indicate whether the parameter was measured in peat or porewater (H_2O). B) Median %MeHg and weighted %MeHg by fractional distribution within Taiga Plains peatland classes (fens, plateaus, and bogs) from BAWLD land cover product (Olefeldt et al., 2021) in the present and in the future. Peatland class distributions were explored based on SSP4.5 with the mid-scenario plotted. Ranges and uncertainties are in Table A.4.5.

Given the projected losses of peat plateaus and expansion of bogs and fens across the Taiga Plains, we anticipate increases of 65% (SSP4.5 mid-scenario; range: 47%–80%) in the %MeHg of near-surface soils (Figure 4.5B, Table A.4.5). The weighted %MeHg decreases in peat plateaus (-50%, -75%–25%) and increases in bogs (+118%, +80%–145%) and fens (+62%, +47–78%). By taking %MeHg as a proxy for landscape-scale net methylation, we see an apparent effect of permafrost thaw leading to enhanced Hg^{II} methylation potential across the landscape of northwestern Canada by 2100.

The MeHg production in expanding bogs and fens across the Taiga Plains may have a temporal aspect. Forecasting could be improved by integrating thermokarst wetland age, which has been

linked to net methylation, with higher %MeHg observed in younger Fennoscandian fens (Tarbier et al., 2021) and seen in experimentally flooded peatlands where near-surface MeHg production rapidly increased (Heyes et al., 2000) but quickly fell in favor of microbial demethylation (St. Louis et al., 2004). The long-term landscape trajectory of thawed peatlands remains uncertain, with a possible outcome of widespread basin drainage and drying (Carpino et al., 2021) that could impede near-surface methylation.

Drivers of permafrost thaw could further shift the methylation efficiency of near-surface soils. The Taiga Plains are warming over twice the national and global average (Vincent et al., 2015); incubation experiments have linked warming to increases in net MeHg production (Loseto et al., 2004; Yang et al., 2016). Water table fluctuations from projections of increased drought coupled with altered intensity and frequency of precipitation events (Tam et al., 2019) may increase Hg^{II} methylation (Coleman Wasik et al., 2015; Haynes et al., 2017). Finally, wildfire activity will likely accelerate in the region (Flannigan et al., 2013), which can shift Hg partitioning in peatlands and increase %MeHg (Ackley et al., 2021).

4.4 Conclusions

We found that the production and potential mobility of MeHg in permafrost peatland complexes in northwestern Canada varied across thermokarst wetlands that emerged after the thawing of drier peat plateaus. Thermokarst wetlands had higher but more variable MeHg concentrations and k_m in thermokarst wetlands compared to intact permafrost peat plateaus. Moderate-rich fens were the optimal environments for MeHg production, with hydrological function as conveyors of integrated water sources and low water residence times likely elevating MeHg mobility. We project enhanced MeHg production in near-surface soils as northern peatlands continue thawing and as reducing conditions establish, although trophic status, groundwater connectivity, and hydrological functioning will pivotally control MeHg production and export. Future work connecting shifts in landscape MeHg production with potential uptake in downstream aquatic food webs will be essential for assessing risks to public health and food security, which has the potential to impact Indigenous communities and nations in the Taiga Plains.

5. Summary, conclusions, and directions for future research

5.1 Summary of findings

In this body of research, I investigated the effects of permafrost thaw on MeHg production and downstream export in peatland-rich catchments of the Interior Plains of boreal western Canada. The extensive peatlands in the Interior Plains are rapidly thawing, leading to land cover shifts and the potential mobilization of previously frozen constituents such as carbon and Hg (Wright et al., 2022). While the expansion of thermokarst wetlands can enhance Hg^{II} methylation potential (Chapter 4), and peatlands are MeHg sources at a catchment scale (Chapter 2), the rivers and lakes that integrate terrestrial solute loads in the Interior Plains were primarily found to have low-moderate concentrations and export of MeHg (Chapter 2, Chapter 3). Quantity and composition of DOM were of central importance for MeHg cycling across the terrestrial-aquatic continuum, whether facilitating co-transport in streams, inhibiting photodemethylation in the water column of lakes, or enhancing Hg^{II} methylation in thawing wetlands.

Chapter 2 examined MeHg and THg concentrations in streams and lakes within boreal western Canada using a space-for-time approach across a permafrost gradient. The delivery of MeHg to streams was closely tied to peatland cover, where higher stream MeHg concentrations were associated with aromatic DOC, Fe, and lower pH. Concentrations of MeHg were not consistently elevated in the rapidly thawing sporadic-discontinuous permafrost regions as predicted, although a direct link between permafrost extent and MeHg concentration may have been confounded due to variable catchment sizes. Small peatland lakes were potential MeHg sinks, although their UV photodemethylation sink capacity will likely be sensitive to increased DOC concentrations predicted with continued permafrost thaw. Hg^{II}-reducing microbes were most abundant within lake sediments relative to Hg^{II}-methylating and MeHg-demethylating microbes, which may reflect a detoxification mechanism of Hg^{II} reduction following abiotic MeHg demethylation. We further observed a negative relationship between the abundance of Hg^{II}-methylating genes in sediment and MeHg concentrations in the lake water column, which may be linked to the inhibition of methylation from high concentrations of SO_4.

In Chapter 3, the export of THg, MeHg, and DOC in two catchments within the discontinuous permafrost region was explored in connection with catchment land cover and controls on runoff

generation. From three years of measuring open-water season solute concentrations, contrasting patterns in solute concentrations vs. yields emerged between the two sites. At the peatland-dominated Scotty Creek, concentrations of MeHg and DOC were consistently high, while THg concentrations were consistently low and not primarily connected to discharge. However, inter-annual solute yields varied substantially as the peatlands stored water in drier periods and generated runoff during wetter periods. At Smith Creek, with a mixed-landscape of mountains, peatlands, and forests, DOC and THg concentrations increased during high-flow events as terrestrial contributions increased, while MeHg concentrations were less variable. Throughout the monitoring period, solute yields at the mixed-landscape catchment varied less due to more consistent runoff inputs from groundwater and steeper slopes. With ongoing permafrost thaw and changes in temperature and precipitation, solute yields will likely be sensitive to changes in runoff patterns and biogeochemical controls on DOC and MeHg production.

Chapter 4 determined how MeHg concentrations and production varied in thermokarst wetlands relative to peat plateaus with intact permafrost. We found that the potential for MeHg production varied with the distinct vegetation and biogeochemical characteristics of plateaus, nutrient-poor bogs, and fens on a spectrum of nutrient richness. Concentrations of MeHg in soil and porewater were higher in thermokarst wetlands than in peat plateaus, with an indication of the most optimal Hg^{II} methylation in moderate-rich fens based on %MeHg and potential methylation rates. Conditions supporting greater methylation potential included a water table closer to the peat surface, labile organic matter, higher pH, and SO_4 and Fe that can stimulate methylating bacteria. Based on projected land cover shifts, MeHg production will be enhanced in near-surface soils in the Taiga Plains by 2100. Still, the effects of thermokarst expansion on the downstream delivery of MeHg to aquatic environments will depend on the hydrological functioning of the landscape.

5.2 Directions for future research

This thesis assessed climate change impacts on MeHg cycling in boreal sub-Arctic regions, focusing on MeHg production in thawing permafrost peatlands and export to streams and lakes. Below, I suggest potential research directions that build upon findings within this thesis. However, these suggestions are from my position as a southern scientist who has conducted research in the North; all future research on MeHg within the Interior Plains should ensure that the priorities of

nations and Indigenous communities most connected to and affected by the changing land and environment are at the forefront (Figure 5.1; Houde et al., 2022; Lafferty et al., 2022).

Figure 5.1. A collective visual representation of the Five R's of Indigenous research and guiding questions for early career researchers: respect, relevance, reciprocity, and responsibility, with relationships intersecting all aspects. Reproduced from Lafferty et al., 2022 under CC BY 4.0 license. Photo credits: S. Bandara.

Our findings in Chapter 2 represented a snapshot of summer THg and MeHg through the synoptic sampling of many streams and lakes across the Interior Plains. In contrast to observations of elevated THg and MeHg in surface waters of discontinuous permafrost regions of eastern Canada and the West Siberian Lowlands (Lim et al., 2019; Richardson et al., 2021), we found less apparent linkages between permafrost extent and MeHg concentrations while THg concentrations increased with latitude. The northernmost extent of the sampling region included tundra wetlands, where plants and soils strongly absorb atmospheric Hg (Obrist et al., 2017); associations between gaseous Hg uptake and enhanced mobility of THg in surface waters merit further exploration. As previously recognized (Åkerblom et al., 2022; Zolkos et al., 2020) and investigated in Chapter 3, concentrations and yields of THg and MeHg vary seasonally and depend on the contributing catchment's runoff patterns and land cover. Repeated sampling of multiple catchments that encompass a narrower range of catchment areas and sampling periods that span a wider range of hydrological conditions could elucidate more explicit effects of permafrost extent on MeHg concentrations in the Interior Plains.

In Chapter 3, we provided insight into the role that midsized catchments in high latitudes have in the export of MeHg, THg, and DOC. This study further provided baseline information on concentrations and yields of MeHg, THg, and DOC for comparison in the future. These data will be particularly valuable as the peatland-dominated catchment experienced a large wildfire in the autumn of 2022. While paired catchment studies have shown relatively muted effects of wildfire on water chemistry (Tank et al., 2018), porewater %MeHg and MeHg concentrations have increased post-fire in peatlands (Ackley et al., 2021). Therefore, tracking post-fire solute concentrations, export, and changes in peat chemistry to compare with data from Chapters 3 and 4 is highly recommended. Precipitation and runoff patterns will likely determine how strongly the outlet water chemistry responds to the direct wildfire effects in the coming years.

Considering the variability in biogeochemical conditions of Interior Plains lakes (Kuhn, Thompson, et al., 2021), mass balance budgets of MeHg fluxes in lakes (e.g., (Sellers et al., 2001) would provide a fascinating insight into biotic and abiotic pathways of transformation. In Chapter 2, the negative relationship between MeHg concentrations in the water column and *hgcA* abundance in sediments was likely confounded by sedimentation, photodemethylation, and water column MeHg production. Methylation and demethylation assays (Lehnherr & St. Louis, 2009) and photodemethylation experiments (Klapstein et al., 2018) could be used to determine the role of lakes as landscape-scale MeHg sources or sinks with greater specificity. Catchment water coverage negatively correlated with MeHg concentrations in boreal rivers throughout northern Quebec (Fink-Mercier, Lapierre, et al., 2022), pointing to the importance of lakes and reservoirs as modulating downstream MeHg concentrations.

Our findings in Chapter 4 indicate that thawing wetlands have greater MeHg production than intact peat plateaus, although we observed high variability in biogeochemical conditions among thermokarst bogs and fens. Temporal variability in MeHg production in wetlands should be explored on seasonal and longer-term scales. As observed in Chapter 3, concentrations of MeHg increased with the water temperature at the peatland-dominated stream, suggesting higher MeHg production during warmer temperatures. High Arctic wetlands had a similar effect of warmer periods stimulating Hg^{II} methylation and increasing MeHg delivery to downstream waters (Varty et al., 2021). Additionally, the connection between thermokarst wetland age and MeHg production should be determined, as emergent features may provide optimal conditions for Hg^{II} methylation

(Tarbier et al., 2021), which could wane over time, as seen in experimentally flooded peatlands (St. Louis et al., 2004). Understanding hot moments of MeHg production seasonally and thermokarst wetland methylation efficiency over time would improve forecasting of MeHg delivery to downstream waters.

Linkages between DOM and MeHg were apparent throughout all studies, affirming the long-recognized and pivotal role of DOM in Hg cycling (Branfireun et al., 2020; Bravo & Cosio, 2020). Labile DOM had strong associations with MeHg production in wetlands (Chapter 4), while aromatic DOM was a control on modeled photodemethylation rates (Chapter 2) and acted as a vector for transport to downstream aquatic environments (Chapter 2, Chapter 3). We utilized various analytical techniques to assess DOM composition. The simpler indices of DOM composition (e.g., from absorbance spectroscopy) explained variability in MeHg concentrations as effectively as more complex methods (e.g., from fluorescence spectroscopy and FTICR-MS analysis). Given the potential enhancement of MeHg transport and dampening of photodemethylation with the projected increases of DOM (Frey & Smith, 2005; Olefeldt et al., 2014), future research and community-led projects can consider the use of relatively inexpensive and readily available techniques to robustly explore linkages between DOM composition and the concentrations and export of MeHg.

Finally, I suggest integrating findings from this thesis into ongoing work tracing MeHg mobility in aquatic food webs of the Interior Plains. For example, wetland cover and permafrost thaw have been linked to Hg bioaccumulation and biomagnification in northern pike within lakes of the Dehcho (Moslemi-Aqdam et al., 2023). From Chapters 2 and 4, groundwater-fed fens are likely MeHg sources to downstream lakes, which could guide targeted biotic Hg sampling in the region. Although measured MeHg and THg concentrations in surface waters (wetlands, lakes, and rivers) were largely below water quality guidelines relating to the protection of aquatic life (Canadian Council of Ministers of the Environment, 2003), there is urgency in understanding linkages between Hg loadings in the watershed and concentrations in country food such as fish (Blanchfield et al., 2021) for land-use planning and public health in Indigenous communities and nations.

References

Ackley, C., Tank, S. E., Haynes, K. M., Rezanezhad, F., McCarter, C., & Quinton, W. L. (2021). Coupled hydrological and geochemical impacts of wildfire in peatland-dominated regions of discontinuous permafrost. *Science of The Total Environment*, *782*, 146841. https://doi.org/10.1016/j.scitotenv.2021.146841

Åkerblom, S., Nilsson, M. B., Skyllberg, U., Björn, E., Jonsson, S., Ranneby, B., & Bishop, K. (2020). Formation and mobilization of methylmercury across natural and experimental sulfur deposition gradients. *Environmental Pollution*, *263*, 114398. https://doi.org/10.1016/j.envpol.2020.114398

Åkerblom, S., Zdanowicz, C., Campeau, A., Soerensen, A. L., & Hewitt, J. (2022). Spatial and temporal variations in riverine mercury in the Mackenzie River Basin, Canada, from community-based water quality monitoring data. *Science of The Total Environment*, *853*, 158674. https://doi.org/10.1016/j.scitotenv.2022.158674

Alberta Environment and Sustainable Resource Development. (2015). *Alberta Wetland Classification System*. Water Policy Branch, Policy and Planning Division, Edmonton, AB.

AMAP. (2019). *Technical background report to the global mercury assessment 2018*. Tromsø, Norway: Arctic Monitoring and Assessment Programme and United Nations Environment Programme.

AMAP. (2021). *AMAP Assessment 2021: Mercury in the Arctic.* (p. vii + 324). Tromsø, Norway: Arctic Monitoring and Assessment Programme.

Amos, H. M., Jacob, D. J., Holmes, C. D., Fisher, J. A., Wang, Q., Yantosca, R. M., et al. (2012). Gas-particle partitioning of atmospheric Hg(II) and its effect on global mercury deposition. *Atmospheric Chemistry and Physics*, *12*(1), 591–603. https://doi.org/10.5194/acp-12-591-2012

Ariya, P. A., Amyot, M., Dastoor, A., Deeds, D., Feinberg, A., Kos, G., et al. (2015). Mercury Physicochemical and Biogeochemical Transformation in the Atmosphere and at Atmospheric Interfaces: A Review and Future Directions. *Chemical Reviews*, *115*(10), 3760–3802. https://doi.org/10.1021/cr500667e

Armstrong, F., & Hamilton, A. (1973). Pathways of mercury in a polluted northwestern Ontario lake. In *Toxic Metals and Metal-Organic Interactions in Natural Waters* (pp. 131–156). Ann Arbor, Michigan: Ann Arbor Science Publishers.

Aukes, P. J. K., Schiff, S. L., Venkiteswaran, J. J., Elgood, R. J., & Spoelstra, J. (2021). SIZE-BASED characterization of freshwater dissolved organic matter finds similarities within a waterbody type across different Canadian ecozones. *Limnology and Oceanography Letters*, *6*(2), 85–95. https://doi.org/10.1002/lol2.10180

Aylsworth, J. M., Burgess, M. M., Desrochers, D. T., Duk-Rodkin, A., Robertson, T., & Traynor, J. A. (2000). Surficial geology, subsurface materials, and thaw sensitivity of sediments. In *The Physical Environment of the Mackenzie Valley, Northwest Territories: a Base Line for the Assessment of Environmental Change* (Vol. 547, pp. 41–48). Ottawa, Ontario: Natural Resources Canada.

Bae, H.-S., Dierberg, F. E., & Ogram, A. (2019). Periphyton and Flocculent Materials Are Important Ecological Compartments Supporting Abundant and Diverse Mercury Methylator Assemblages in the Florida Everglades. *Applied and Environmental Microbiology*, *85*(13), e00156-19. https://doi.org/10.1128/AEM.00156-19

Barkay, T., & Gu, B. (2021). Demethylation─The Other Side of the Mercury Methylation Coin: A Critical Review. *ACS Environmental Au*, acsenvironau.1c00022. https://doi.org/10.1021/acsenvironau.1c00022

Basu, N., Destouni, G., Jawitz, J. W., Thompson, S. E., Loukinova, N. V., Darracq, A., et al. (2010). Nutrient loads exported from managed catchments reveal emergent biogeochemical stationarity. *Geophysical Research Letters*, *37*(23), L23404. https://doi.org/10.1029/2010GL045168

Basu, N., Abass, K., Dietz, R., Krümmel, E., Rautio, A., & Weihe, P. (2022). The impact of mercury contamination on human health in the Arctic: A state of the science review. *Science of The Total Environment*, *831*, 154793. https://doi.org/10.1016/j.scitotenv.2022.154793

Blanchfield, P. J., Rudd, J. W. M., Hrenchuk, L. E., Amyot, M., Babiarz, C. L., Beaty, K. G., et al. (2021). Experimental evidence for recovery of mercury-contaminated fish populations. *Nature*. https://doi.org/10.1038/s41586-021-04222-7

Bolyen, E., Rideout, J. R., Dillon, M. R., Bokulich, N. A., Abnet, C. C., Al-Ghalith, G. A., et al. (2019). Reproducible, interactive, scalable and extensible microbiome data science using QIIME 2. *Nature Biotechnology*, *37*(8), 852–857. https://doi.org/10.1038/s41587-019-0209-9

Bourbonniere, R. A. (2009). Review of Water Chemistry Research in Natural and Disturbed Peatlands. *Canadian Water Resources Journal*, *34*(4), 393–414. https://doi.org/10.4296/cwrj3404393

Boyd, E. S., & Barkay, T. (2012). The Mercury Resistance Operon: From an Origin in a Geothermal Environment to an Efficient Detoxification Machine. *Frontiers in Microbiology*, *3*. https://doi.org/10.3389/fmicb.2012.00349

Boyd, J. A., Woodcroft, B. J., & Tyson, G. W. (2018). GraftM: a tool for scalable, phylogenetically informed classification of genes within metagenomes. *Nucleic Acids Research*, *46*(10), e59–e59. https://doi.org/10.1093/nar/gky174

Branfireun, B. A., Cosio, C., Poulain, A. J., Riise, G., & Bravo, A. G. (2020). Mercury cycling in freshwater systems - An updated conceptual model. *Science of The Total Environment*, *745*, 140906. https://doi.org/10.1016/j.scitotenv.2020.140906

Bravo, A. G., & Cosio, C. (2020). Biotic formation of methylmercury: A bio–physico–chemical conundrum. *Limnology and Oceanography*, *65*(5), 1010–1027. https://doi.org/10.1002/lno.11366

Bravo, A. G., Bouchet, S., Guédron, S., Amouroux, D., Dominik, J., & Zopfi, J. (2015). High methylmercury production under ferruginous conditions in sediments impacted by sewage treatment plant discharges. *Water Research*, *80*, 245–255. https://doi.org/10.1016/j.watres.2015.04.039

Bravo, A. G., Bouchet, S., Tolu, J., Björn, E., Mateos-Rivera, A., & Bertilsson, S. (2017). Molecular composition of organic matter controls methylmercury formation in boreal lakes. *Nature Communications*, *8*(1), 14255. https://doi.org/10.1038/ncomms14255

Bravo, A. G., Peura, S., Buck, M., Ahmed, O., Mateos-Rivera, A., Herrero Ortega, S., et al. (2018). Methanogens and Iron-Reducing Bacteria: the Overlooked Members of Mercury-Methylating Microbial Communities in Boreal Lakes. *Applied and Environmental Microbiology*, *84*(23), e01774-18. https://doi.org/10.1128/AEM.01774-18

Bravo, A. G., Kothawala, D. N., Attermeyer, K., Tessier, E., Bodmer, P., Ledesma, J. L. J., et al. (2018). The interplay between total mercury, methylmercury and dissolved organic

matter in fluvial systems: A latitudinal study across Europe. *Water Research*, *144*, 172–182. https://doi.org/10.1016/j.watres.2018.06.064

Brown, J., Ferrians, O., Melnikov, E. S., & Melnikov, E. S. (2002). Circum-Arctic Map of Permafrost and Ground-Ice Conditions, Version 2. Boulder, Colorado USA: NSIDC. Retrieved from https://doi.org/10.7265/skbg-kf16

Brown, J., Ferrians, O., Heginbottom, J., & Melnikov, E. S. (2002). Circum-Arctic Map of Permafrost and Ground-Ice Conditions, Version 2 [Data set]. Boulder, Colorado USA: NSIDC: National Snow and Ice Data Center. https://doi.org/10.7265/SKBG-KF16

Burd, K., Tank, S. E., Dion, N., Quinton, W. L., Spence, C., Tanentzap, A. J., & Olefeldt, D. (2018). Seasonal shifts in export of DOC and nutrients from burned and unburned peatland-rich catchments, Northwest Territories, Canada. *Hydrology and Earth System Sciences*, *22*(8), 4455–4472. https://doi.org/10.5194/hess-22-4455-2018

Canadian Council of Ministers of the Environment. (2003). Canadian Water Quality Guidelines for the Protection of Aquatic Life - Mercury - Inorganic mercury and methylmercury, 6.

Carpino, O., Haynes, K., Connon, R., Craig, J., Devoie, É., & Quinton, W. (2021). Long-term climate-influenced land cover change in discontinuous permafrost peatland complexes. *Hydrology and Earth System Sciences*, *25*(6), 3301–3317. https://doi.org/10.5194/hess-25-3301-2021

Chasmer, L., & Hopkinson, C. (2017). Threshold loss of discontinuous permafrost and landscape evolution. *Global Change Biology*, *23*(7), 2672–2686. https://doi.org/10.1111/gcb.13537

Chen, S., Zhou, Y., Chen, Y., & Gu, J. (2018). fastp: an ultra-fast all-in-one FASTQ preprocessor. *Bioinformatics*, *34*(17), i884–i890. https://doi.org/10.1093/bioinformatics/bty560

Chételat, J., Amyot, M., Arp, P., Blais, J. M., Depew, D., Emmerton, C. A., et al. (2015). Mercury in freshwater ecosystems of the Canadian Arctic: Recent advances on its cycling and fate. *Science of The Total Environment*, *509–510*, 41–66. https://doi.org/10.1016/j.scitotenv.2014.05.151

Chételat, J., McKinney, M. A., Amyot, M., Dastoor, A., Douglas, T. A., Heimbürger-Boavida, L.-E., et al. (2022). Climate change and mercury in the Arctic: Abiotic interactions. *Science of The Total Environment*, *824*, 153715. https://doi.org/10.1016/j.scitotenv.2022.153715

Chiasson-Gould, S. A., Blais, J. M., & Poulain, A. J. (2014). Dissolved Organic Matter Kinetically Controls Mercury Bioavailability to Bacteria. *Environmental Science & Technology*, *48*(6), 3153–3161. https://doi.org/10.1021/es4038484

Christakis, C. A., Barkay, T., & Boyd, E. S. (2021). Expanded Diversity and Phylogeny of mer Genes Broadens Mercury Resistance Paradigms and Reveals an Origin for MerA Among Thermophilic Archaea. *Frontiers in Microbiology*, *12*, 682605. https://doi.org/10.3389/fmicb.2021.682605

Christensen, G. A., Wymore, A. M., King, A. J., Podar, M., Hurt, R. A., Santillan, E. U., et al. (2016). Development and Validation of Broad-Range Qualitative and Clade-Specific Quantitative Molecular Probes for Assessing Mercury Methylation in the Environment. *Applied and Environmental Microbiology*, *82*(19), 6068–6078. https://doi.org/10.1128/AEM.01271-16

Christensen, G. A., Gionfriddo, C. M., King, A. J., Moberly, J. G., Miller, C. L., Somenahally, A. C., et al. (2019). Determining the Reliability of Measuring Mercury Cycling Gene Abundance with Correlations with Mercury and Methylmercury Concentrations.

Environmental Science & Technology, *53*(15), 8649–8663. https://doi.org/10.1021/acs.est.8b06389

Ci, Z., Peng, F., Xue, X., & Zhang, X. (2020). Permafrost Thaw Dominates Mercury Emission in Tibetan Thermokarst Ponds. *Environmental Science & Technology*, *54*(9), 5456–5466. https://doi.org/10.1021/acs.est.9b06712

Cohen, E., Levy, G. J., & Borisover, M. (2014). Fluorescent components of organic matter in wastewater: efficacy and selectivity of the water treatment. *Water Research*, *55*, 323–334. https://doi.org/10.1016/j.watres.2014.02.040

Coleman Wasik, J. K., Engstrom, D. R., Mitchell, C. P. J., Swain, E. B., Monson, B. A., Balogh, S. J., et al. (2015). The effects of hydrologic fluctuation and sulfate regeneration on mercury cycling in an experimental peatland. *Journal of Geophysical Research: Biogeosciences*, *120*(9), 1697–1715. https://doi.org/10.1002/2015JG002993

Connon, R. F., Quinton, W. L., Craig, J. R., & Hayashi, M. (2014). Changing hydrologic connectivity due to permafrost thaw in the lower Liard River valley, NWT, Canada. *Hydrological Processes*, *28*(14), 4163–4178. https://doi.org/10.1002/hyp.10206

Copernicus Climate Change Service. (2019). ERA5-Land hourly data from 2001 to present [Data set]. ECMWF. https://doi.org/10.24381/CDS.E2161BAC

Dastoor, A., Angot, H., Bieser, J., Christensen, J. H., Douglas, T. A., Heimbürger-Boavida, L.-E., et al. (2022). Arctic mercury cycling. *Nature Reviews Earth & Environment*, *3*, 270–286. https://doi.org/10.1038/s43017-022-00269-w

Dittmar, T., Koch, B., Hertkorn, N., & Kattner, G. (2008). A simple and efficient method for the solid-phase extraction of dissolved organic matter (SPE-DOM) from seawater: SPE-DOM from seawater. *Limnology and Oceanography: Methods*, *6*(6), 230–235. https://doi.org/10.4319/lom.2008.6.230

Donahue, W. F., Turner, M. A., Findlay, D. L., & Leavitt, P. R. (2003). The role of solar radiation in structuring the shallow benthic communities of boreal forest lakes. *Limnology and Oceanography*, *48*(1), 31–47. https://doi.org/10.4319/lo.2003.48.1.0031

Ecosystem Classification Group. (2009). *Ecological Regions of the Northwest Territories – Taiga Plains* (p. viii + 173 pp. + folded insert map). Yellowknife, NT, Canada: Department of Environment and Natural Resources, Government of the Northwest Territories.

Ecosystem Classification Group (Ed.). (2010). *Ecological regions of the Northwest Territories: Cordillera*. Yellowknife, NWT: Dept. of Environment and Natural Resources, Govt. of the Northwest Territories.

Emmerton, C. A., Graydon, J. A., Gareis, J. A. L., St. Louis, V. L., Lesack, L. F. W., Banack, J. K. A., et al. (2013). Mercury Export to the Arctic Ocean from the Mackenzie River, Canada. *Environmental Science & Technology*, *47*(14), 7644–7654. https://doi.org/10.1021/es400715r

Emmerton, C. A., Drevnick, P. E., Serbu, J. A., Cooke, C. A., Graydon, J. A., Reichert, M., et al. (2022). Downstream Modification of Mercury in Diverse River Systems Underscores the Role of Local Conditions in Fish Bioaccumulation. *Ecosystems*, *26*, 114–133. https://doi.org/10.1007/s10021-022-00745-w

Environment and Climate Change Canada. (2021). *Historical Hydrometric Data Search*. Government of Canada, Ottawa, ON.

Esdaile, L. J., & Chalker, J. M. (2018). The Mercury Problem in Artisanal and Small-Scale Gold Mining. *Chemistry – A European Journal*, *24*(27), 6905–6916. https://doi.org/10.1002/chem.201704840

Evans, M., Lockhart, W. L., Doetzel, L., Low, G., Muir, D., Kidd, K., et al. (2005). Elevated mercury concentrations in fish in lakes in the Mackenzie River Basin: The role of physical, chemical, and biological factors. *Science of The Total Environment*, *351–352*, 479–500. https://doi.org/10.1016/j.scitotenv.2004.12.086

Fahnestock, M. F., Bryce, J. G., McCalley, C. K., Montesdeoca, M., Bai, S., Li, Y., et al. (2019). Mercury reallocation in thawing subarctic peatlands. *Geochemical Perspectives Letters*, 33–38. https://doi.org/10.7185/geochemlet.1922

Fick, S. E., & Hijmans, R. J. (2017). WorldClim 2: new 1-km spatial resolution climate surfaces for global land areas. *International Journal of Climatology*, *37*(12), 4302–4315. https://doi.org/10.1002/joc.5086

Fink-Mercier, C., Lapierre, J., Amyot, M., & del Giorgio, P. A. (2022). Concentrations and Yields of Total Hg and MeHg in Large Boreal Rivers Linked to Water and Wetland Coverage in the Watersheds. *Journal of Geophysical Research: Biogeosciences*, *127*(5), e2022JG006892. https://doi.org/10.1029/2022JG006892

Fink-Mercier, C., del Giorgio, P., Amyot, M., & Lapierre, J. (2022). Hydrology and seasonality shape the coupling of dissolved Hg and methyl-Hg with DOC in boreal rivers in northern Québec. *Water Resources Research*, *58*, e2022WR033036. https://doi.org/10.1029/2022WR033036

Flannigan, M., Cantin, A. S., de Groot, W. J., Wotton, M., Newbery, A., & Gowman, L. M. (2013). Global wildland fire season severity in the 21st century. *Forest Ecology and Management*, *294*, 54–61. https://doi.org/10.1016/j.foreco.2012.10.022

Fleming, E. J., Mack, E. E., Green, P. G., & Nelson, D. C. (2006). Mercury Methylation from Unexpected Sources: Molybdate-Inhibited Freshwater Sediments and an Iron-Reducing Bacterium. *Applied and Environmental Microbiology*, *72*(1), 457–464. https://doi.org/10.1128/AEM.72.1.457-464.2006

FLUXNET Canada. (2016). FLUXNET Canada Research Network - Canadian Carbon Program Data Collection, 1993-2014, 1646.222627 MB. https://doi.org/10.3334/ORNLDAAC/1335

French, T. D., Houben, A. J., Desforges, J.-P. W., Kimpe, L. E., Kokelj, S. V., Poulain, A. J., et al. (2014). Dissolved organic carbon thresholds affect mercury bioaccumulation in Arctic lakes. *Environmental Science and Technology*, *48*(6), 3162–3168. https://doi.org/10.1021/es403849d

Frey, K. E., & McClelland, J. W. (2009). Impacts of permafrost degradation on arctic river biogeochemistry. *Hydrological Processes: An International Journal*, *23*(1), 169–182.

Frey, K. E., & Smith, L. C. (2005). Amplified carbon release from vast West Siberian peatlands by 2100. *Geophysical Research Letters*, *32*(9), 1–4. https://doi.org/10.1029/2004GL022025

Friedlingstein, P., Jones, M. W., O'Sullivan, M., Andrew, R. M., Bakker, D. C. E., Hauck, J., et al. (2022). Global Carbon Budget 2021. *Earth System Science Data*, *14*(4), 1917–2005. https://doi.org/10.5194/essd-14-1917-2022

Fulton, R. J. (1995). *Surficial materials of Canada* (No. 1880A) (p. 1880A). https://doi.org/10.4095/205040

Gagnon, C., & Fisher, N. S. (1997). Bioavailability of Sediment-Bound Methyl and Inorganic Mercury to a Marine Bivalve. *Environmental Science & Technology*, *31*(4), 993–998. https://doi.org/10.1021/es960364k

Gandois, L., Hoyt, A. M., Hatté, C., Jeanneau, L., Teisserenc, R., Liotaud, M., & Tananaev, N. (2019). Contribution of Peatland Permafrost to Dissolved Organic Matter along a Thaw Gradient in North Siberia. *Environmental Science & Technology*, *53*(24), 14165–14174. https://doi.org/10.1021/acs.est.9b03735

Gandois, L., Tananaev, N. I., Prokushkin, A., Solnyshkin, I., & Teisserenc, R. (2021). Seasonality of DOC Export From a Russian Subarctic Catchment Underlain by Discontinuous Permafrost, Highlighted by High-Frequency Monitoring. *Journal of Geophysical Research: Biogeosciences*, *126*(10), e2020JG006152. https://doi.org/10.1029/2020JG006152

Gao, Z., & Guéguen, C. (2017). Size distribution of absorbing and fluorescing DOM in Beaufort Sea, Canada Basin. *Deep Sea Research Part I: Oceanographic Research Papers*, *121*, 30–37. https://doi.org/10.1016/j.dsr.2016.12.014

Gibson, C. M., Chasmer, L. E., Thompson, D. K., Quinton, W. L., Flannigan, M. D., & Olefeldt, D. (2018). Wildfire as a major driver of recent permafrost thaw in boreal peatlands. *Nature Communications*, *9*(1), 3041. https://doi.org/10.1038/s41467-018-05457-1

Gibson, C. M., Cottenie, K., Gingras-Hill, T., Kokelj, S. V., Baltzer, J. L., Chasmer, L., & Turetsky, M. R. (2021). Mapping and understanding the vulnerability of northern peatlands to permafrost thaw at scales relevant to community adaptation planning. *Environmental Research Letters*, *16*(5), 055022. https://doi.org/10.1088/1748-9326/abe74b

Gilmour, C. C., Henry, E. A., & Mitchell, R. (1992). Sulfate stimulation of mercury methylation in freshwater sediments. *Environmental Science & Technology*, *26*(11), 2281–2287. https://doi.org/10.1021/es00035a029

Gilmour, C. C., Riedel, G. S., Ederington, M. C., Bell, J. T., Gill, G. A., & Stordal, M. C. (1998). Methylmercury concentrations and production rates across a trophic gradient in the northern Everglades. *Biogeochemistry*, *40*(2/3), 327–345. https://doi.org/10.1023/A:1005972708616

Gilmour, C. C., Podar, M., Bullock, A. L., Graham, A. M., Brown, S. D., Somenahally, A. C., et al. (2013). Mercury Methylation by Novel Microorganisms from New Environments. *Environmental Science & Technology*, *47*(20), 11810–11820. https://doi.org/10.1021/es403075t

Gionfriddo, C. M., Wymore, A. M., Jones, D. S., Wilpiszeski, R. L., Lynes, M. M., Christensen, G. A., et al. (2020). An Improved hgcAB Primer Set and Direct High-Throughput Sequencing Expand Hg-Methylator Diversity in Nature. *Frontiers in Microbiology*, *11*, 541554. https://doi.org/10.3389/fmicb.2020.541554

Girard, C., Leclerc, M., & Amyot, M. (2016). Photodemethylation of Methylmercury in Eastern Canadian Arctic Thaw Pond and Lake Ecosystems. *Environmental Science and Technology*, *50*(7), 3511–3520. https://doi.org/10.1021/acs.est.5b04921

Gonçalves-Araujo, R., Stedmon, C. A., Heim, B., Dubinenkov, I., Kraberg, A., Moiseev, D., & Bracher, A. (2015). From Fresh to Marine Waters: Characterization and Fate of Dissolved Organic Matter in the Lena River Delta Region, Siberia. *Frontiers in Marine Science*, *2*. https://doi.org/10.3389/fmars.2015.00108

Gonçalves-Araujo, R., Granskog, M. A., Bracher, A., Azetsu-Scott, K., Dodd, P. A., & Stedmon, C. A. (2016). Using fluorescent dissolved organic matter to trace and distinguish the origin of Arctic surface waters. *Scientific Reports*, *6*(1), 33978. https://doi.org/10.1038/srep33978

Goodbrand, A., Westbrook, C. J., & Kamp, G. (2019). Hydrological functions of a peatland in a Boreal Plains catchment. *Hydrological Processes*, *33*(4), 562–574. https://doi.org/10.1002/hyp.13343

Google. (2015). Satellite imagery.

Gordon, J., Quinton, W., Branfireun, B. A., & Olefeldt, D. (2016). Mercury and methylmercury biogeochemistry in a thawing permafrost wetland complex, Northwest Territories, Canada. *Hydrological Processes*, *30*(20), 3627–3638. https://doi.org/10.1002/hyp.10911

Graham, A. M., Aiken, G. R., & Gilmour, C. C. (2012). Dissolved Organic Matter Enhances Microbial Mercury Methylation Under Sulfidic Conditions. *Environmental Science & Technology*, *46*(5), 2715–2723. https://doi.org/10.1021/es203658f

Grigal, D. F. (2003). Mercury sequestration in forests and peatlands: A review. *Journal of Environmental Quality*, *32*(2), 393–405. https://doi.org/10.2134/jeq2003.3930

Guéguen, C., Cuss, C. W., Cassels, C. J., & Carmack, E. C. (2014). Absorption and fluorescence of dissolved organic matter in the waters of the Canadian Arctic Archipelago, Baffin Bay, and the Labrador Sea. *Journal of Geophysical Research: Oceans*, *119*(3), 2034–2047. https://doi.org/10.1002/2013JC009173

Hall, B. D., St. Louis, V. L., & Bodaly, R. A. (Drew). (2004). The stimulation of methylmercury production by decomposition of flooded birch leaves and jack pine needles. *Biogeochemistry*, *68*(1), 107–129. https://doi.org/10.1023/B:BIOG.0000025745.28447.8b

Halsey, L. A., Vitt, D. H., & Zoltai, S. C. (1995). Disequilibrium response of permafrost in boreal continental western Canada to climate change. *Climatic Change*, *30*(1), 57–73. https://doi.org/10.1007/BF01093225

Hamelin, S., Amyot, M., Barkay, T., Wang, Y., & Planas, D. (2011). Methanogens: Principal Methylators of Mercury in Lake Periphyton. *Environmental Science & Technology*, *45*(18), 7693–7700. https://doi.org/10.1021/es2010072

Hammerschmidt, C. R., Fitzgerald, W. F., Lamborg, C. H., Balcom, P. H., & Tseng, C.-M. (2006). Biogeochemical Cycling of Methylmercury in Lakes and Tundra Watersheds of Arctic Alaska. *Environmental Science & Technology*, *40*(4), 1204–1211. https://doi.org/10.1021/es051322b

Harris, L. I., Moore, T. R., Roulet, N. T., & Pinsonneault, A. J. (2020). Limited effect of drainage on peat properties, porewater chemistry, and peat decomposition proxies in a boreal peatland. *Biogeochemistry*, *151*(1), 43–62. https://doi.org/10.1007/s10533-020-00707-1

Harris, L. I., Schulze, C., Marouelli, K., Shewan, R., & Olefeldt, D. (In prep.). The 13C isotopic signature of methane emissions in thawing permafrost landscapes.

Hayashi, M., Quinton, W. L., Pietroniro, A., & Gibson, J. J. (2004). Hydrologic functions of wetlands in a discontinuous permafrost basin indicated by isotopic and chemical signatures. *Journal of Hydrology*, *296*(1–4), 81–97. https://doi.org/10.1016/j.jhydrol.2004.03.020

Haynes, K. M., Kane, E. S., Potvin, L., Lilleskov, E. A., Kolka, R. K., & Mitchell, C. P. J. (2017). Mobility and transport of mercury and methylmercury in peat as a function of

changes in water table regime and plant functional groups. *Global Biogeochemical Cycles*, *31*(2), 233–244. https://doi.org/10.1002/2016GB005471

Haynes, K. M., Connon, R. F., & Quinton, W. L. (2018). Permafrost thaw induced drying of wetlands at Scotty Creek, NWT, Canada. *Environmental Research Letters*, *13*(11), 114001. https://doi.org/10.1088/1748-9326/aae46c

Haynes, K. M., Frederick, I., Disher, B., Carpino, O., & Quinton, W. L. (2022). Long-term trends in wetland event response with permafrost thaw-induced landscape transition and hummock development. *Ecohydrology*, e2515. https://doi.org/10.1002/eco.2515

Heffernan, L., Estop-Aragonés, C., Knorr, K., Talbot, J., & Olefeldt, D. (2020). Long-term impacts of permafrost thaw on carbon storage in peatlands: deep losses offset by surficial accumulation. *Journal of Geophysical Research: Biogeosciences*, *125*(3), e2019JG005501. https://doi.org/doi.org/10.1029/2019JG005501

Hermosilla, T., Wulder, M. A., White, J. C., & Coops, N. C. (2022). Land cover classification in an era of big and open data: Optimizing localized implementation and training data selection to improve mapping outcomes. *Remote Sensing of Environment*, *268*, 112780. https://doi.org/10.1016/j.rse.2021.112780

Herrero Ortega, S., Catalán, N., Björn, E., Gröntoft, H., Hilmarsson, T. G., Bertilsson, S., et al. (2018). High methylmercury formation in ponds fueled by fresh humic and algal derived organic matter: High methylmercury formation in ponds. *Limnology and Oceanography*, *63*(S1), S44–S53. https://doi.org/10.1002/lno.10722

Heyes, A., Moore, T. R., Rudd, J. W. M., & Dugoua, J. J. (2000). Methyl mercury in pristine and impounded boreal peatlands, Experimental Lakes Area, Ontario. *Canadian Journal of Fisheries and Aquatic Sciences*, *57*, 2211–2222. https://doi.org/10.1139/f00-197

Hintelmann, H., & Ogrinc, N. (2003). Determination of stable mercury isotopes by ICP/MS and their application in environmental studies. *ACS Symposium Series*, *835*, 321–338.

Holloway, J. E., & Lewkowicz, A. G. (2020). Half a century of discontinuous permafrost persistence and degradation in western Canada. *Permafrost and Periglacial Processes*, *31*(1), 85–96. https://doi.org/10.1002/ppp.2017

Houde, M., Krümmel, E. M., Mustonen, T., Brammer, J., Brown, T. M., Chételat, J., et al. (2022). Contributions and perspectives of Indigenous Peoples to the study of mercury in the Arctic. *Science of The Total Environment*, *841*, 156566. https://doi.org/10.1016/j.scitotenv.2022.156566

Hsu-Kim, H., Kucharzyk, K. H., Zhang, T., & Deshusses, M. A. (2013). Mechanisms Regulating Mercury Bioavailability for Methylating Microorganisms in the Aquatic Environment: A Critical Review. *Environmental Science & Technology*, *47*(6), 2441–2456. https://doi.org/10.1021/es304370g

Hugelius, G., Loisel, J., Chadburn, S., Jackson, R. B., Jones, M., MacDonald, G., et al. (2020). Large stocks of peatland carbon and nitrogen are vulnerable to permafrost thaw. *Proceedings of the National Academy of Sciences*, *117*(34), 20438–20446. https://doi.org/10.1073/pnas.1916387117

Huguet, A., Vacher, L., Relexans, S., Saubusse, S., Froidefond, J. M., & Parlanti, E. (2009). Properties of fluorescent dissolved organic matter in the Gironde Estuary. *Organic Geochemistry*, *40*(6), 706–719. https://doi.org/10.1016/j.orggeochem.2009.03.002

Ilyniak, N. (2014). Mercury poisoning in Grassy Narrows: Environmental injustice, colonialism, and capitalist expansion in Canada. *McGill Sociological Review*, *4*, 43–66.

Jensen, S., & Jernelöv, A. (1969). Biological Methylation of Mercury in Aquatic Organisms. *Nature*, *223*(5207), 753–754. https://doi.org/10.1038/223753a0

Jiskra, M., Wiederhold, J. G., Skyllberg, U., Kronberg, R.-M., Hajdas, I., & Kretzschmar, R. (2015). Mercury Deposition and Re-emission Pathways in Boreal Forest Soils Investigated with Hg Isotope Signatures. *Environmental Science & Technology*, *49*(12), 7188–7196. https://doi.org/10.1021/acs.est.5b00742

Jiskra, M., Sonke, J. E., Obrist, D., Bieser, J., Ebinghaus, R., Myhre, C. L., et al. (2018). A vegetation control on seasonal variations in global atmospheric mercury concentrations. *Nature Geoscience*, *11*(4), 244–250. https://doi.org/10.1038/s41561-018-0078-8

Jonsson, S., Skyllberg, U., Nilsson, M. B., Westlund, P.-O., Shchukarev, A., Lundberg, E., & Björn, E. (2012). Mercury Methylation Rates for Geochemically Relevant Hg^{II} Species in Sediments. *Environmental Science & Technology*, *46*(21), 11653–11659. https://doi.org/10.1021/es3015327

Jonsson, S., Mastromonaco, M. N., Wang, F., Bravo, A. G., Cairns, W. R. L., Chételat, J., et al. (2022). Arctic methylmercury cycling. *Science of The Total Environment*, 157445. https://doi.org/10.1016/j.scitotenv.2022.157445

Kaiser, K., & Kalbitz, K. (2012). Cycling downwards – dissolved organic matter in soils. *Soil Biology and Biochemistry*, *52*, 29–32. https://doi.org/10.1016/j.soilbio.2012.04.002

Kellerman, A. M., Kothawala, D. N., Dittmar, T., & Tranvik, L. J. (2015). Persistence of dissolved organic matter in lakes related to its molecular characteristics. *Nature Geoscience*, *8*(6), 454–457. https://doi.org/10.1038/ngeo2440

Kelly, C. A., Rudd, J. W. M., & Holoka, M. H. (2003). Effect of pH on Mercury Uptake by an Aquatic Bacterium: Implications for Hg Cycling. *Environmental Science & Technology*, *37*(13), 2941–2946. https://doi.org/10.1021/es026366o

Kim, S., Kramer, R. W., & Hatcher, P. G. (2003). Graphical Method for Analysis of Ultrahigh-Resolution Broadband Mass Spectra of Natural Organic Matter, the Van Krevelen Diagram. *Analytical Chemistry*, *75*(20), 5336–5344. https://doi.org/10.1021/ac034415p

Kirk, J. L., & St. Louis, V. L. (2009). Multiyear Total and Methyl Mercury Exports from Two Major Sub-Arctic Rivers Draining into Hudson Bay, Canada. *Environmental Science & Technology*, *43*(7), 2254–2261. https://doi.org/10.1021/es803138z

Klaminder, J., Yoo, K., Rydberg, J., & Giesler, R. (2008). An explorative study of mercury export from a thawing palsa mire. *Journal of Geophysical Research: Biogeosciences*, *113*(4). https://doi.org/10.1029/2008JG000776

Klapstein, S. J., & O'Driscoll, N. J. (2018). Methylmercury Biogeochemistry in Freshwater Ecosystems: A Review Focusing on DOM and Photodemethylation. *Bulletin of Environmental Contamination and Toxicology*, *100*(1), 14–25. https://doi.org/10.1007/s00128-017-2236-x

Klapstein, S. J., Ziegler, S. E., & O'Driscoll, N. J. (2018). Methylmercury photodemethylation is inhibited in lakes with high dissolved organic matter. *Environmental Pollution*, *232*, 392–401. https://doi.org/10.1016/j.envpol.2017.09.049

Koch, B. P., & Dittmar, T. (2006). From mass to structure: an aromaticity index for high-resolution mass data of natural organic matter. *Rapid Communications in Mass Spectrometry*, *20*(5), 926–932. https://doi.org/10.1002/rcm.2386

Koger, J. M., Newman, B. D., & Goering, T. J. (2018). Chemostatic behaviour of major ions and contaminants in a semiarid spring and stream system near Los Alamos, NM, USA. *Hydrological Processes*, *32*(11), 1709–1716. https://doi.org/10.1002/hyp.11624

Kothawala, D. N., Roehm, C., Blodau, C., & Moore, T. R. (2012). Selective adsorption of dissolved organic matter to mineral soils. *Geoderma*, *189–190*, 334–342. https://doi.org/10.1016/j.geoderma.2012.07.001

Kothawala, D. N., Stedmon, C. A., Müller, R. A., Weyhenmeyer, G. A., Köhler, S. J., & Tranvik, L. J. (2014). Controls of dissolved organic matter quality: Evidence from a large-scale boreal lake survey. *Global Change Biology*, *20*(4), 1101–1114. https://doi.org/10.1111/gcb.12488

Krylov, I. N., Drozdova, A. N., & Labutin, T. A. (2020). Albatross R package to study PARAFAC components of DOM fluorescence from mixing zones of arctic shelf seas. *Chemometrics and Intelligent Laboratory Systems*, *207*, 104176. https://doi.org/10.1016/j.chemolab.2020.104176

Kuhn, M. A., Varner, R. K., Bastviken, D., Crill, P., MacIntyre, S., Turetsky, M., et al. (2021). BAWLD-CH₄: a comprehensive dataset of methane fluxes from boreal and arctic ecosystems. *Earth System Science Data*, *13*(11), 5151–5189. https://doi.org/10.5194/essd-13-5151-2021

Kuhn, M. A., Thompson, L. M., Winder, J. C., Braga, L. P. P., Tanentzap, A. J., Bastviken, D., & Olefeldt, D. (2021). Opposing Effects of Climate and Permafrost Thaw on CH_4 and CO_2 Emissions From Northern Lakes. *AGU Advances*, *2*(4). https://doi.org/10.1029/2021AV000515

Kuhn, M. A., Olefeldt, D., McGuire, D., Arndt, K., Bastviken, D., Crill, P., et al. (In prep.). Boreal-Arctic methane emissions: Influence of warming, permafrost thaw, and hydrologic change.

Lafferty, A., Gonet, J., Wasilik, T., Thompson, L., Ertman, S., & Bandara, S. (2023). Navigating the Shifting Landscape of Engagement in Northern Research: Perspectives from Early Career Researchers. *The Northern Review*, *54*. https://doi.org/10.22584/nr54.2023.001

Lafrenière, M. J., & Lamoureux, S. F. (2019). Effects of changing permafrost conditions on hydrological processes and fluvial fluxes. *Earth-Science Reviews*, *191*, 212–223. https://doi.org/10.1016/j.earscirev.2019.02.018

Laird, M. J., Henao, J. J. A., Reyes, E. S., Stark, K. D., Low, G., Swanson, H. K., & Laird, B. D. (2018). Mercury and omega-3 fatty acid profiles in freshwater fish of the Dehcho Region, Northwest Territories: Informing risk benefit assessments. *Science of The Total Environment*, *637–638*, 1508–1517. https://doi.org/10.1016/j.scitotenv.2018.04.381

Lam, W. Y., Mackereth, R. W., & Mitchell, C. P. J. (2022). Landscape controls on total mercury and methylmercury export from small boreal forest catchments. *Biogeochemistry*, *160*(1), 89–104. https://doi.org/10.1007/s10533-022-00941-9

Lamberink, L. (2022, October 22). N.W.T. First Nation to rebuild climate research station ravaged by late-season wildfire. *CBC News*. Retrieved from https://www.cbc.ca/news/canada/north/scotty-creek-research-station-fire-1.6625171

Lavoie, R. A., Amyot, M., & Lapierre, J. (2019). Global Meta-Analysis on the Relationship Between Mercury and Dissolved Organic Carbon in Freshwater Environments. *Journal of Geophysical Research: Biogeosciences*, *124*(6), 1508–1523. https://doi.org/10.1029/2018JG004896

Le Faucheur, S., Campbell, P. G. C., Fortin, C., & Slaveykova, V. I. (2014). Interactions between mercury and phytoplankton: Speciation, bioavailability, and internal handling: Mercury-phytoplankton interactions. *Environmental Toxicology and Chemistry*, *33*(6), 1211–1224. https://doi.org/10.1002/etc.2424

Lefcheck, J. S. (2016). PIECEWISESEM : Piecewise structural equation modelling in R for ecology, evolution, and systematics. *Methods in Ecology and Evolution*, *7*(5), 573–579. https://doi.org/10.1111/2041-210X.12512

Lehnherr, I., & St. Louis, V. L. (2009). Importance of Ultraviolet Radiation in the Photodemethylation of Methylmercury in Freshwater Ecosystems. *Environmental Science & Technology*, *43*(15), 5692–5698. https://doi.org/10.1021/es9002923

Lehnherr, I., St. Louis, V. L., & Kirk, J. L. (2012). Methylmercury cycling in high arctic wetland ponds: Controls on sedimentary production. *Environmental Science and Technology*, *46*(19), 10523–10531. https://doi.org/10.1021/es300577e

Lehnherr, I., St. Louis, V. L., Emmerton, C. A., Barker, J. D., & Kirk, J. L. (2012). Methylmercury Cycling in High Arctic Wetland Ponds: Sources and Sinks. *Environmental Science & Technology*, *46*(19), 10514–10522. https://doi.org/10.1021/es300576p

Lei, P., Nunes, L. M., Liu, Y.-R., Zhong, H., & Pan, K. (2019). Mechanisms of algal biomass input enhanced microbial Hg methylation in lake sediments. *Environment International*, *126*, 279–288. https://doi.org/10.1016/j.envint.2019.02.043

Lescord, G. L., Emilson, E. J. S., Johnston, T. A., Branfireun, B. A., & Gunn, J. M. (2018). Optical Properties of Dissolved Organic Matter and Their Relation to Mercury Concentrations in Water and Biota Across a Remote Freshwater Drainage Basin. *Environmental Science & Technology*, *52*(6), 3344–3353. https://doi.org/10.1021/acs.est.7b05348

Lescord, G. L., Johnston, T., Branfireun, B. A., & Gunn, J. M. (2019). Mercury bioaccumulation in relation to changing physicochemical and ecological factors across a large and undisturbed boreal watershed. *Canadian Journal of Fisheries and Aquatic Sciences*, *76*(12), 2165–2175. https://doi.org/10.1139/cjfas-2018-0465

Lim, A. G., Sonke, J. E., Krickov, I. V., Manasypov, R. M., Loiko, S. V., & Pokrovsky, O. S. (2019). Enhanced particulate Hg export at the permafrost boundary, western Siberia. *Environmental Pollution*, *254*, 113083. https://doi.org/10.1016/j.envpol.2019.113083

Lim, A. G., Jiskra, M., Sonke, J. E., Loiko, S. V., Kosykh, N., & Pokrovsky, O. S. (2020). A revised pan-Arctic permafrost soil Hg pool based on Western Siberian peat Hg and carbon observations. *Biogeosciences*, *17*(12), 3083–3097. https://doi.org/10.5194/bg-17-3083-2020

Lin, Y., Campbell, A. N., Bhattacharyya, A., DiDonato, N., Thompson, A. M., Tfaily, M. M., et al. (2021). Differential effects of redox conditions on the decomposition of litter and soil organic matter. *Biogeochemistry*, *154*(1), 1–15. https://doi.org/10.1007/s10533-021-00790-y

Liu, S., Wang, P., Huang, Q., Yu, J., Pozdniakov, S. P., & Kazak, E. S. (2022). Seasonal and spatial variations in riverine DOC exports in permafrost-dominated Arctic river basins. *Journal of Hydrology*, *612*, 128060. https://doi.org/10.1016/j.jhydrol.2022.128060

Loseto, L. L., Siciliano, S. D., & Lean, D. R. S. (2004). Methylmercury production in high arctic wetlands. *Environmental Toxicology and Chemistry*, *23*(1), 17–23. https://doi.org/10.1897/02-644

Mack, M., Connon, R., Makarieva, O., McLaughlin, J., Nesterova, N., & Quinton, W. (2021). Heterogenous runoff trends in peatland-dominated basins throughout the circumpolar North. *Environmental Research Communications*, *3*(7), 075006. https://doi.org/10.1088/2515-7620/ac11ed

MacMillan, G. A., Girard, C., Chételat, J., Laurion, I., & Amyot, M. (2015). High Methylmercury in Arctic and Subarctic Ponds is Related to Nutrient Levels in the Warming Eastern Canadian Arctic. *Environmental Science & Technology*, *49*(13), 7743–7753. https://doi.org/10.1021/acs.est.5b00763

Mangal, V., DeGasparro, S., Beresford, D. V., & Guéguen, C. (2020). Linking molecular and optical properties of dissolved organic matter across a soil-water interface on Akimiski Island (Nunavut, Canada). *Science of The Total Environment*, *704*, 135415. https://doi.org/10.1016/j.scitotenv.2019.135415

Mangal, V., Lam, W. Y., Huang, H., Emilson, E. J. S., Mackereth, R. W., & Mitchell, C. P. J. (2022). Molecular correlations of dissolved organic matter with inorganic mercury and methylmercury in Canadian boreal streams. *Biogeochemistry*, *160*(1), 127–144. https://doi.org/10.1007/s10533-022-00944-6

Martino, C., Morton, J. T., Marotz, C. A., Thompson, L. R., Tripathi, A., Knight, R., & Zengler, K. (2019). A Novel Sparse Compositional Technique Reveals Microbial Perturbations. *MSystems*, *4*(1), e00016-19, /msystems/4/1/msys.00016-19.atom. https://doi.org/10.1128/mSystems.00016-19

Matilainen, A., Vepsäläinen, M., & Sillanpää, M. (2010). Natural organic matter removal by coagulation during drinking water treatment: A review. *Advances in Colloid and Interface Science*, *159*(2), 189–197. https://doi.org/10.1016/j.cis.2010.06.007

Mattsson, T., Kortelainen, P., & Räike, A. (2005). Export of DOM from Boreal Catchments: Impacts of Land Use Cover and Climate. *Biogeochemistry*, *76*(2), 373–394. https://doi.org/10.1007/s10533-005-6897-x

Mattsson, T., Kortelainen, P., Räike, A., Lepistö, A., & Thomas, D. N. (2015). Spatial and temporal variability of organic C and N concentrations and export from 30 boreal rivers induced by land use and climate. *Science of The Total Environment*, *508*, 145–154. https://doi.org/10.1016/j.scitotenv.2014.11.091

Mawowa, S. (2013). The Political Economy of Artisanal and Small-Scale Gold Mining in Central Zimbabwe. *Journal of Southern African Studies*, *39*(4), 921–936. https://doi.org/10.1080/03057070.2013.858540

McDaniel, E. A., Peterson, B. D., Stevens, S. L. R., Tran, P. Q., Anantharaman, K., & McMahon, K. D. (2020). Expanded Phylogenetic Diversity and Metabolic Flexibility of Mercury-Methylating Microorganisms. *MSystems*, *5*(4), e00299-20. https://doi.org/10.1128/mSystems.00299-20

McKnight, D. M., Boyer, E. W., Westerhoff, P. K., Doran, P. T., Kulbe, T., & Andersen, D. T. (2001). Spectrofluorometric characterization of dissolved organic matter for indication of precursor organic material and aromaticity. *Limnology and Oceanography*, *46*(1), 38–48. https://doi.org/10.4319/lo.2001.46.1.0038

de Melo, M. L., Gérardin, M.-L., Fink-Mercier, C., & del Giorgio, P. A. (2022). Patterns in riverine carbon, nutrient and suspended solids export to the Eastern James Bay: links to climate, hydrology and landscape. *Biogeochemistry*, *161*(3), 291–314. https://doi.org/10.1007/s10533-022-00983-z

Mergler, D., Anderson, H. A., Chan, L. H. M., Mahaffey, K. R., Murray, M., Sakamoto, M., & Stern, A. H. (2007). Methylmercury exposure and health effects in humans: a worldwide concern. *AMBIO: A Journal of the Human Environment*, *36*(1), 3–11. https://doi.org/10.1579/0044-7447(2007)36[3:MEAHEI]2.0.CO;2

Mistry, J., Chuguransky, S., Williams, L., Qureshi, M., Salazar, G. A., Sonnhammer, E. L. L., et al. (2021). Pfam: The protein families database in 2021. *Nucleic Acids Research*, *49*(D1), D412–D419. https://doi.org/10.1093/nar/gkaa913

Mitchell, C. P. J., Branfireun, B. A., & Kolka, R. K. (2008a). Assessing sulfate and carbon controls on net methylmercury production in peatlands: An in situ mesocosm approach. *Applied Geochemistry*, *23*(3), 503–518. https://doi.org/10.1016/j.apgeochem.2007.12.020

Mitchell, C. P. J., Branfireun, B. A., & Kolka, R. K. (2008b). Spatial Characteristics of Net Methylmercury Production Hot Spots in Peatlands. *Environmental Science & Technology*, *42*(4), 1010–1016. https://doi.org/10.1021/es0704986

Mitchell, C. P. J., Branfireun, B. A., & Kolka, R. K. (2008c). Total mercury and methylmercury dynamics in upland–peatland watersheds during snowmelt. *Biogeochemistry*, *90*(3), 225–241. https://doi.org/10.1007/s10533-008-9246-z

Moslemi-Aqdam, M., Low, G., Low, M., Laird, B. D., Branfireun, B. A., & Swanson, H. K. (2023). Estimates, spatial variability, and environmental drivers of mercury biomagnification rates through lake food webs in the Canadian subarctic. *Environmental Research*, *217*, 114835. https://doi.org/10.1016/j.envres.2022.114835

Murphy, K. R., Hambly, A., Singh, S., Henderson, R. K., Baker, A., Stuetz, R., & Khan, S. J. (2011). Organic Matter Fluorescence in Municipal Water Recycling Schemes: Toward a Unified PARAFAC Model. *Environmental Science & Technology*, *45*(7), 2909–2916. https://doi.org/10.1021/es103015e

Murphy, K. R., Stedmon, C. A., Wenig, P., & Bro, R. (2014). OpenFluor- an online spectral library of auto-fluorescence by organic compounds in the environment. *Analytical Methods*, *6*(3), 658–661. https://doi.org/10.1039/C3AY41935E

Musolff, A., Schmidt, C., Selle, B., & Fleckenstein, J. H. (2015). Catchment controls on solute export. *Advances in Water Resources*, *86*, 133–146. https://doi.org/10.1016/j.advwatres.2015.09.026

Nagorski, S. A., Engstrom, D. R., Hudson, J. P., Krabbenhoft, D. P., Hood, E., DeWild, J. F., & Aiken, G. R. (2014). Spatial distribution of mercury in southeastern Alaskan streams influenced by glaciers, wetlands, and salmon. *Environmental Pollution*, *184*, 62–72. https://doi.org/10.1016/j.envpol.2013.07.040

Natural Resources Canada. (2013). *Canadian Digital Elevation Model*. Government of Canada.

Natural Resources Canada. (2022). *National Hydrometric Network Basin Polygons*. Government of Canada.

Nelson, K., Thompson, D., Hopkinson, C., Petrone, R., & Chasmer, L. (2021). Peatland-fire interactions: A review of wildland fire feedbacks and interactions in Canadian boreal peatlands. *Science of The Total Environment*, *769*, 145212. https://doi.org/10.1016/j.scitotenv.2021.145212

Nercessian, O., Noyes, E., Kalyuzhnaya, M. G., Lidstrom, M. E., & Chistoserdova, L. (2005). Bacterial Populations Active in Metabolism of C $_1$ Compounds in the Sediment of Lake Washington, a Freshwater Lake. *Applied and Environmental Microbiology*, *71*(11), 6885–6899. https://doi.org/10.1128/AEM.71.11.6885-6899.2005

Obrist, D., Agnan, Y., Jiskra, M., Olson, C. L., Colegrove, D. P., Hueber, J., et al. (2017). Tundra uptake of atmospheric elemental mercury drives Arctic mercury pollution. *Nature*, *547*(7662), 201–204. https://doi.org/10.1038/nature22997

Ohno, T. (2002). Fluorescence Inner-Filtering Correction for Determining the Humification Index of Dissolved Organic Matter. *Environmental Science & Technology*, *36*(4), 742–746. https://doi.org/10.1021/es0155276

Oksanen, J., Blanchet, F. G., Kindt, R., Legendre, P., Minchin, P. R., O'Hara, R. B., et al. (2022). vegan: Community Ecology Package. R Package Version 2.2-0. Retrieved from http://CRAN.Rproject.org/package=vegan

Olefeldt, D., & Roulet, N. T. (2012). Effects of permafrost and hydrology on the composition and transport of dissolved organic carbon in a subarctic peatland complex. *Journal of Geophysical Research: Biogeosciences*, *117*, G01005. https://doi.org/10.1029/2011JG001819

Olefeldt, D., Turetsky, M. R., & Blodau, C. (2013). Altered Composition and Microbial versus UV-Mediated Degradation of Dissolved Organic Matter in Boreal Soils Following Wildfire. *Ecosystems*, *16*(8), 1396–1412. https://doi.org/10.1007/s10021-013-9691-y

Olefeldt, D., Roulet, N., Giesler, R., & Persson, A. (2013). Total waterborne carbon export and DOC composition from ten nested subarctic peatland catchments-importance of peatland cover, groundwater influence, and inter-annual variability of precipitation patterns. *Hydrological Processes*, *27*(16), 2280–2294. https://doi.org/10.1002/hyp.9358

Olefeldt, D., Persson, A., & Turetsky, M. R. (2014). Influence of the permafrost boundary on dissolved organic matter characteristics in rivers within the Boreal and Taiga plains of western Canada. *Environmental Research Letters*, *9*(3), 035005. https://doi.org/10.1088/1748-9326/9/3/035005

Olefeldt, D., Hovemyr, M., Kuhn, M. A., Bastviken, D., Bohn, T. J., Connolly, J., et al. (2021). The Boreal–Arctic Wetland and Lake Dataset (BAWLD). *Earth System Science Data*, *13*(11), 5127–5149. https://doi.org/10.5194/essd-13-5127-2021

Oliver, A. A., Tank, S. E., Giesbrecht, I., Korver, M. C., Floyd, W. C., Sanborn, P., et al. (2017). A global hotspot for dissolved organic carbon in hypermaritime watersheds of coastal British Columbia. *Biogeosciences*, *14*(15), 3743–3762. https://doi.org/10.5194/bg-14-3743-2017

Osburn, C. L., Boyd, T. J., Montgomery, M. T., Bianchi, T. S., Coffin, R. B., & Paerl, H. W. (2016). Optical proxies for terrestrial dissolved organic matter in estuaries and coastal waters. *Frontiers in Marine Science*, *2*(Journal Article), 127.

Osburn, C. L., Anderson, N. J., Stedmon, C. A., Giles, M. E., Whiteford, E. J., McGenity, T. J., et al. (2017). Shifts in the Source and Composition of Dissolved Organic Matter in Southwest Greenland Lakes Along a Regional Hydro-climatic Gradient. *Journal of Geophysical Research: Biogeosciences*, *122*(12), 3431–3445. https://doi.org/10.1002/2017JG003999

Pacyna, J. M., Travnikov, O., De Simone, F., Hedgecock, I. M., Sundseth, K., Pacyna, E. G., et al. (2016). Current and future levels of mercury atmospheric pollution on a global scale. *Atmospheric Chemistry and Physics*, *16*(19), 12495–12511. https://doi.org/10.5194/acp-16-12495-2016

Parada, A. E., Needham, D. M., & Fuhrman, J. A. (2016). Every base matters: assessing small subunit rRNA primers for marine microbiomes with mock communities, time series and global field samples: Primers for marine microbiome studies. *Environmental Microbiology*, *18*(5), 1403–1414. https://doi.org/10.1111/1462-2920.13023

Park, Y., Engel, B., Frankenberger, J., & Hwang, H. (2015). A Web-Based Tool to Estimate Pollutant Loading Using LOADEST. *Water*, *7*(12), 4858–4868. https://doi.org/10.3390/w7094858

Parks, J. M., Johs, A., Podar, M., Bridou, R., Hurt, R. A., Smith, S. D., et al. (2013). The Genetic Basis for Bacterial Mercury Methylation. *Science*, *339*(6125), 1332–1335. https://doi.org/10.1126/science.1230667

Pelletier, N., Talbot, J., Olefeldt, D., Turetsky, M., Blodau, C., Sonnentag, O., & Quinton, W. L. (2017). Influence of Holocene permafrost aggradation and thaw on the paleoecology and carbon storage of a peatland complex in northwestern Canada. *The Holocene*, *27*(9), 1391–1405. https://doi.org/10.1177/0959683617693899

Peterson, B. D., Krabbenhoft, D. P., McMahon, K. D., Ogorek, J. M., Tate, M. T., Orem, W. H., & Poulin, B. A. (2023). Environmental formation of methylmercury is controlled by synergy of inorganic mercury bioavailability and microbial mercury-methylation capacity. *Environmental Microbiology*, 1462-2920.16364. https://doi.org/10.1111/1462-2920.16364

Podar, M., Gilmour, C. C., Brandt, C. C., Soren, A., Brown, S. D., Crable, B. R., et al. (2015). Global prevalence and distribution of genes and microorganisms involved in mercury methylation. *Science Advances*, *1*(9), e1500675. https://doi.org/10.1126/sciadv.1500675

Pohle, I., Baggaley, N., Palarea-Albaladejo, J., Stutter, M., & Glendell, M. (2021). A Framework for Assessing Concentration-Discharge Catchment Behavior From Low-Frequency Water Quality Data. *Water Resources Research*, *57*(9), e2021WR029692. https://doi.org/10.1029/2021WR029692

Porter, J. (2017). Children of the poisoned river. *CBC News*. Retrieved from https://www.cbc.ca/news2/interactives/children-of-the-poisoned-river-mercury-poisoning-grassy-narrows-first-nation/

Poulin, B. A., Ryan, J. N., Tate, M. T., Krabbenhoft, D. P., Hines, M. E., Barkay, T., et al. (2019). Geochemical Factors Controlling Dissolved Elemental Mercury and Methylmercury Formation in Alaskan Wetlands of Varying Trophic Status. *Environmental Science & Technology*, *53*(11), 6203–6213. https://doi.org/10.1021/acs.est.8b06041

Pracht, L. E., Tfaily, M. M., Ardissono, R. J., & Neumann, R. B. (2018). Molecular characterization of organic matter mobilized from Bangladeshi aquifer sediment: tracking carbon compositional change during microbial utilization. *Biogeosciences*, *15*(6), 1733–1747. https://doi.org/10.5194/bg-15-1733-2018

Pucher, M., Wünsch, U., Weigelhofer, G., Murphy, K., Hein, T., & Graeber, D. (2019). staRdom: Versatile Software for Analyzing Spectroscopic Data of Dissolved Organic Matter in R. *Water*, *11*(11), 2366. https://doi.org/10.3390/w11112366

Pugh, E. A., Olefeldt, D., Leader, S. N., Hokanson, K. J., & Devito, K. J. (2021). Characteristics of Dissolved Organic Carbon in Boreal Lakes: High Spatial and Inter-Annual Variability Controlled by Landscape Attributes and Wet-Dry Periods. *Water Resources Research*, *57*(11). https://doi.org/10.1029/2021WR030021

Queimaliños, C., Reissig, M., Pérez, G. L., Soto Cárdenas, C., Gerea, M., Garcia, P. E., et al. (2019). Linking landscape heterogeneity with lake dissolved organic matter properties assessed through absorbance and fluorescence spectroscopy: Spatial and seasonal patterns in temperate lakes of Southern Andes (Patagonia, Argentina). *Science of The*

Total Environment, *686*(Generic), 223–235. https://doi.org/10.1016/j.scitotenv.2019.05.396

Quinton, W. L., Hayashi, M., & Pietroniro, A. (2003). Connectivity and storage functions of channel fens and flat bogs in northern basins. *Hydrological Processes*, *17*(18), 3665–3684. https://doi.org/10.1002/hyp.1369

Quinton, W. L., Hayashi, M., & Chasmer, L. E. (2009). Peatland Hydrology of Discontinuous Permafrost in the Northwest Territories: Overview and Synthesis. *Canadian Water Resources Journal*, *34*(4), 311–328. https://doi.org/10.4296/cwrj3404311

Quinton, W. L., Hayashi, M., & Chasmer, L. E. (2011). Permafrost-thaw-induced land-cover change in the Canadian subarctic: implications for water resources. *Hydrological Processes*, *25*(1), 152–158. https://doi.org/10.1002/hyp.7894

R Core Team. (2022). R: A language and environment for statistical computing. R Foundation for Statistical Computing. Retrieved from https://www.R-project.org/

Ren, W., Wu, X., Ge, X., Lin, G., Zhou, M., Long, Z., et al. (2021). Characteristics of dissolved organic matter in lakes with different eutrophic levels in southeastern Hubei Province, China. *Journal of Oceanology and Limnology*, *39*(4), 1256–1276. https://doi.org/10.1007/s00343-020-0102-x

Richardson, M., Chételat, J., MacMillan, G. A., & Amyot, M. (2021). Mercury concentrations and associations with dissolved organic matter are modified by water residence time in eastern Canadian lakes along a 30° latitudinal gradient. *Limnology and Oceanography*, *66*(S1). https://doi.org/10.1002/lno.11580

Riedel, T., Biester, H., & Dittmar, T. (2012). Molecular Fractionation of Dissolved Organic Matter with Metal Salts. *Environmental Science & Technology*, *46*(8), 4419–4426. https://doi.org/10.1021/es203901u

Robins, N. A. (2011). *Mercury, mining, and empire: the human and ecological cost of colonial silver mining in the Andes*. Bloomington: Indiana University Press.

Roth, S., Poulin, B. A., Baumann, Z., Liu, X., Zhang, L., Krabbenhoft, D. P., et al. (2021). Nutrient Inputs Stimulate Mercury Methylation by Syntrophs in a Subarctic Peatland. *Frontiers in Microbiology*, *12*, 741523. https://doi.org/10.3389/fmicb.2021.741523

Rudd, J. W., Kelly, C. A., Sellers, P., Flett, R. J., & Townsend, B. E. (2021). Why the English–Wabigoon river system is still polluted by mercury 57 years after its contamination. *FACETS*, *6*(1), 2002–2027. https://doi.org/10.1139/facets-2021-0093

Runkel, R. L., Crawford, C. G., & Cohn, T. A. (2004). Load estimator (LOADEST): a FORTRAN program for estimating constituent loads in streams and rivers. *Techniques and Methods 4-A5*. https://doi.org/10.3133/tm4A5

Rydberg, J., Klaminder, J., Rosén, P., & Bindler, R. (2010). Climate driven release of carbon and mercury from permafrost mires increases mercury loading to sub-arctic lakes. *Science of The Total Environment*, *408*(20), 4778–4783. https://doi.org/10.1016/j.scitotenv.2010.06.056

Salopree, R. (2022, September 17). Oral teaching at Mbehcho.

Schaefer, K., Elshorbany, Y., Jafarov, E., Schuster, P. F., Striegl, R. G., Wickland, K. P., & Sunderland, E. M. (2020). Potential impacts of mercury released from thawing permafrost. *Nature Communications*, *11*(1), 4650. https://doi.org/10.1038/s41467-020-18398-5

Schelker, J., Burns, D. A., Weiler, M., & Laudon, H. (2011). Hydrological mobilization of mercury and dissolved organic carbon in a snow-dominated, forested watershed:

Conceptualization and modeling. *Journal of Geophysical Research*, *116*(G1), G01002. https://doi.org/10.1029/2010JG001330

Schmidt, O., Hink, L., Horn, M. A., & Drake, H. L. (2016). Peat: home to novel syntrophic species that feed acetate- and hydrogen-scavenging methanogens. *The ISME Journal*, *10*(8), 1954–1966. https://doi.org/10.1038/ismej.2015.256

Schulze, C., Sonnentag, O., Voigt, C., Thompson, L., van Delden, L., Heffernan, L., et al. (2023). Nitrous Oxide Fluxes in Permafrost Peatlands remain negligible after Wildfire and Thermokarst Disturbance. *Journal of Geophysical Research: Biogeosciences*, e2022JG007322. https://doi.org/10.1029/2022JG007322

Schuster, P. F., Schaefer, K. M., Aiken, G. R., Antweiler, R. C., Dewild, J. F., Gryziec, J. D., et al. (2018). Permafrost Stores a Globally Significant Amount of Mercury. *Geophysical Research Letters*, *45*(3), 1463–1471. https://doi.org/10.1002/2017GL075571

Scully, N. M., & Lean, D. R. S. (1994). The attenuation of ultraviolet radiation in temperate lakes. *Arch Hydrobiol Beih Ergebn Limnol*, *43*, 135–144.

Sellers, P., Kelly, C. A., & Rudd, J. W. M. (2001). Fluxes of methylmercury to the water column of a drainage lake: The relative importance of internal and external sources. *Limnology and Oceanography*, *46*(3), 623–631. https://doi.org/10.4319/lo.2001.46.3.0623

Shanley, J. B., Taylor, V. F., Ryan, K. A., Chalmers, A. T., Perdrial, J., & Stubbins, A. (2022). Using dissolved organic matter fluorescence to predict total mercury and methylmercury in forested headwater streams, Sleepers River, Vermont USA. *Hydrological Processes*, *36*(5), e14572. https://doi.org/10.1002/hyp.14572

Shao, D., Kang, Y., Wu, S., & Wong, M. H. (2012). Effects of sulfate reducing bacteria and sulfate concentrations on mercury methylation in freshwater sediments. *Science of The Total Environment*, *424*, 331–336. https://doi.org/10.1016/j.scitotenv.2011.09.042

Shipley, B. (2000). A New Inferential Test for Path Models Based on Directed Acyclic Graphs. *Structural Equation Modeling: A Multidisciplinary Journal*, *7*(2), 206–218. https://doi.org/10.1207/S15328007SEM0702_4

Shogren, A. J., Zarnetske, J. P., Abbott, B. W., Iannucci, F., Medvedeff, A., Cairns, S., et al. (2021). Arctic concentration–discharge relationships for dissolved organic carbon and nitrate vary with landscape and season. *Limnology and Oceanography*, *66*(S1), S197–S215. https://doi.org/10.1002/lno.11682

Skyllberg, U. (2008). Competition among thiols and inorganic sulfides and polysulfides for Hg and MeHg in wetland soils and sediments under suboxic conditions: Illumination of controversies and implications for MeHg net production. *Journal of Geophysical Research: Biogeosciences*, *113*(G2). https://doi.org/10.1029/2008JG000745

Soerensen, A. L., Jacob, D. J., Schartup, A. T., Fisher, J. A., Lehnherr, I., St. Louis, V. L., et al. (2016). A mass budget for mercury and methylmercury in the Arctic Ocean. *Global Biogeochemical Cycles*, *30*(4), 560–575. https://doi.org/10.1002/2015GB005280

Sonke, J. E., Teisserenc, R., Heimbürger-Boavida, L.-E., Petrova, M. V., Marusczak, N., Le Dantec, T., et al. (2018). Eurasian river spring flood observations support net Arctic Ocean mercury export to the atmosphere and Atlantic Ocean. *Proceedings of the National Academy of Sciences*, *115*(50), E11586–E11594. https://doi.org/10.1073/pnas.1811957115

Sonnentag, O. (2022). AmeriFlux AmeriFlux CA-SMC Smith Creek [Data set]. AmeriFlux; Universite de Montreal, Departement de geographie. https://doi.org/10.17190/AMF/1767830

Sonnentag, O., & Quinton, W. (2022). AmeriFlux AmeriFlux CA-SCC Scotty Creek Landscape [Data set]. AmeriFlux; Université de Montréal; Wilfrid Laurier University. https://doi.org/10.17190/AMF/1480303

Spence, C., Norris, M., Bickerton, G., Bonsal, B. R., Brua, R., Culp, J. M., et al. (2020). The Canadian Water Resource Vulnerability Index to Permafrost Thaw (CWRVIPT). *Arctic Science*, (0), 1–26. https://doi.org/10.1139/as-2019-0028

St. Louis, V. L., Rudd, J. W. M., Kelly, C. A., Beaty, K. G., Bloom, N. S., & Flett, R. J. (1994). Importance of Wetlands as Sources of Methyl Mercury to Boreal Forest Ecosystems. *Canadian Journal of Fisheries and Aquatic Sciences*, *51*(5), 1065–1076. https://doi.org/10.1139/f94-106

St. Louis, V. L., Rudd, J. W. M., Kelly, C. A., Bodaly, R. A. (Drew), Paterson, M. J., Beaty, K. G., et al. (2004). The Rise and Fall of Mercury Methylation in an Experimental Reservoir. *Environmental Science & Technology*, *38*(5), 1348–1358. https://doi.org/10.1021/es034424f

St. Louis, V. L., Sharp, M. J., Steffen, A., May, A., Barker, J., Kirk, J. L., et al. (2005). Some Sources and Sinks of Monomethyl and Inorganic Mercury on Ellesmere Island in the Canadian High Arctic. *Environmental Science & Technology*, *39*(8), 2686–2701. https://doi.org/10.1021/es049326o

St. Pierre, K. A., Zolkos, S., Shakil, S., Tank, S. E., St. Louis, V. L., & Kokelj, S. V. (2018). Unprecedented Increases in Total and Methyl Mercury Concentrations Downstream of Retrogressive Thaw Slumps in the Western Canadian Arctic. *Environmental Science & Technology*, *52*(24), 14099–14109. https://doi.org/10.1021/acs.est.8b05348

St. Pierre, K. A., Danielsen, B. K., Hermesdorf, L., D'Imperio, L., Iversen, L. L., & Elberling, B. (2019). Drivers of net methane uptake across Greenlandic dry heath tundra landscapes. *Soil Biology and Biochemistry*, *138*, 107605. https://doi.org/10.1016/j.soilbio.2019.107605

Staniszewska, K. J., Reyes, A. V., Cooke, C. A., Miller, B. S., & Woywitka, R. J. (2022). Permafrost, geomorphic, and hydroclimatic controls on mercury, methylmercury, and lead concentrations and exports in Old Crow River, arctic western Canada. *Chemical Geology*, *596*, 120810. https://doi.org/10.1016/j.chemgeo.2022.120810

Stedmon, C. A., & Markager, S. (2005). Tracing the production and degradation of autochthonous fractions of dissolved organic matter by fluorescence analysis. *Limnology and Oceanography*, *50*(5), 1415–1426. https://doi.org/10.4319/lo.2005.50.5.1415

Tam, B. Y., Szeto, K., Bonsal, B., Flato, G., Cannon, A. J., & Rong, R. (2019). CMIP5 drought projections in Canada based on the Standardized Precipitation Evapotranspiration Index. *Canadian Water Resources Journal / Revue Canadienne Des Ressources Hydriques*, *44*(1), 90–107. https://doi.org/10.1080/07011784.2018.1537812

Tanentzap, A. J., Burd, K., Kuhn, M. A., Estop-Aragonés, C., Tank, S. E., & Olefeldt, D. (2021). Aged soils contribute little to contemporary carbon cycling downstream of thawing permafrost peatlands. *Global Change Biology*, *27*(20), 5368–5382. https://doi.org/10.1111/gcb.15756

Tank, S. E., Lesack, L. F. W., Gareis, J. A. L., Osburn, C. L., & Hesslein, R. H. (2011). Multiple tracers demonstrate distinct sources of dissolved organic matter to lakes of the Mackenzie Delta, western Canadian Arctic. *Limnology and Oceanography*, *56*(4), 1297–1309. https://doi.org/10.4319/lo.2011.56.4.1297

Tank, S. E., Olefeldt, D., Quinton, W. L., Spence, C., Dion, N., Ackley, C., et al. (2018). Fire in the Arctic: The effect of wildfire across diverse aquatic ecosystems of the Northwest Territories. *Polar Knowledge: Aqhaliat*, *1*(1), 31–38.

Tank, S. E., Vonk, J. E., Walvoord, M. A., McClelland, J. W., Laurion, I., & Abbott, B. W. (2020). Landscape matters: Predicting the biogeochemical effects of permafrost thaw on aquatic networks with a state factor approach. *Permafrost and Periglacial Processes*, *31*(3), 358–370. https://doi.org/10.1002/ppp.2057

Tarbier, B., Hugelius, G., Kristina Sannel, A. B., Baptista-Salazar, C., & Jonsson, S. (2021). Permafrost Thaw Increases Methylmercury Formation in Subarctic Fennoscandia. *Environmental Science & Technology*, *55*(10), 6710–6717. https://doi.org/10.1021/acs.est.0c04108

Teickner, H. (2021). ir: A simple package to handle and preprocess infrared spectra. Retrieved from https://zenodo.org/record/5747170

Teickner, H., & Hodgkins, S. (2021, December 20). irpeat: Simple Functions to Analyze Mid Infrared Spectra of Peat Samples. (Version v0.0.0.9100). Zenodo. https://doi.org/10.5281/ZENODO.5792919

Teickner, H., Gao, C., & Knorr, K. (2022). Electrochemical Properties of Peat Particulate Organic Matter on a Global Scale: Relation to Peat Chemistry and Degree of Decomposition. *Global Biogeochemical Cycles*, *36*(2). https://doi.org/10.1029/2021GB007160

Thompson, L. M. (2021). Taking the pulse of streams with spectrometer probes. *Nature Reviews Earth & Environment*, *2*(8), 524–524. https://doi.org/10.1038/s43017-021-00202-7

Thompson, L. M., Olefeldt, D., Mangal, V., & Knorr, K. H. (2022). Soil and porewater chemistry from peatlands of the Interior Plains, northwestern Canada (dataset). *University of Alberta Education & Research Archive*. https://doi.org/10.7939/r3-vp5e-aj53

Thompson, L. M., Kuhn, M. A., Winder, J. C., Braga, L. P. P., Hutchins, R. H. S., Tanentzap, A. J., et al. (2023). Controls on methylmercury concentrations in lakes and streams of peatland-rich catchments along a 1700 km permafrost gradient. *Limnology and Oceanography*, *68*, 583–597. https://doi.org/10.1002/lno.12296

Thompson, L. M., Low, M., Shewan, R., Schulze, C., Simba, M., Sonnentag, O., et al. (Under review). Landscape drives variability in concentrations and yields of mercury, methylmercury, and dissolved organic carbon in boreal catchments.

Tjerngren, I., Karlsson, T., Björn, E., & Skyllberg, U. (2012). Potential Hg methylation and MeHg demethylation rates related to the nutrient status of different boreal wetlands. *Biogeochemistry*, *108*(1–3), 335–350. https://doi.org/10.1007/s10533-011-9603-1

Todorova, S. G., Driscoll, C. T., Matthews, D. A., Effler, S. W., Hines, M. E., & Henry, E. A. (2009). Evidence for Regulation of Monomethyl Mercury by Nitrate in a Seasonally Stratified, Eutrophic Lake. *Environmental Science & Technology*, *43*(17), 6572–6578. https://doi.org/10.1021/es900887b

Tsui, M. T. K., & Finlay, J. C. (2011). Influence of Dissolved Organic Carbon on Methylmercury Bioavailability across Minnesota Stream Ecosystems. *Environmental Science & Technology*, *45*(14), 5981–5987. https://doi.org/10.1021/es200332f

Turnipseed, D. P., & Sauer, V. B. (2010). Discharge Measurements at Gaging Stations. *USGS Numbered Series 3-A8.* https://doi.org/10.3133/tm3A8

Ullrich, S. M., Tanton, T. W., & Abdrashitova, S. A. (2001). Mercury in the Aquatic Environment: A Review of Factors Affecting Methylation. *Critical Reviews in*

Environmental Science and Technology, *31*(3), 241–293. https://doi.org/10.1080/20016491089226

University of Alberta. (2022). CIMP 199: Water quality of peatland ponds and streams on a latitudinal transect (dataset) (Version 4.0.0). *Mackenzie DataStream*. https://doi.org/10.25976/rzkg-7n02

University of Alberta, & Dehcho-AAROM. (2022). Seasonal Monitoring of Smith Creek and Scotty Creek, 2019-2021 (dataset) (Version 1.0.0). *Mackenzie DataStream*. https://doi.org/10.25976/y9yi-no57

Utting, N., Lauriol, B., Mochnacz, N., Aeschbach-Hertig, W., & Clark, I. (2013). Noble gas and isotope geochemistry in western Canadian Arctic watersheds: tracing groundwater recharge in permafrost terrain. *Hydrogeology Journal*, *21*(1), 79–91. https://doi.org/10.1007/s10040-012-0913-8

Varty, S., Lehnherr, I., St. Pierre, K., Kirk, J., & Wisniewski, V. (2021). Methylmercury Transport and Fate Shows Strong Seasonal and Spatial Variability along a High Arctic Freshwater Hydrologic Continuum. *Environmental Science & Technology*, *55*(1), 331–340. https://doi.org/10.1021/acs.est.0c05051

Vaughan, M. C. H., Bowden, W. B., Shanley, J. B., Vermilyea, A., Sleeper, R., Gold, A. J., et al. (2017). High-frequency dissolved organic carbon and nitrate measurements reveal differences in storm hysteresis and loading in relation to land cover and seasonality. *Water Resources Research*, *53*(7), 5345–5363. https://doi.org/10.1002/2017WR020491

Vermilyea, A. W., Nagorski, S. A., Lamborg, C. H., Hood, E. W., Scott, D., & Swarr, G. J. (2017). Continuous proxy measurements reveal large mercury fluxes from glacial and forested watersheds in Alaska. *Science of The Total Environment*, *599–600*, 145–155. https://doi.org/10.1016/j.scitotenv.2017.03.297

Vincent, L. A., Zhang, X., Brown, R. D., Feng, Y., Mekis, E., Milewska, E. J., et al. (2015). Observed Trends in Canada's Climate and Influence of Low-Frequency Variability Modes. *Journal of Climate*, *28*(11), 4545–4560. https://doi.org/10.1175/JCLI-D-14-00697.1

Vines, M., & Terry, L. G. (2020). Evaluation of the biodegradability of fluorescent dissolved organic matter via biological filtration. *AWWA Water Science*, *2*(5). https://doi.org/10.1002/aws2.1201

Vitt, D. H., & Chee, W.-L. (1990). The relationships of vegetation to surface water chemistry and peat chemistry in fens of Alberta, Canada. *Vegetatio*, *89*(2), 87–106. https://doi.org/10.1007/BF00032163

Vonk, J. E., Tank, S. E., & Walvoord, M. A. (2019). Integrating hydrology and biogeochemistry across frozen landscapes. *Nature Communications*, *10*(1), 5377. https://doi.org/10.1038/s41467-019-13361-5

Wauthy, M., Rautio, M., Christoffersen, K. S., Forsström, L., Laurion, I., Mariash, H. L., et al. (2018). Increasing dominance of terrigenous organic matter in circumpolar freshwaters due to permafrost thaw. *Limnology and Oceanography Letters*, *3*(3), 186–198. https://doi.org/10.1002/lol2.10063

Weishaar, J. L., Aiken, G. R., Bergamaschi, B. A., Fram, M. S., Fujii, R., & Mopper, K. (2003). Evaluation of Specific Ultraviolet Absorbance as an Indicator of the Chemical Composition and Reactivity of Dissolved Organic Carbon. *Environmental Science & Technology*, *37*(20), 4702–4708. https://doi.org/10.1021/es030360x

Wheatley, B., & Wheatley, M. A. (2000). Methylmercury and the health of indigenous peoples: a risk management challenge for physical and social sciences and for public health policy. *Science of The Total Environment*, *259*(1–3), 23–29. https://doi.org/10.1016/S0048-9697(00)00546-5

Wheeler, B., & Torchiano, M. (2016). Package 'lmPerm'. *R Package Version 2.0*.

Wheeler, J. O., Hoffman, P. F., Card, K. D., Davidson, A., Sanford, B. V., Okulitch, A. V., & Roest, W. R. (1996). *Geological map of Canada* (No. 1860A) (p. 1860A). https://doi.org/10.4095/208175

Woerndle, G. E., Tsz-Ki Tsui, M., Sebestyen, S. D., Blum, J. D., Nie, X., & Kolka, R. K. (2018). New Insights on Ecosystem Mercury Cycling Revealed by Stable Isotopes of Mercury in Water Flowing from a Headwater Peatland Catchment. *Environmental Science & Technology*, *52*(4), 1854–1861. https://doi.org/10.1021/acs.est.7b04449

Wright, S. N., Thompson, L. M., Olefeldt, D., Connon, R. F., Carpino, O. A., Beel, C. R., & Quinton, W. L. (2022). Thaw-induced impacts on land and water in discontinuous permafrost: A review of the Taiga Plains and Taiga Shield, northwestern Canada. *Earth-Science Reviews*, *232*, 104104. https://doi.org/10.1016/j.earscirev.2022.104104

Wu, Z., Li, Z., Shao, B., Zhang, Y., He, W., Lu, Y., et al. (2022). Impact of dissolved organic matter and environmental factors on methylmercury concentrations across aquatic ecosystems inferred from a global dataset. *Chemosphere*, *294*, 133713. https://doi.org/10.1016/j.chemosphere.2022.133713

Wünsch, U. J., Murphy, K. R., & Stedmon, C. A. (2017). The One-Sample PARAFAC Approach Reveals Molecular Size Distributions of Fluorescent Components in Dissolved Organic Matter. *Environmental Science & Technology*, *51*(20), 11900–11908. https://doi.org/10.1021/acs.est.7b03260

Xu, J., Buck, M., Eklöf, K., Ahmed, O. O., Schaefer, J. K., Bishop, K., et al. (2019). Mercury methylating microbial communities of boreal forest soils. *Scientific Reports*, *9*(1), 518. https://doi.org/10.1038/s41598-018-37383-z

Yang, Z., Fang, W., Lu, X., Sheng, G.-P., Graham, D. E., Liang, L., et al. (2016). Warming increases methylmercury production in an Arctic soil. *Environmental Pollution*, *214*, 504–509. https://doi.org/10.1016/j.envpol.2016.04.069

Yusoff, K. (2018). *A billion black Anthropocenes or none*. Retrieved from https://search.ebscohost.com/login.aspx?direct=true&scope=site&db=nlebk&db=nlabk&AN=2458652

Zhang, D., Yin, Y., Li, Y., Cai, Y., & Liu, J. (2017). Critical role of natural organic matter in photodegradation of methylmercury in water: Molecular weight and interactive effects with other environmental factors. *Science of The Total Environment*, *578*, 535–541. https://doi.org/10.1016/j.scitotenv.2016.10.222

Zhou, J., Riccardi, D., Beste, A., Smith, J. C., & Parks, J. M. (2014). Mercury Methylation by HgcA: Theory Supports Carbanion Transfer to Hg(II). *Inorganic Chemistry*, *53*(2), 772–777. https://doi.org/10.1021/ic401992y

Zhou, Y., Martin, P., & Müller, M. (2019). Composition and cycling of dissolved organic matter from tropical peatlands of coastal Sarawak, Borneo, revealed by fluorescence spectroscopy and parallel factor analysis. *Biogeosciences*, *16*(13), 2733–2749. https://doi.org/10.5194/bg-16-2733-2019

Zhuang, W.-E., Chen, W., Cheng, Q., & Yang, L. (2021). Assessing the priming effect of dissolved organic matter from typical sources using fluorescence EEMs-PARAFAC. *Chemosphere*, *264*, 128600. https://doi.org/10.1016/j.chemosphere.2020.128600

Zolkos, S., Tank, S. E., Striegl, R. G., & Kokelj, S. V. (2019). Thermokarst Effects on Carbon Dioxide and Methane Fluxes in Streams on the Peel Plateau (NWT, Canada). *Journal of Geophysical Research: Biogeosciences*, *124*(7), 1781–1798. https://doi.org/10.1029/2019JG005038

Zolkos, S., Krabbenhoft, D. P., Suslova, A., Tank, S. E., McClelland, J. W., Spencer, R. G. M., et al. (2020). Mercury Export from Arctic Great Rivers. *Environmental Science & Technology*, *54*(7), 4140–4148. https://doi.org/10.1021/acs.est.9b07145

Zoltai, S. C. (1993). Cyclic Development of Permafrost in the Peatlands of Northwestern Alberta, Canada. *Arctic and Alpine Research*, *25*(3), 240–246. https://doi.org/10.1080/00040851.1993.12003011

Zoltai, S. C., & Tarnocai, C. (1974). Perennially Frozen Peatlands in the Western Arctic and Subarctic of Canada. *Canadian Journal of Earth Sciences*. https://doi.org/10.1139/e75-004

Appendices

A.1. Supporting information for Chapter 1

There is no supporting information for Chapter 1

A.2. Supporting information for Chapter 2

A.2.1 Quality assurance and quality control

Detection limits for total mercury (THg) and methylmercury (MeHg) were determined annually at the Canadian Association of Laboratory Accreditation certified Biogeochemical Analytical Service Laboratory (BASL - University of Alberta) where samples were analyzed. Detection limits were 0.08 ng L^{-1} for THg and 0.01 ng L^{-1} for MeHg.

THg was analyzed following EPA Method 1631. Samples were first oxidized with bromine chloride (BrCl) for at least 12 hours and presence of excess BrCl was established by pipetting a sample onto potassium iodide starch paper (Hintelmann & Ogrinc, 2003). 10% of the samples were spiked by a known quantity of $HgCl_2$ to assess procedural recoveries (Spex-CertiPrep, US), approximately equivalent to the sample concentration. Spike recoveries were >94%, with mean value of 106.2%. 20% of the samples were duplicated with a mean difference of 9.7% and standard deviation of 6.7%. The Tekran 2600 was standardized by a 9-point standard curve (0 – 40 ng L^{-1}) at the start of each analytical day, using certified Brooks Rand $HgCl_2$ standards (R^2> 0.99).

MeHg was analyzed following EPA Method 1630. All samples were spiked before distillation with $Me^{201}Hg$ as an internal standard to correct for MeHg loss or formation during analysis. $Me^{202}Hg$ was used as the ambient tracer. 20% of the samples were duplicated with a mean difference of 7.1% and a standard deviation of 8.1%. Blanks of Milli-Q® water and the reagents ran with samples beginning at the distillation stage and prior to the analysis by gas chromatograph paired with an inductively coupled plasma mass spectrometer.

Dissolved organic carbon (DOC) and total dissolved nitrogen (TDN) were analyzed by a Chemiluminesence detector following combustion to carbon dioxide gas and nitrous oxide gas, respectively, for TDN. Photon emission is measured by a Chemiluminesence detector. Final concentrations were the mean result of three injections per sample with a standard deviation of 0.13 mg C L^{-1} and 0.009 mg N L^{-1}. Analysis of anions involved separation of anions followed by quantification by a conductivity detector. To analyze cations, atoms were excited, producing characteristic emission patterns unique to each element detected by a spectrometer.

A.2.2 DOM Characterization Methods

The protocol to examine dissolved organic matter (DOM) quality was adapted from a study on DOM in watersheds from coastal British Columbia (Oliver et al., 2017), where samples were scanned from excitation wavelengths of 230–500 nm at 5 nm increments and emission wavelengths of 210–620 nm at 2 nm increments. Corrections for excitation and emission, inner

filter effects, and Raman signal calibration were applied before analysis. We then characterized the biological index (BIX) and humification index (HIX) using the R package (R Foundation for Statistical Computing, Austria) staRdom (Pucher et al., 2019). BIX characterizes autochthonous biological activity in water samples and is calculated by dividing fluorescence at excitation 310 nm and emission at 380 nm by fluorescence at excitation 310 nm and emission 430 nm. Higher values of BIX correspond to the increased presence of organic matter freshly released by microbial activity (Huguet et al., 2009). HIX indicates the extent of humification, with higher values indicating increased humification, and is calculated at 254 nm excitation from dividing the sum of fluorescence intensities between emission 435 – 480 nm by the sum of fluorescence intensities between 300 – 345 nm (Ohno, 2002).

We further characterized the DOM using parallel factor analysis (PARAFAC) for each EEM with the drEEM toolbox for Matlab (Mathworks, US). PARAFAC decomposes the DOM pool into individual components. We identified five unique components and found multiple matches for each component on the online fluorescence database, OpenFluor (Murphy et al., 2014). The maximum fluorescence of excitation and emission in Raman units (Fmax) was used to calculate the percent contribution of each component to total fluorescence, as the fluorophores' actual structure is unknown (Oliver et al., 2017).

A.2.3 Path Analysis

The path analysis approach tests the statistical significance of inferred causal pathways using individual linear regressions. Previous work shows that MeHg concentrations vary with DOC concentrations (Lavoie et al., 2019), which vary with peatland cover (Olefeldt et al., 2014), catchment size (Mattsson et al., 2005), and permafrost extent (Olefeldt et al., 2014). Therefore, we examined the influence of these three variables through DOC concentrations on % unfiltered MeHg in streams and lakes, with catchment area log-normalized. Path analysis code was adapted from (St. Pierre et al., 2019).

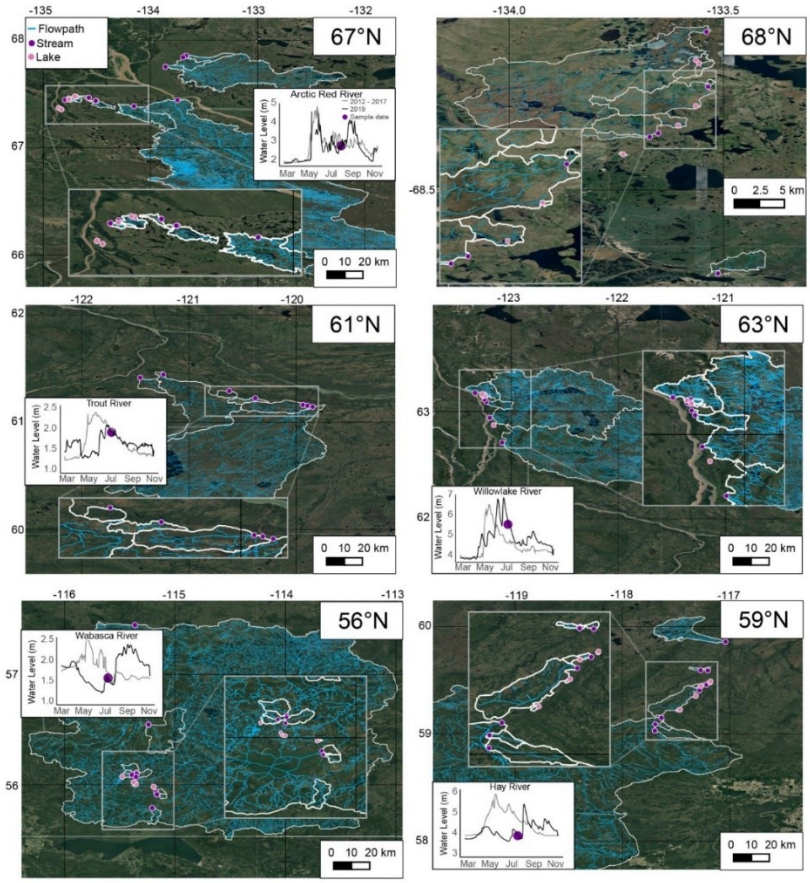

Figure A.2.1. Satellite imagery (Google, 2015), hydrographs of major rivers (Environment and Climate Change Canada, 2021), and flow paths (Natural Resources Canada, 2022). Each inset box is a 2x magnification of the base imagery. Hydrographs show 2019 water levels, the mean 2012-2017 levels, and the 2019 sampling date. Note that 68°N has a different scale than the other regions.

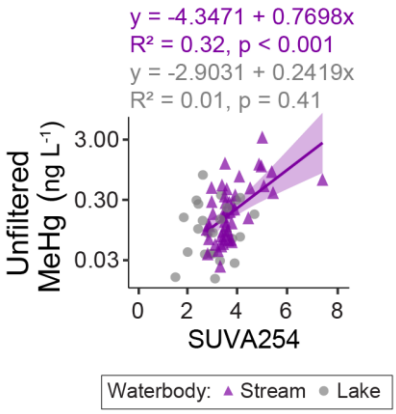

Figure A.2.2. Regression of unfiltered methylmercury (MeHg) with the specific ultraviolet absorbance at 254 nm ($SUVA_{254}$), separated into lakes (n=25) and streams (n=47). Model formula, adjusted R^2 values, and p-values of the regressions are displayed, a 95% confidence interval surrounds the best-fit line, and the y-axis is on a log scale.

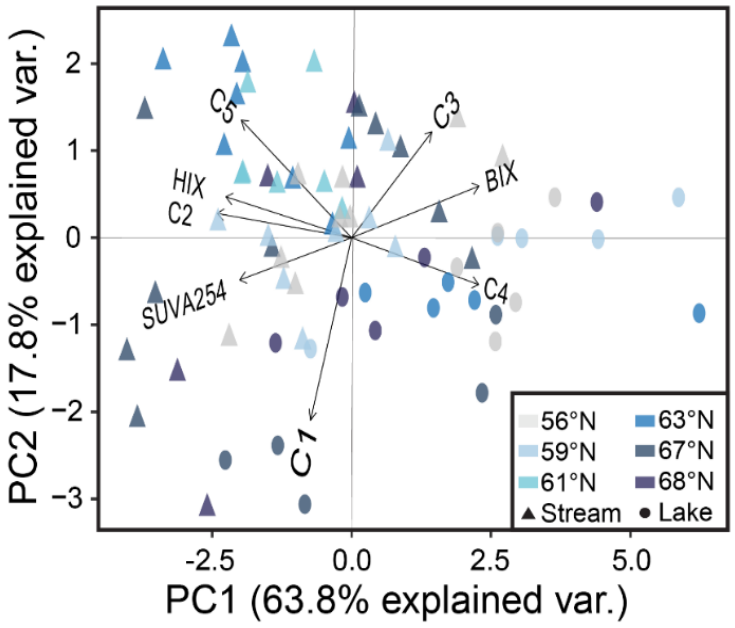

Figure A.2.3. Principal component analysis (PCA) biplot of log-normalized dissolved organic matter quality variables for the 6 sample regions (colored points) separated by lake (n=25) and stream (n=47). PCA accounts for 81.6% of the variation among sites (Axis 1, 63.8% and Axis 2, 17.8%). Parallel factor analysis components (C1 – C5) are expressed as the percent of total fluorescence, and are visualized in Figure A.2.4 and described in Table A.2.3.

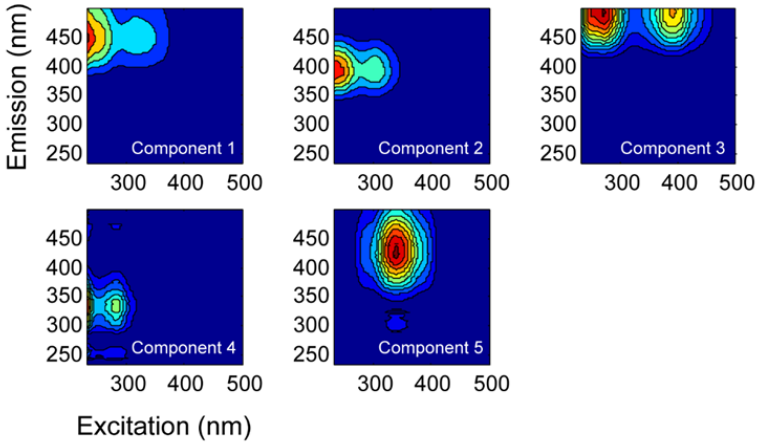

Figure A.2.4. Components identified by parallel factor analysis for measured excitation-emission spectra from the sampling sites.

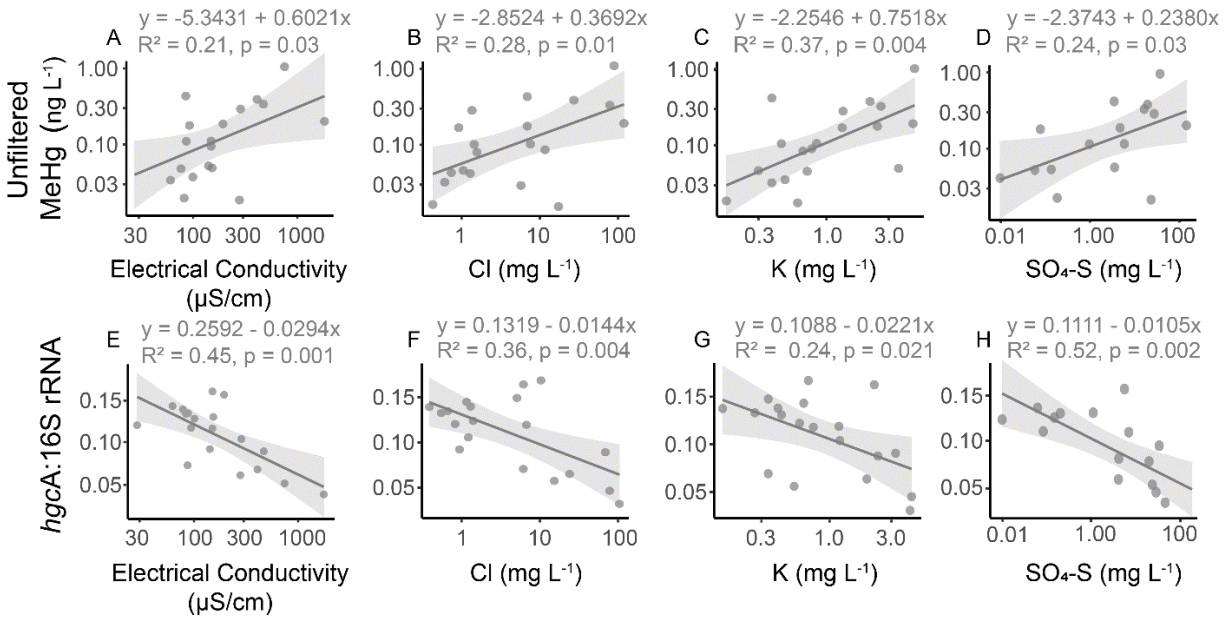

Figure A.2.5. Regression of unfiltered methylmercury (MeHg) and the ratio of *hgc*A to 16S rRNA in lake sediments with water chemistry parameters. MeHg with A) electrical conductivity, B) chloride (Cl), C) potassium (K), and D) sulfate-as-sulfur (SO_4-S) in the lake surface waters and the ratio of *hgcA* to 16S rRNA in lake sediments with E) electrical conductivity, F) Cl, G) K, H) SO_4-S in lake surface waters (n=19). Model formula, adjusted R^2 values, and p-values of the regressions are displayed, a 95% confidence interval surrounds the best-fit line, and the axes are on a log scale except for the y-axis of E–H.

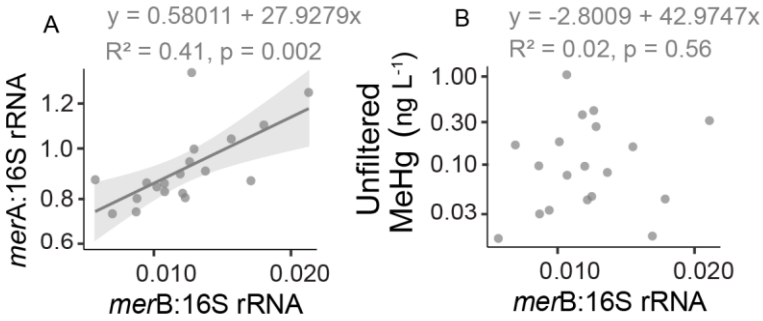

Figure A.2.6. Regression of A) *merA* with *merB* abundance in lake sediments (n=19), separately normalized by 16S rRNA, and B) unfiltered methylmercury (MeHg) in lake surface waters with normalized *merB* abundance. The model formula, adjusted R^2 values, and p-values of the regressions are displayed, and a 95% confidence interval surrounds the best-fit line.

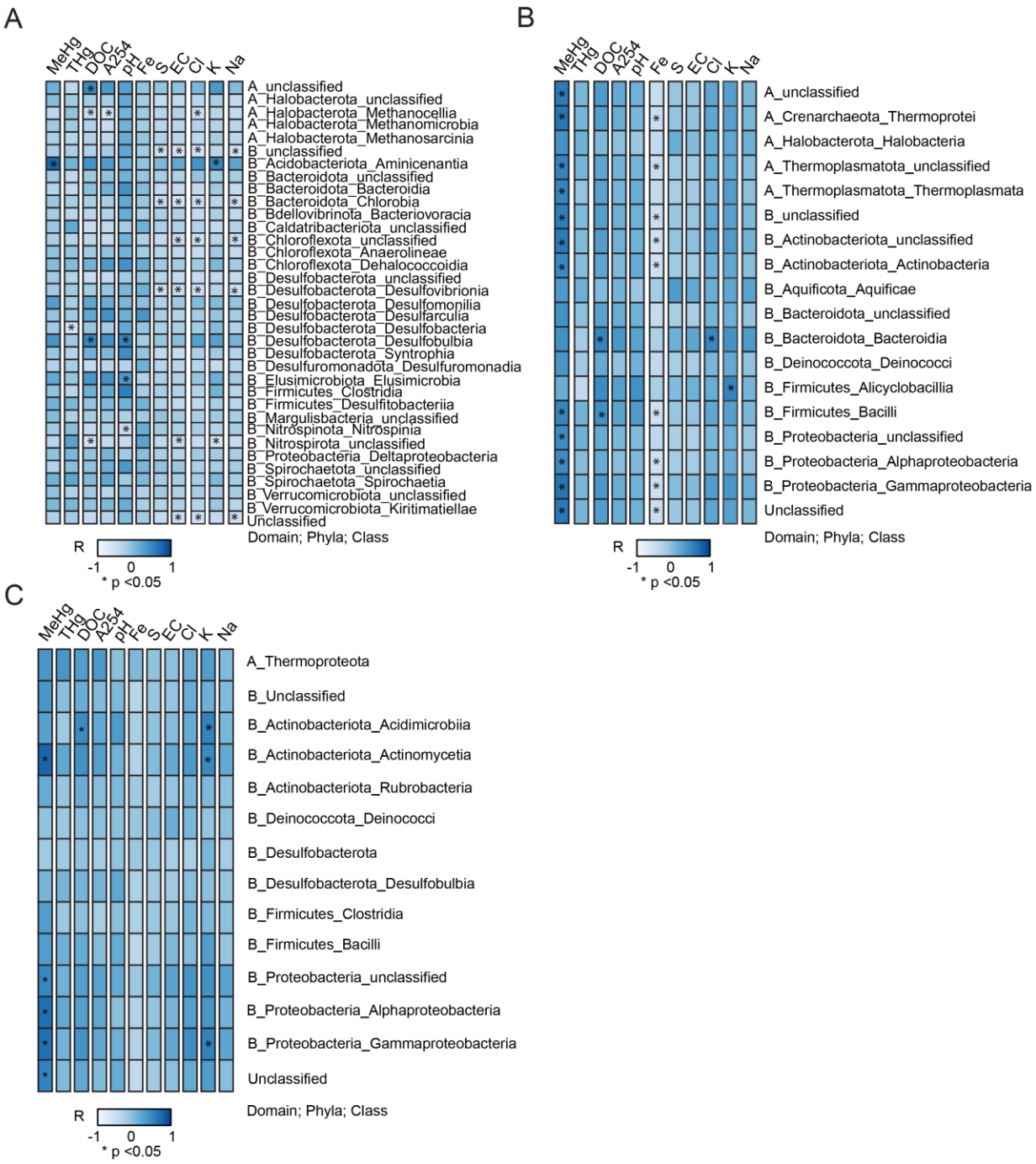

Figure A.2.7. Heat maps of water chemistry in lake surface waters against identified classes with A) Hg^{II} methylating (*hgcA*), B) Hg^{II} reducing (*merA*), and C) MeHg demethylating (*merB*) genes in lake sediments. Water chemistry parameters include unfiltered methylmercury (MeHg), total mercury (THg), dissolved organic carbon (DOC), absorbance at 254 nm (A_{254}), pH, iron (Fe), sulfur (S), electrical conductivity (EC), chloride (Cl), potassium (K), sodium (Na).

Table A.2.1. Results of perANOVA analysis on A) iron (Fe), B) pH, C) dissolved organic carbon (DOC), D) sulfur (S), and E) electrical conductivity (EC), separated by waterbody type (stream or pond) and region (68°N, 67°N, 63°N, 61°N, 59°N, 56°N).

A. Fe						
	Df	SS	MS	F	P	
Stream vs Pond	1	0.33	0.33	0.07	0.78	
Region	5	42.3	8.47	1.91	0.10	
Waterbody::Region	4	21.5	5.37	1.21	0.31	
Residuals	61	269.6	4.42			
B. pH						
	Df	SS	MS	F	P	
Stream vs Pond	1	1.54	1.54	4.37	0.04	*
Region	5	14.08	2.81	7.97	<0.001	***
Waterbody::Region	4	2.47	0.61	1.75	0.15	
Residuals	61	21.55	0.35			
C. DOC						
	Df	SS	MS	F	P	
Stream vs Pond	1	1423.5	1423.4	17.16	<0.001	***
Region	5	5050.9	1010.1	12.17	<0.001	***
Waterbody::Region	4	1815.4	453.8	5.47	<0.001	***
Residuals	61	5059.9	82.95			
D. S						
	Df	SS	MS	F	P	
Stream vs Pond	1	6208	6207.6	7.13	0.009	**
Region	5	13715	2742.9	3.15	0.01	*
Waterbody::Region	4	6003	1500.9	1.72	0.15	
Residuals	61	53085	870.2			
E. EC						
	Df	SS	MS	F	P	
Stream vs Pond	1	145993	145993	3.38	0.07	
Region	5	1548864	309773	7.17	<0.001	***
Waterbody::Region	4	247075	61769	1.43	0.23	
Residuals	61	2634029	43181			

Table A.2.2. Results of perANOVA analysis on A) total unfiltered mercury (U-THg), B) total unfiltered methylmercury (U-TMeHg), C) total THg:MeHg (%U-TMeHg), D) total filtered mercury (F-THg), E) total filtered methylmercury (F-TMeHg), and F) filtered THg:MeHg (%F-TMeHg), separated by waterbody type (stream or pond) and region (68°N, 67°N, 63°N, 61°N, 59°N, 56°N).

A. U-THg						
	Df	SS	MS	F	P	
Stream vs Pond	1	4.03	4.02	2.37	0.13	
Region	5	42.1	8.42	4.97	<0.001	***
Waterbody::Region	4	4.15	1.04	0.61	0.67	
Residuals	61	103	1.69			
B. U-TMeHg						
	Df	SS	MS	F	P	
Stream vs Pond	1	2.87	2.87	7.65	0.007	**
Region	5	5.41	1.08	2.88	0.02	*
Waterbody::Region	4	1.67	0.42	1.11	0.36	
Residuals	61	22.9	0.37			

C. %U-TMeHg						
	Df	SS	MS	F	P	
Stream vs Pond	1	1915	1915	9.23	0.003	**
Region	5	4968	993	4.79	<0.001	***
Waterbody::Region	4	1161	290	1.40	0.24	
Residuals	61	12647	207			
D. F-THg						
	Df	SS	MS	F	P	
Stream vs Pond	1	1.50	1.50	2.22	0.14	
Region	5	10.5	2.11	3.11	0.01	*
Waterbody::Region	4	1.8	0.43	0.65	0.63	
Residuals	61	41.3	0.67			
E. F-TMeHg						
	Df	SS	MS	F	P	
Stream vs Pond	1	2.1	2.1	7.41	0.008	**
Region	5	3.6	0.72	2.52	0.03	*
Waterbody::Region	4	1.0	0.25	0.91	0.46	
Residuals	61	16.8	0.28			
F. %F-TMeHg						
	Df	SS	MS	F	P	
Stream vs Pond	1	1898.8	1898.8	10.5	0.002	**
Region	5	4260.2	852.0	4.70	0.001	***
Waterbody::Region	4	867.5	216.8	1.19	0.32	
Residuals	61	10689.0	181.2			

Table A.2.3. Spectral composition of the five fluorescence compounds identified using parallel factor analysis, including excitation (Ex), emission (Em), peak values, and likely structure and characteristics of the component based on previous studies. Italics indicate a secondary excitation peak.

Component	Ex (nm)	Em (nm)	Potential structure/ characteristics	Previous studies with comparable results
C1	<230, *320*	446	Terrestrial humic-like, with fulvic acid and high molecular weight	C1 (Guéguen et al., 2014), C2 (Queimaliños et al., 2019), C4 (Kothawala et al., 2014), Cc (Olefeldt et al., 2014)
C2	<230, *300*	395	Microbial humic-like, with fulvic acid and lower molecular weight	C2 (Gonçalves-Araujo et al., 2016), Cm (Olefeldt et al., 2014), C4 (Osburn et al., 2017), C2 (Kothawala et al., 2014)
C3	270, *390*	492	Terrestrial humic-like, with fulvic acid and high molecular weight	C3 (Kothawala et al., 2014), C3 (Guéguen et al., 2014), C4 (Cohen et al., 2014)
C4	<230*, 280*	333	Protein-like or amino-acid like	C4 (Osburn et al., 2016), C6 (Kothawala et al., 2014), C5 (Osburn et al., 2017), Ctr (Olefeldt et al., 2014)
C5	340	430	Not commonly reported, microbial humic-like	G3 (Murphy et al., 2011), C5 (Stedmon & Markager, 2005)

Table A.2.4. Results of perANOVA analysis on proportion of A) *hgcA*, B) *merA,* and C) *merB* to housekeeping gene 16S rRNA, separated by permafrost extent (absent, sporadic, discontinuous, continuous).

A. *hgcA*:16S rRNA					
	Df	SS	MS	F	P
Region	3	0.008	0.002	1.87	0.17
Residuals	15	0.02	0.001		
B. *merA*:16S rRNA					
	Df	SS	MS	F	P
Region	3	0.009	0.003	0.09	0.95
Residuals	15	0.03	0.03		
C. *merB*:16S rRNA					
	Df	SS	MS	F	P
Region	3	0.00005	0.00002	1.25	0.33
Residuals	15	0.0002	0.00001		

Table A.2.5. Results of perMANOVA analysis on gene diversity data (collapsed at taxonomic class level) in lake sediments for A) *hgcA*, B) *merA*, and C) *merB* with Aitchison distance.

A. *hgcA*						
Group 1	Group 2	n	Perm.	F	P	Q
Continuous	Sporadic	10	999	0.34	0.72	0.73
Continuous	Absent	10	999	2.00	0.95	0.73
Continuous	Discontinuous	9	999	0.63	0.61	0.73
Sporadic	Absent	10	999	0.45	0.66	0.73
Sporadic	Discontinuous	9	999	0.32	0.72	0.73
Absent	Discontinuous	9	999	1.23	0.32	0.73
B. *merA*						
Group 1	Group 2	n	Perm.	F	P	Q
Continuous	Sporadic	10	999	0.95	0.46	0.67
Continuous	Absent	10	999	0.08	0.96	0.96
Continuous	Discontinuous	9	999	1.09	0.33	0.66
Sporadic	Absent	10	999	0.74	0.55	0.67
Sporadic	Discontinuous	9	999	2.46	0.12	0.42
Absent	Discontinuous	9	999	1.86	0.14	0.42
C. *merB*						
Group 1	Group 2	n	Perm.	F	P	Q
Continuous	Sporadic	10	999	0.77	0.48	0.48
Continuous	Absent	10	999	2.63	0.10	0.27
Continuous	Discontinuous	9	999	1.78	0.20	0.31
Sporadic	Absent	10	999	2.43	0.13	0.27
Sporadic	Discontinuous	9	999	0.77	0.48	0.48
Absent	Discontinuous	9	999	0.84	0.46	0.48

A.3. Supporting information for Chapter 3

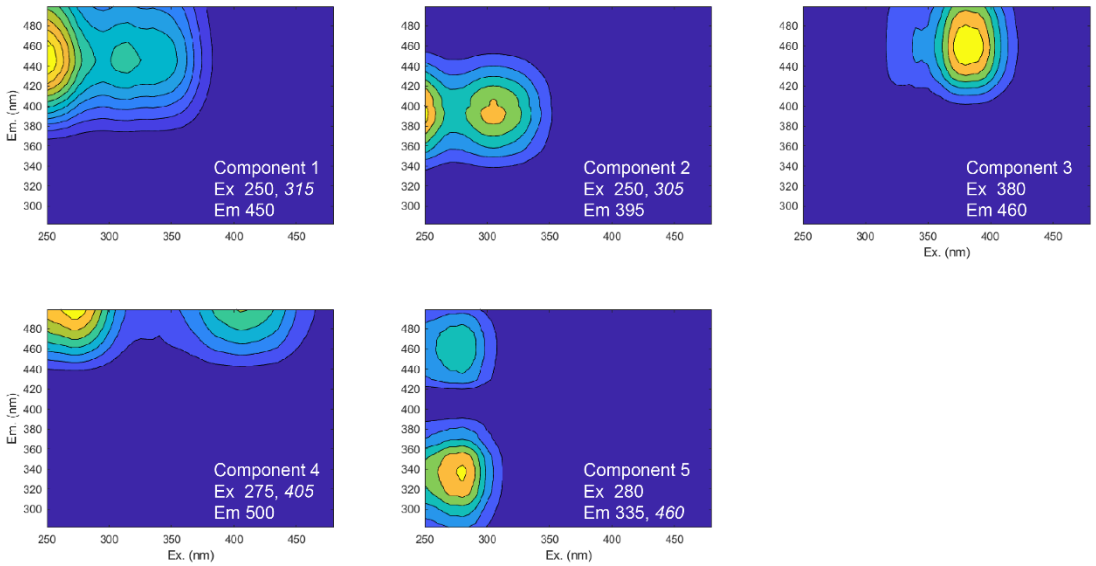

Figure A.3.1. Validated PARAFAC components. Component descriptions in Table A.3.1 and peaks indicated on the figure with secondary peaks italicized.

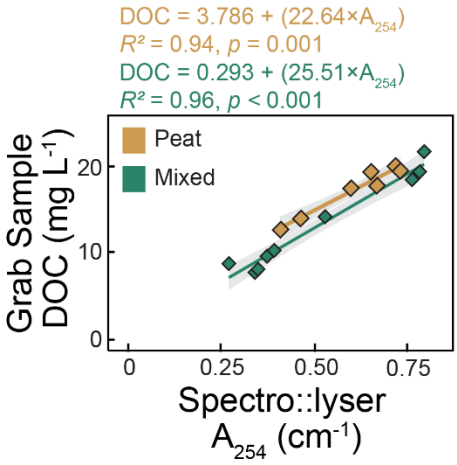

Figure A.3.2. Regression to predict dissolved organic carbon (DOC) concentrations in 2019 for LOADEST model. Based on high-frequency absorbance at 254 (A_{254}) at Scotty Creek – Peat (n=7) and Smith Creek – Mixed (n=9).

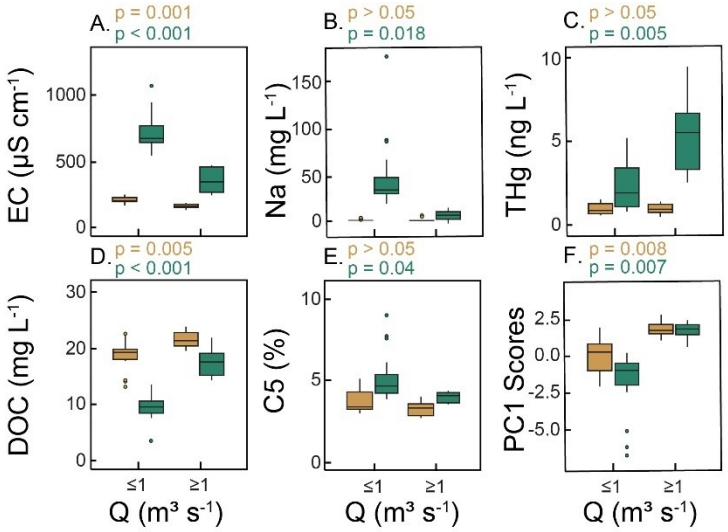

Figure A.3.3. Boxplots of water chemistry during high (discharge, Q≥1 m^3 s^{-1}) and low (Q≤1 m^3 s^{-1}) flow periods in Scotty Creek – Peat, and Smith Creek – Mixed (Q≤1, *n*=17, 15; Q≥, *n*=7, 8). A) electrical conductivity (EC), B) sodium (Na), C) total mercury (THg), D) dissolved organic carbon (DOC), E) scores of PC1 from the PCA, and F) tryptophan, protein-like PARAFAC component (C5). *p*-values describe results from pairwise t-tests comparing values at Q<1 m^3 s^{-1} and Q>1 m^3 s^{-1}.

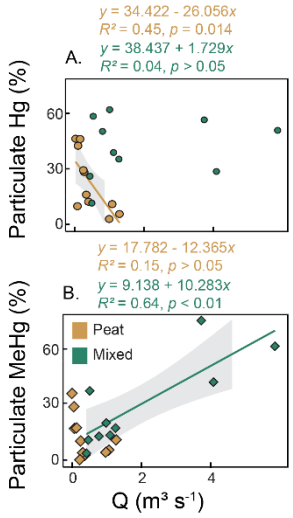

Figure A.3.4. Regressions of discharge (Q) against A) fraction of particulate mercury (Hg) and B) fraction of particulate methylmercury (MeHg), separated by Scotty Creek – Peat, and Smith Creek – Mixed. Model formula, adjusted R^2, and *p*-values of the regressions are displayed, and a 95% confidence interval surrounds the best-fit line if statistically significant ($p<0.05$).

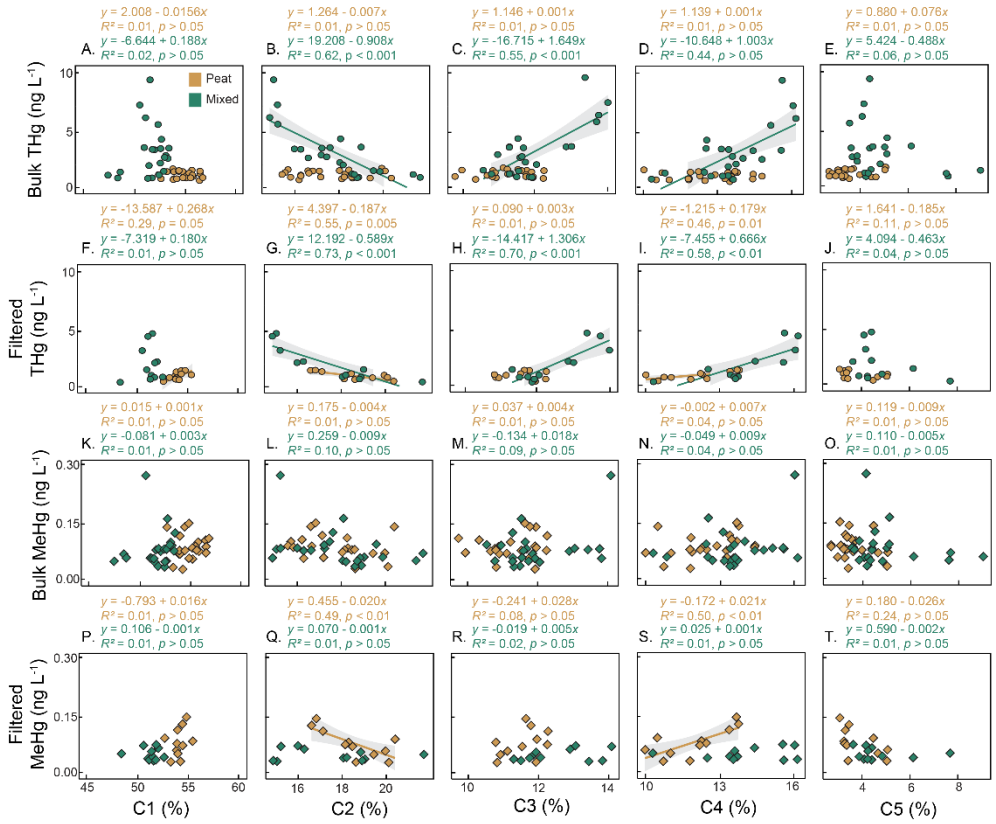

Figure A.3.5. Regressions of PARAFAC Components 1-5 against bulk and filtered A)–J) total mercury (THg) and K)–T) methylmercury (MeHg), separated by Scotty Creek – Peat, and Smith Creek – Mixed. Model formula, adjusted R^2, and p-values of the regressions are displayed, and a 95% confidence interval surrounds the best-fit line if statistically significant (p<0.05). C1=terrestrial humic-like, C2=microbial humic-like, C3=fulvic-like, C4=terrestrial humic-like, C5=protein, tryptophan-like (Table A.3.1).

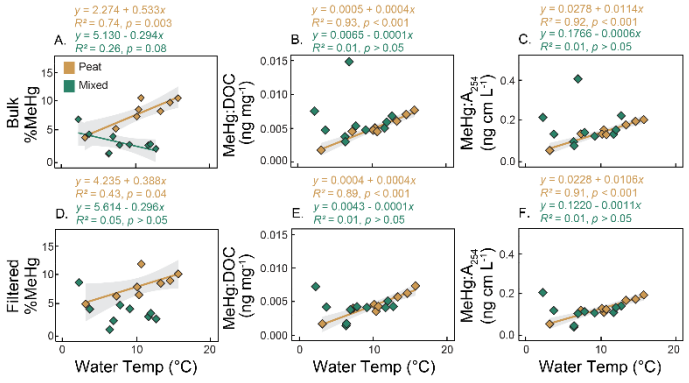

Figure A.3.6. Regressions of water temperature against ratios of A)-C) bulk and D)-F) filtered methylmercury to total mercury (%MeHg), methylmercury to dissolved organic carbon (MeHg:DOC), and methylmercury to absorbance at 254 nm (MeHg:A_{254}) separated by Scotty Creek – Peat, and Smith Creek – Mixed. Model formula, adjusted R^2, and p-values of the regressions are displayed, and a 95% confidence interval surrounds the best-fit line if statistically significant (p<0.05).

Table A.3.1. Dissolved organic matter (DOM) indices analyzed through UV-visible absorbance and fluorescence spectroscopy and parallel factor analysis (PARAFAC). Ex.=excitation, Em.=emission.

Optical Indices	Abbreviation (unit)	Calculation	Characteristic	Citation
Specific ultraviolet absorbance at 254 nm	SUVA (L mg^{-1} C m^{-1})	(Absorbance at 254 nm)/(Dissolved organic carbon concentration)	Aromaticity	Weishaar et al., 2003
Biological Index	BIX	(Ex. 310, Em. 380)/(Ex. 310, Em. 430)	Presence of fresh DOM	Huguet et al., 2009
Humification index	HIX	(Ex. 254, Σ Em. 435-480)/ (Ex. 254, Σ Em. 300-345)	Extent of humification	Ohno, 2002
PARAFAC Component	**Abbreviation (unit)**	**Peaks**	**Characteristic**	**Matching Components**
Component 1	C1 (%)	Ex. <250, *315* Em. 450	Terrestrial humic-like	C1 (Guéguen et al., 2014); C1 (Vines & Terry, 2020); C1 (Zhuang et al., 2021)
Component 2	C2 (%)	Ex. <250, *305* Em. 395	Microbial humic-like	C2 (Kothawala et al., 2014); C4 (Wauthy et al., 2018); C4 (Zhou et al., 2019)
Component 3	C3 (%)	Ex. 380 Em. 460	Fulvic acid, humic-like	C2 (Ren et al., 2021); C4 (Wünsch et al., 2017)
Component 4	C4 (%)	Ex. 275, *405* Em. 500	Terrestrial humic-like	C4 (Gonçalves-Araujo et al., 2015); C3 (Guéguen et al., 2014); C3 (Krylov et al., 2020)
Component 5	C5 (%)	Ex. 280 Em. 335, 460	Protein, tryptophan-like	C2 (Gao & Guéguen, 2017); C4 (Krylov et al., 2020)

Table A.3.2. Data quality checks for turbidity corrected Spectro::lyser (absorbance at 254 nm; A_{254}) and autosampler (A_{254} and dissolved organic carbon; DOC) against grab samples for Smith Creek and Scotty Creek in 2019.

Stream	Instrument	Constituent	n	R^2
Smith Creek	Spectro::lyser	A_{254}	9	0.99
Smith Creek	Autosampler	A_{254}	9	0.96
Smith Creek	Autosampler	DOC	9	0.99
Scotty Creek	Spectro::lyser	A_{254}	7	0.97
Scotty Creek	Autosampler	A_{254}	7	0.99
Scotty Creek	Autosampler	DOC	7	0.92

Table A.3.3. Characteristics of the Ochre River, gauged by the Water Survey of Canada since 2005.

Characteristic	Ochre River
Gauging location	63.489444, -123.6125
Permafrost zone	Extensive discontinuous
Catchment area (km^2)	1125
Mean slope (degrees)	7.3
Mean elevation (m)	491
Wetland (%)	2
Forest (%)	76
Shrub (%)	18
Barren (%)	3
Water (%)	1
Utility in predicting Smith Creek discharge	
Regression formula	0.3781+0.0513x
n	139
p-value	<0.001
Adjusted R^2	0.74

Table A.3.4. Models and coefficients from LOADEST for 2006-2021. Models were nested within: ln Load=a0+ a1lnQ+a2lnQ2+a3sin(2πdtime)+a4cos(2πdtime). THg=total mercury, MeHg=methylmercury, DOC=dissolved organic carbon. Q and dtime are centered estimates as described in the main text; THg, MeHg flux=g d^{-1}; DOC=kg d^{-1}.

Stream	Solute	*n*	Model	R^2	a0	a1	a2	a3	a4
Scotty Creek	MeHg	23	2	0.937	-13.0900	1.0179	0.0763		
Scotty Creek	THg	24	4	0.972	-10.3118	1.0583	-0.1922	0.1351	
Scotty Creek	DOC	125	6	0.994	6.3357	1.0281	0.026	0.2890	0.1248
Smith Creek	MeHg	22	4	0.924	-12.3316	0.8411	-0.1625	0.6715	
Smith Creek	THg	23	4	0.975	-8.2766	1.2228	-0.6708	0.4776	
Smith Creek	DOC	133	6	0.992	7.2599	1.2865	-0.0522	-0.1983	0.0710

Table A.3.5. Seasonal runoff and solute yields. Runoff and LOADEST quantified yields of bulk total mercury (THg) and methylmercury (MeHg), and dissolved organic carbon (DOC) normalized by catchment area at A) Scotty Creek and B) Smith Creek from April to September 2019–2021 and mean and range of yield estimates based on longer-term discharge record (2006–2021) and concentrations from the monitoring period (2019–2021).

	A) Scotty Creek – Peat			Mean (range)	B) Smith Creek – Mixed			Mean (range)
Yields	2019	2020	2021	2006 – 2021	2019*	2020	2021	2006 – 2021
Runoff (mm)	61	311	142	151 (24-311)	87	146	86	96 (70-146)
Spring runoff	12 (20%)	79 (25%)	112 (79%)	68 (12-122)	22 (25%)	45 (31%)	44 (51%)	43 (22-76)
Summer runoff	49 (80%)	232 (75%)	30 (21%)	83 (12-232)	65 (75%)	101 (69%)	42 (49%)	54 (29-106)
Cumulative Bulk THg (ng m^{-2})	75.5	406	203	209 (32–406)	406	645	405	443 (334–645)
Spring THg	16.0 (21%)	120 (30%)	170 (84%)	99 (16–191)	139 (34%)	311 (48%)	297 (73%)	285 (134–536)
Summer THg	59.5 (79%)	286 (70%)	32.7 (16%)	98 (14–286)	267 (66%)	334 (52%)	108 (27%)	159 (56–334)
Cumulative Bulk MeHg (ng m^{-2})	5.21	36.3	16.5	18 (2–40)	6.56	10.0	6.06	6.6 (4.9–10.0)
Spring MeHg	0.96 (18%)	9.66 (27%)	13.6 (82%)	9 (0.9–18)	1.67 (26%)	3.22 (32%)	3.11 (51%)	2.8 (1.4–4.8)
Summer MeHg	4.25 (82%)	26.7 (73%)	2.86 (18%)	9 (0.9–27)	4.89 (74%)	6.80 (68%)	2.95 (49%)	3.8 (2.0–6.8)
Cumulative DOC (g m^{-2})	1.16	6.63	2.63	3.0 (0.4–6.6)	1.45	2.37	1.37	1.5 (1.1–2.4)
Spring DOC	0.19 (16%)	1.41 (21%)	2.02 (77%)	1.2 (0.2–2.3)	0.43 (30%)	0.94 (40%)	0.90 (65%)	0.9 (0.4–1.6)
Summer DOC	0.97 (84%)	5.23 (79%)	0.61 (23%)	1.7 (0.2–5.2)	1.02 (70%)	1.43 (60%)	0.47 (35%)	0.7 (0.3–1.4)

*Smith Creek flow record in 2019 ranges from May 27 to Sept 28; yields are based on this period.

Table A.3.6. Summary statistics of cumulative annual (January-December) runoff for Ochre River (proxy for Smith Creek) and Scotty Creek, 2006 – 2021.

Cumulative Runoff (mm)	Ochre River near Smith Creek	Scotty Creek
Minimum	169	28
Mean	236	164
Median	240	155
Maximum	301	338
Standard Deviation	42	91
Coefficient of Variation	18	56

Table A.3.7. PCA on absorbance and fluorescence indices.

	PC1	PC2	PC3
Importance of components:			
Eigenvalue	4.81	1.94	0.54
Proportion of variance	0.60	0.24	0.06
Cumulative variance	0.60	0.84	0.91
Loadings:			
SUVA	0.76	0.01	-0.58
BIX	-0.92	0.01	-0.08
HIX	0.91	-0.24	0.19
C1	0.65	-0.73	0.05
C2	-0.89	-0.33	0.05
C3	0.28	0.87	0.29
C4	0.68	0.63	-0.11
C5	-0.88	0.31	-0.24

A.4. Supporting information for Chapter 4

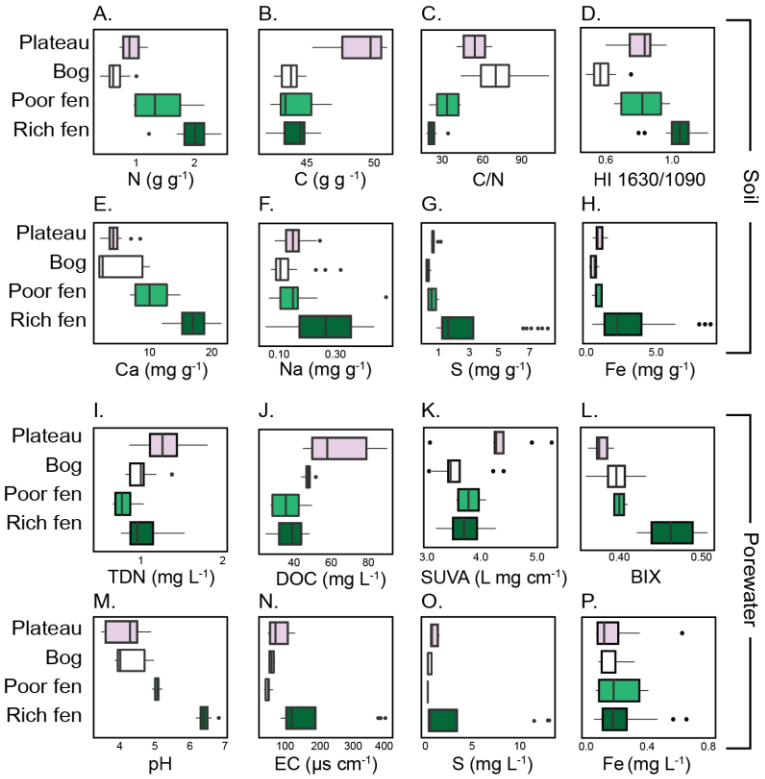

Figure A.4.1. Geochemistry and organic matter composition of porewater and soil. Boxplots of the median, first, and third quartiles, whiskers of 1.5 times the interquartile range, and outliers from A)–H) soil samples (triplicates from 0-12 cm depth) and I)–P) porewater samples (triplicates) including nitrogen (N), carbon (C), C/N, humification index at 1630/1090 cm^{-1}, calcium (Ca), sodium (Na), sulfur (S), iron (Fe), total dissolved nitrogen (TDN), dissolved organic

carbon (DOC), specific ultraviolet absorption at 254 nm ($SUVA_{254}$), biological index (BIX), pH, and electrical conductivity (EC).

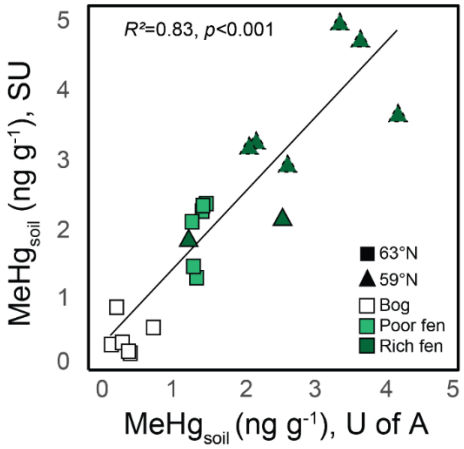

Figure A.4.2. Comparison of methylmercury (MeHg) concentrations (n=20) from the calculation of ambient MeHg in soil samples amended with tracer and incubated before analysis at the University of Alberta (U of A) vs. adjacent soil samples not amended with tracer/incubated before analysis at Stockholm University (SU). Fens are separated by moderate-rich and poor classification, with two moderate-rich fens at 59°N; the relatively richer fen at 59°N has a dashed border.

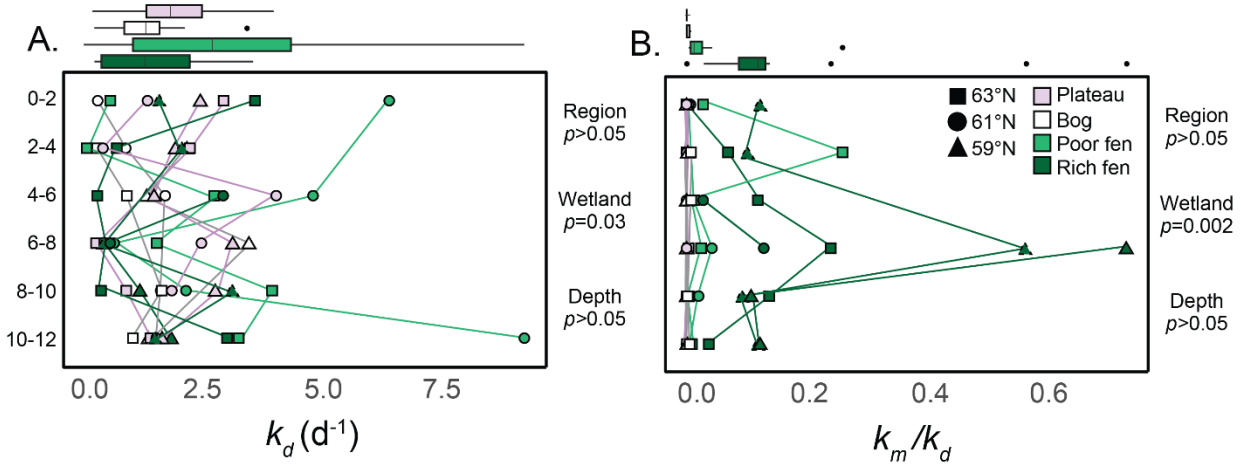

Figure A.4.3. Soil profiles from 0–12 cm depth for A) potential demethylation rate (k_d) and B) the ratio of potential methylation to demethylation (km/k_d). Values are the mean of triplicate samples grouped by wetland classification. Fens are separated by moderate-rich and poor classification, with two moderate-rich fens at 59°N; the relatively richer fen at 59°N has a dashed border. The p-values from testing the variability of the region, wetland class, and depth with permutational analysis of variance (perANOVA) are displayed beside the plots, and boxplots of the median, first, and third quartiles, whiskers of 1.5 times the interquartile range, and outliers grouped by wetland classification are above each plot. No demethylation was detected during the incubation period in several samples.

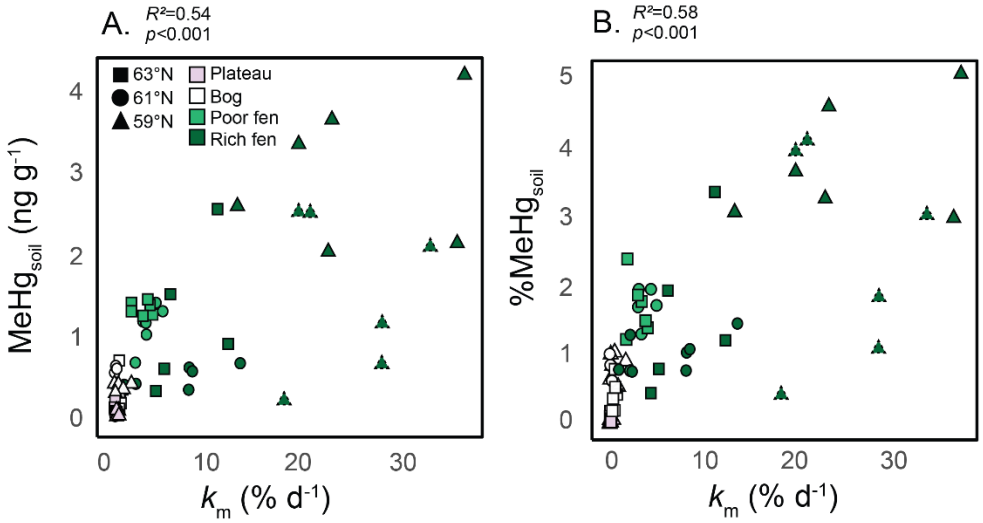

Figure A.4.4. Utility of potential methylation rates (k_m) as predictors of A) methylmercury (MeHg) concentrations and B) %MeHg (ratio of MeHg to total mercury) in soils. Fens are separated by moderate-rich and poor classification, with two moderate-rich fens at 59°N; the relatively richer fen at 59°N has a dashed border.

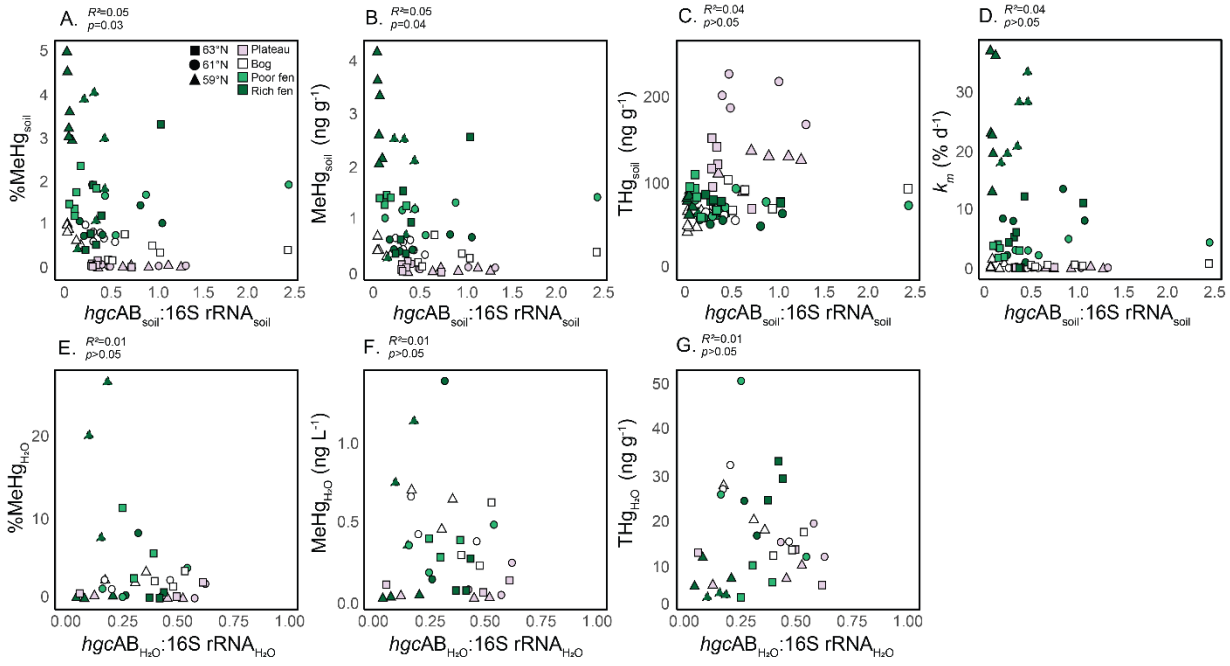

Figure A.4.5. Relationships between soil (A–D) and porewater (E–G) chemistry and methylating gene *hgc*AB normalized by 16S rRNA, including %MeHg (methylmercury to total mercury concentration ratio, [MeHg]/[THg]), MeHg, THg, and potential methylation rates (*km*). Fens are separated by moderate-rich and poor classification, with two moderate-rich fens at 59°N; the relatively richer fen at 59°N has a dashed border.

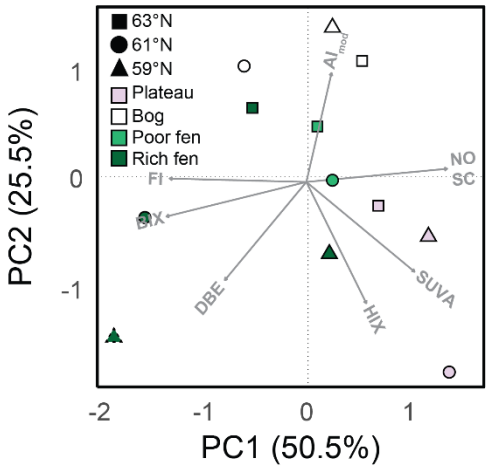

Figure A.4.6. Principle component analysis (PCA) on dissolved organic matter (DOM) indices; DOM indices are described in Table A.4.3. Fens are separated by moderate-rich and poor classification, with two moderate-rich fens at 59°N; the relatively richer fen at 59°N has a dashed border.

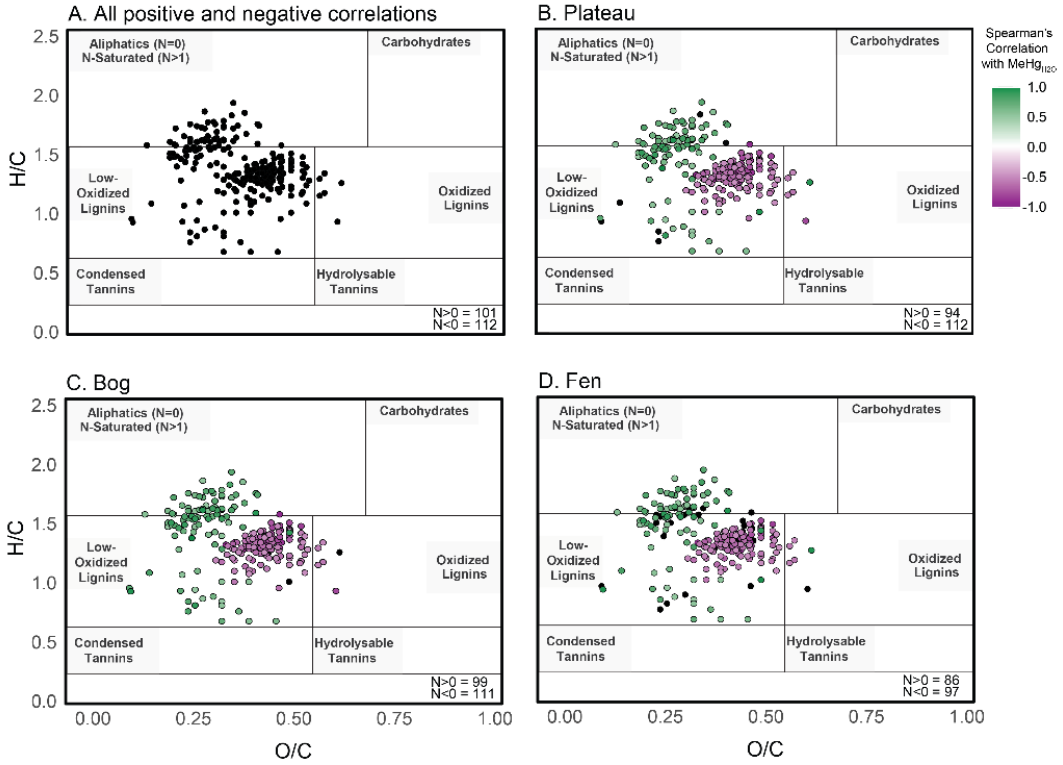

Figure A.4.7. Correlations between dissolved organic matter (DOM) compound classes and methylmercury (MeHg) concentrations shown per wetland class. Van Krevelen plot of oxygen/carbon (O/C) and hydrogen/carbon (H/C) wherein each data point represents the strength of significant correlations (Spearman's Rank, $p<0.05$ after 999 permutations) between the relative intensity of a specific DOM molecule with MeHg concentrations in porewaters. Boxed regions denote biomolecular compound classes and molecules from panel A underlie molecules in panels B, C, and D.

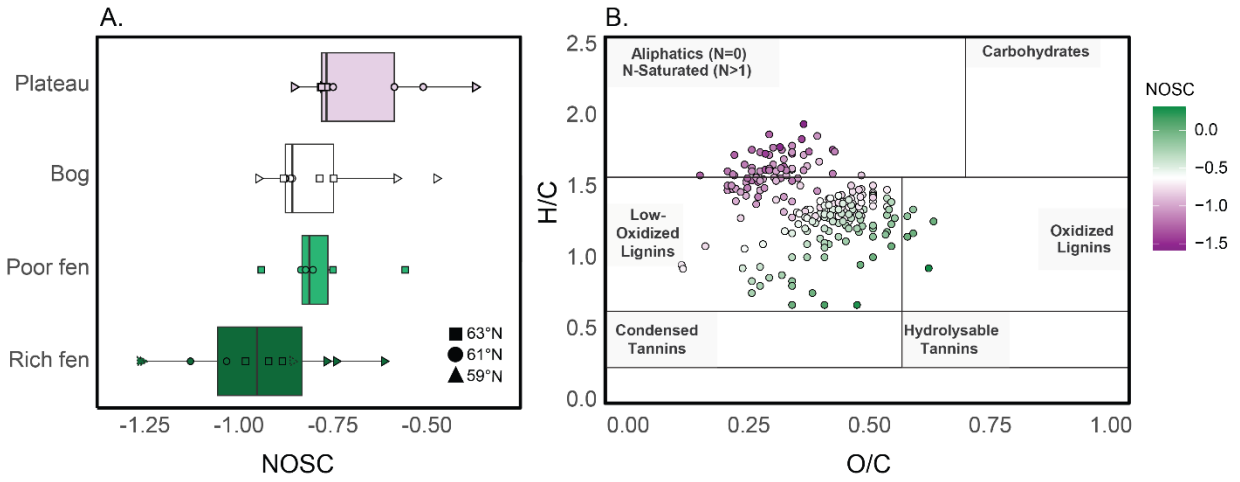

Figure A.4.8. Exploring the nominal oxidation state of carbon (NOSC) among A) wetland classes and B) within DOM compound classes that correlate with methylmercury (MeHg). Panel B is a Van Krevelen plot of oxygen/carbon (O/C) and hydrogen/carbon (H/C) wherein each data point shows the NOSC values of molecules that significantly correlate (Spearman's Rank, $p<0.05$ after 999 permutations) between the relative intensity of a specific DOM molecule with MeHg concentrations in porewaters.

Table A.4.1. Sampling region characteristics.

Site characteristics	59°N	61°N	63°N
Monitoring location	59.484, -117.178	61.304, -121.299	63.149, -123.258
Sampling dates	July 27 – 30, 2021	July 5 – 8, 2021	July 13 – 16, 2021
Permafrost zone	Sporadic discontinuous	Sporadic discontinuous	Extensive discontinuous
Thaw Depth (cm)	39	32	33

Table A.4.2. Species list for each sampled wetland. PP=peat plateau; BG=bog; RF=moderate-rich fen; PF=poor fen. [1]Relatively richer 59°N fen. Dark grey indicates presence.

		59°N				61°N				63°N			
Type	Species	PP	BG	RF	RF[1]	PP	BG	PF	RF	PP	BG	PF	RF
Lichenous	Cladina rangiferina	■				■				■			
	Cladina stellaris	■								■			
	Cladina sp.									■			
Nonvascular	Sphagnum fuscum	■	■			■				■	■		
	Sphagnum medium		■				■				■		
	Sphagnum angustifolium							■					
	Sphagnum majus										■		
	Sphagnum riparium		■										
	Sphagnum teres			■							■		
	Sphagnum subfulvum											■	
	Sphagnum balticum						■				■		
	Sphagnum russowi							■					
	Sphagnum rubellum					■							
	Mylia anomala										■		
	Pleurozium schreberi					■				■			
	Scorpidium scorpioides												■
	Dichodontium flavescens												

	Warnstorfia exannulata	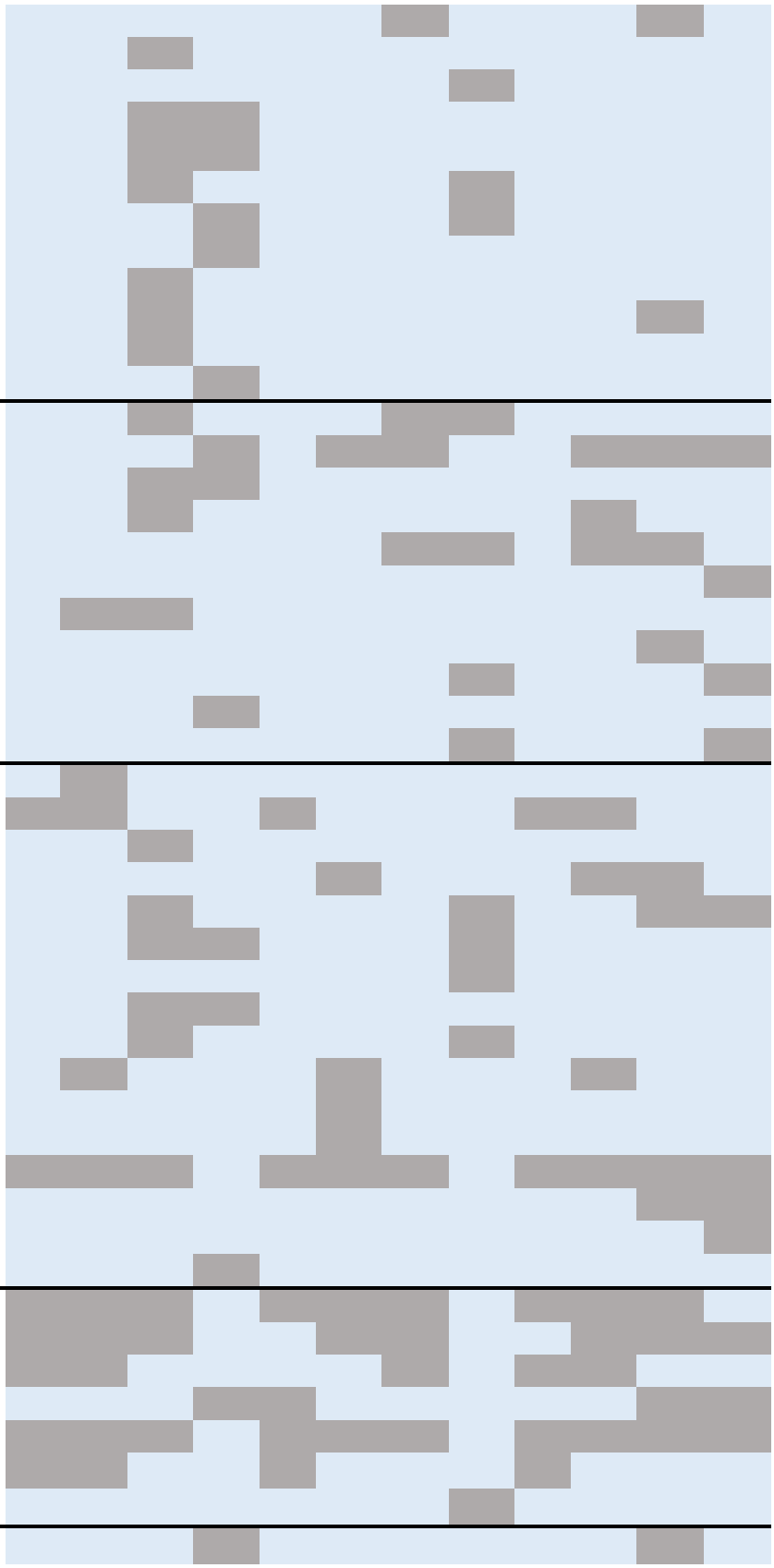
	Calliergon richardsonii	
	Calliergon giganteum	
	Brachythecium acutum	
	Bryum pseudotriquetrum	
	Hamatocaulis vernicosus	
	Drepanocladus polygamus	
	Drepanocladus aduncus	
	Plagiomnium ellipticum	
	Straminergon stramineum	
	Paludella squarrosa	
	Cinclidium stygium	
Graminoid	Carex aquatilis	
	Carex utriculata	
	Carex diandra	
	Carex magellanica	
	Carex limosa	
	Carex sp.	
	Eriophorum vaginatum	
	Eriophorum angustifolium	
	Trichophorum alpinum	
	Calamagrostis canadensis	
	Triglochin maritima	
Forb/herb	Geocaulon lividum	
	Rubus chamaemorus	
	Rubus acaulis	
	Maianthemum trifolium	
	Menyanthes trifoliata	
	Comarum palustre	
	Calla palustris	
	Epilobium palustre	
	Galium trifidum	
	Scheuchzeria palustris	
	Sparganium natans	
	Sarracenia purpurea	
	Drosera rotundifolia	
	Drosera anglica	
	Tofieldia glutinosa	
	Hippuris vulgaris	
Shrub	Chamaedaphne calyculata	
	Andromeda polifolia	
	Rhododendron groenlandicum	
	Myrica gale	
	Vaccinium oxycoccos	
	Vaccinium vitis-idaea	
	Betula glandulosa	
Shrub/tree	Salix sp.	

	Betula pumila	
Tree	Picea mariana	

Table A.4.3. DOM indices from optical (absorbance or fluorescence) spectroscopy and FTICR-MS and compound classes from FTICR-MS. Ex.=excitation, Em.=emission, C=carbon, H=hydrogen, N=nitrogen, O=oxygen, S=sulfur, P=phosphorus.

Indices	Category	Abbreviation (unit)	Calculation	Characteristic	Citation
Specific ultraviolet absorbance at 254 nm	Optical	SUVA (L mg^{-1} C m^{-1})	(Absorbance at 265 nm)/(Dissolved organic carbon concentration)	Aromaticity	(Weishaar et al., 2003)
Biological index	Optical	BIX	(Ex. 310, Em, 380)/(Ex. 310, Em. 430)	Presence of fresh DOM	(Huguet et al., 2009)
Humification index	Optical	HIX	(Ex. 254, Σ Em. 435-480)/ (Ex. 254, Σ Em. 300-345)	Extent of humification	(Ohno, 2002)
Fluorescence index	Optical	FI	(Ex. 370, Em. 450)/(Ex. 370, Em. 500)	Microbially-derived substance	(McKnight et al., 2001)
Nominal oxygenation state of carbon	FTICR-MS	NOSC	$4 - [(4C + H - 3N - 2O - 2S)/C]$	Bioavailability inferred from polarity	(Riedel et al., 2012)
Modified aromaticity index	FTICR-MS	AI_{mod}	$(1 + C - 0.5O - S - 0.5H)/(C - 0.5O - S - N - P)$	Aromaticity	(Koch & Dittmar, 2006)
Double bond equivalence	FTICR-MS	DBE	$1 + 1/2(2C - H + N + P)$	Double bonds and rings in molecule	(Koch & Dittmar, 2006)

Compound class	Calculation	
Aliphatic	$0 < O/C < 0.65$, $1.6 \leq H/C \leq 2.2$	(Kellerman et al., 2015)
N-saturated peptides and amino-sugars	$1 \leq N$, $0.1 \leq O/C \leq 0.65$, $1 \leq H/C < 2.2$	(Kellerman et al., 2015)
Low-oxidized lignins	$0.1 \leq O/C < 0.5$, $0.7 \leq H/C \leq 1.6$	(Kellerman et al., 2015)
Oxidized lignins	$0.5 \leq O/C \leq 1$, $0.7 \leq H/C \leq 1.6$	(Kellerman et al., 2015)
Condensed tannins	$0 < O/C < 0.5$, $0.3 \leq H/C < 0.7$	(Kellerman et al., 2015)
Hydrolysable tannins	$0.5 \leq O/C < 1$, $0.3 \leq H/C \leq 0.7$	(Kellerman et al., 2015)
Carbohydrates	$0.65 \leq O/C < 1$, $1.3 \leq H/C < 2.2$	(Kellerman et al., 2015)

Table A.4.4. PCA (Figure A.4.2) on DOM indices.

	PC1	PC2	PC3
Importance of components:			
Eigenvalue	3.53	1.78	0.76
Proportion of variance	50.47	25.47	10.81
Cumulative variance	50.47	75.94	86.75
Loadings:			
SUVA	0.72	-0.56	0.03
BIX	-0.93	-0.22	-0.03
HIX	0.40	-0.76	-0.37
FI	-0.90	0.02	-0.07
NOSC	0.93	0.08	-0.05
DBE	-0.54	-0.61	-0.35
AI_{mod}	0.17	0.68	-0.70

Table A.4.5. Projections of landscape net methylation. First, second, and third quartiles of %MeHg per BAWLD-harmonized peatland class and fractional distribution within Taiga Plains peatland classes (fens, plateaus, and bogs) from the BAWLD land cover product (Olefeldt et al., 2021). Present and future projections of %MeHg are weighted by peatland complex fractional area, with future scenarios based on SSP4.5 (low, mid, and high).

	%MeHg			Distribution (km^2; % of peatland-complex area)				%MeHg (Q2; Q1-Q3) x peatland-complex fractional area			
Class	Q1	Q2	Q3	Current	2100 low	2100 mid	2100 high	Current	2100 low	2100 mid	2100 high
Perm-Bog	0.04	0.06	0.08	1.08E+05 (61%)	6.58E+04 (37%)	4.95E+04 (28%)	3.49E+04 (20%)	**0.04** *(0.02-0.05)*	**0.02** *(0.01-0.03)*	**0.02** *(0.01-0.02)*	**0.01** *(0.01-0.02)*
Bog	0.53	0.68	0.86	2.95E+04 (17%)	5.31E+04 (30%)	6.25E+04 (35%)	7.11E+04 (40%)	**0.11** *(0.09-0.14)*	**0.20** *(0.16-0.26)*	**0.24** *(0.19-0.30)*	**0.27** *(0.21-0.34)*
Fen	1.08	1.96	2.99	4.13E+04 (23%)	5.97E+04 (34%)	6.65E+04 (37%)	7.24E+04 (41%)	**0.45** *(0.25-0.69)*	**0.66** *(0.36-1.00)*	**0.73** *(0.40-1.12)*	**0.80** *(0.44-1.22)*
							Landscape %MeHg	**0.60** *(0.36-0.88)*	**0.88** *(0.53-1.29)*	**0.99** *(0.60-1.44)*	**1.08** *(0.66-1.58)*